Physics – Uspekhi **44** (2) 135 – 171 (2001)

REVIEWS OF TOPICAL PROBLEMS PACS numbers: 11.30.Er, **25.43 + t**, **36.30.10 – k**, 67.40.Kh

Some problems of the physics of exotic atoms

L I Men'shikov, M K Eseev

DOI: 10.1070/PU2001v044n02ABEH000817

Contents

1. Introduction **135**
2. Current status of the physics of exotic atoms **136**
2.1 Main avenues of investigation, experimental techniques and facilities; 2.2 Cascade processes in exotic atoms; 2.3 Muonic atoms; 2.4 Hadronic atoms; 2.5 Experiments on antihydrogen; 2.6 Metastability of exotic helium. The Condo model.
3. Direct production mechanism of antiproton helium **149**
4. Production of antiproton helium by recombination mechanism. The 'ioncule' **150**
5. Why is metastability inherent only in helium? **150**
6. Quenching of metastability by impurities. Comparison with experiments **150**
7. Metastability of antiprotons in pure helium. The bubble model **153**
8. Electronic states of an ioncule for low helium densities **157**
9. Basic ioncule properties. Comparison of the model with laser-spectroscopy data **158**
10. Conclusions **159**
11. Appendix **161**
I. *CPT* invariance; II. Calculation of the cross section for the direct production of antiproton helium; III. Rate of antiproton helium production by the recombination mechanism (71), (72); IV. Rate of Auger ionization (88) of an ioncule in the ground electronic state; V. Excited electronic states of an ioncule
References **167**

Abstract. The current status of the physics of exotic atoms is reviewed. The problem of the anomalous width of the kaonic helium 2p level is analyzed, experimental *CPT* invariance tests for the antihydrogen are discussed, and results of investigations on the metastability of the antiproton (as well as of π^-, μ^-, K^-, Σ^-, ...) in helium are considered. A comparison is made of the well-known Condo model and the ionic model. In the latter, the ion ($\bar{p}\alpha ee$) — a so-called 'ioncule' — forms after $\bar{p}$ is stopped in its motion in helium. One of the ioncule's electrons is weakly bound, resides at one of the Efimov levels, and orbits at ~ 20 a.u. in the dipole field of the neutral 'atomcule' ($\bar{p}\alpha e$). The lifetime of the ioncule is long ($> 10^{-5}$ s) and the antiproton's vibrational – rotational transition frequencies ω are practically equal to the atomcule value ($\Delta\omega/\omega \sim 10^{-5} - 10^{-6}$) — in agreement with laser-spectroscopy data. While the ionic model results on the quenching cross sections of metastable states by impurity atoms and molecules in helium agree well with experiment, the atomcule-based Condo model underrates the cross sections by 3 – 4 orders of magnitude. The ionic model is also consistent with other experiments. Direct experimental tests of this model are discussed. A new interpretation of E Zavattini's group's laser-spectroscopy results on the 2s – 2p-splitting in muonic helium is presented.

L I Men'shikov Russian Research Centre 'Kurchatov Institute',
pl. Kurchatova 1, 123181 Moscow, Russian Federation
Tel. (7-095) 947-27 72
E-mail: menipel@cityline.ru
Pomor'e State University,
prosp. Lomonosova 4, 163006 Arkhangel'sk, Russian Federation
Tel. (7-8182) 44-17 50
M K Eseev Pomor'e State University,
prosp. Lomonosova 4, 163006 Arkhangel'sk, Russian Federation
Tel. (7-8182) 44-17 50
E-mail: eseev_m@mail.ru

Received 27 June 2000; revised 22 October 2000
Uspekhi Fizicheskikh Nauk **171** (2) 149 – 185 (2001)
Translated by E N Ragozin; edited by A Radzig

1. Introduction

An exotic atom (EA) is a bound or a quasi-stationary complex produced when a heavy negatively charged particle X ($X = \mu^-, \pi^-, K^-, \bar{p}, \Sigma^-, ...$) lands on a conventional atom. Also sometimes classed with EAs are antihydrogen ($\bar{p}e^+$), muonium (μ^+e^-), and other systems. The concept of an EA was first introduced by Fermi, Teller, and Wheeler [1, 2] to provide an interpretation of the experiment conducted by Conversi et al. [3]. The authors of the latter paper discovered that the lifetime of negative muons in heavy-atom materials ($Z \gg 1$, $A \gg 1$) is far shorter than for free muons. It was shown in Refs [1, 2] that μ^- are decelerated in a material and knock electrons out of their parent atoms to produce excited muonic atoms. The dimension of an initial muon orbit (as with any other X particle) is of the order of the Bohr radius a_0 and, accordingly, these states are characterized by large quantum numbers $l \sim n \sim \sqrt{m_\mu/m_e} \sim 15$. Subsequently there occur cascade mesoatom relaxation processes with the effect that the mesons drop back to lower $n \sim 1$ orbits whose dimension [$\sim a_0 m_e/(Zm_\mu)$] is small in comparison with the electron orbits. In these states, the probability that a muon

finds itself close to the nucleus is significant, and the rate (the probability per unit time) of muon capture by the nuclei increases sharply owing to the weak interaction with nucleons. The slowing-down of mesons and the cascade occur in a time $\tau_c \sim 10^{-12}$ s, i.e. in a time far shorter than the muon lifetime ($\tau_\mu \sim 10^{-6}$ s), hence the results of Ref. [3]. In addition, the conclusion that τ_c is negligible in comparison with the particle X lifetime (in the case that the particle is unstable) is general in character and holds good for not-very-low atomic densities in the material, with the exception of the lowest ones ($N < 10^{18}$ cm^{-3}). Hence we draw a conclusion that EAs are by no means scarce, exotic objects: they are always produced after a particle is brought to rest in a material.

Intensive investigations are presently being pursued in the physics of EAs and, despite its 'age' of fifty, the situation continues to change rapidly. Reviews [4–17] and the proceedings of numerous conferences (for instance, see Refs [18–20]) are convincing proof that this is indeed the case. The main objectives of contemporary elementary particle physics are well known: verification of the implications and quest of the violations of the Standard Electroweak Model with the goal of its generalization, the detection of the Higgs boson, the determination of neutrino masses, elucidation of the cosmological implications of the microworld physics, etc. Experiments in this realm advance along two mutually complementary avenues. At the heart of the former are the construction of high-energy accelerators and unique detectors in an effort to discover new particles and interactions and to verify theoretical models. The latter is precisely the physics of exotic atoms or, to put it otherwise, medium energy physics. It has the same purposes as the former. At its heart lies the quest for rare decays and reactions involving known particles, the discovery of violations of fundamental symmetry properties, and the study of atomic and molecular processes with the participation of EAs. In these investigations, advantage is taken of accelerators with intense beams and relatively low-energy particles.

The physics of EAs is quite extensive and highly diverse. It is therefore not surprising that all reviews on this subject focus on some specific fields. Our paper follows the same pattern. First comes a brief review of previous and contemporary investigations. The problems of the kaonic helium 2p state and the experiments on antihydrogen are discussed in greater detail. The main body of our paper is devoted to experiments and theoretical models concerned with the metastability of antiprotons in helium. Naturally, this selection of topics is subjective and reflects the scientific interests of the authors. The missing information can be found in the reviews mentioned and the current scientific literature.

2. Current status of the physics of exotic atoms

2.1 Main avenues of investigation, experimental techniques and facilities

In objectives and experimental techniques, EA research may be divided into three big avenues: the physics of muonic atoms and molecules (mesomolecules), the physics of hadronic atoms and hypernuclei, and experiments on the production of antihydrogen and the comparison of its properties with those of hydrogen.

Hadrons are produced when immobile targets are bombarded by protons. Muons form in the decays of pions $\pi^- \to \mu^- + \tilde{\nu}_\mu$ either in flight or in the near-surface layer of a proton-irradiated target. Facilities of this type are termed meson factories. Devices with a magnetic field are sometimes taken advantage of to form secondary beams out of the cloud of nascent hadrons with the purpose of raising the muon intensity [21]. Meson factories have been built in the LAMPF (USA), PSI (Switzerland), TRIUMF (Canada), IYaF (Troitsk, Russia), RIKEN (Japan), and RAL (Great Britain) laboratories. The intensity of muon beams attained with these facilities ($\sim 10^6$ particles per second) is 2–3 orders of magnitude higher than that in the pioneering experiments with muonic atoms and molecules (see, e.g., Refs [22, 23]). Such facilities permit the detection of a large number of events and hence acquire vast statistics and lower the statistical errors in the quantities under measurement.

As a rule, experiments on EAs follow the pattern outlined below. A charged particle passes through a monitor counter placed in front of the target with the material under investigation. The electric pulse coming from this counter serves as the zero time of the period (the time gate) during which other counters record the time of the origin (the so-called delay time) of secondary particles — the reaction products created by the incident particle in the target. The inevitable background is drastically reduced through an additional selection of events on the basis of coincidence and anticoincidence circuits. To reduce the background arising from nuclear captures of the particles stopped in the target walls (the walls consist of heavy atoms, and therefore nuclear captures are fast to occur), the so-called dead time is sometimes introduced during which the signals generated by the secondary-particle detectors are not recorded. A histogram is plotted after the experiment (the time spectrum of reaction products) — the number of events falling into a given interval of the delay time as a function of this time. This spectrum carries the most important information on the processes at work.

The above scheme should obviously discard those events which see another particle (or several particles) flying into the target through the corresponding time gates. Hence it follows that the beam intensity and, as a consequence, the event counting rate are bound from above. These restrictions are lifted [21, 24] if advantage is taken of pulsed or time-modulated beams instead of constant-intensity beams. For instance, the muon beam in the RIKEN-RAL facility [21] consists of short bursts comprising $\sim 10^4$ muons each and repeating with a rate of 50 Hz. The pulse duration (~ 50 ns) is short in comparison with the muon lifetime, allowing the duration to be neglected. A bunch of $\sim 10^4$ muons is much easier to record than a single muon arriving at a target. The bunch detection triggers the time reading. By measuring the frequency of origination of reaction products produced by all muons of the bunch in relation to the time delay, they obtain the same time spectrum as that obtained by the method outlined above, with an obvious gain in the data acquisition rate. Yet another advantage of the pulsed beams lies in the reduction of the fraction of background events.

Another type of experiments involves the quest for rare decays, for instance, $\mu \to e\gamma$. In this case, it is important to have a beam of as high an intensity as possible.

In experiments with negative kaons at the meson factories, these particles are typically brought to rest at an experimental target with a frequency of ~ 200 events per second (a helium decimeter-sized target with a density $\rho \sim 0.2$ g cm^{-3} [25]). The number of pions stopped in the target is higher by an

order of magnitude, and they produce a strong background. Electron–positron factories are void of this drawback — the Φ and B factories whose concept was framed in the G I Budker Institute of Nuclear Physics, Siberian Branch of the Russian Academy of Sciences [19, 26–29] and elaborated on the VÉPP-2M and VÉPP-4 facilities. A virtual photon originating in the annihilation of particles in counter-propagating e^+ and e^- beams (Fig. 1) transforms into a short-lived vector meson, which decays through the strong-interaction channel into $K\bar{K}$ mesons (Φ factory) or $B\bar{B}$ mesons (B factory). The reaction cross section has a resonance when the total energy of e^+ and e^- corresponds to the rest mass of a vector meson. The typical number of K^- stopping events in a hydrogen target with a density of $\sim 4 \times 10^{-3}$ g cm^{-3} at the DAΦNE Φ factory (Frascati, Italy) is, according to the DEAR (DAΦNE Exotic Atom Research [30]) project, ~ 0.3 particles per second. From this and from the previously given example we conclude that the number of kaon stopping events at the Φ factory is, when the targets are similar, an order of magnitude lower than at a meson factory. This disadvantage is compensated for by a drastic lowering of the background.

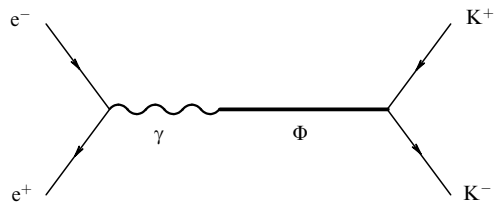

Figure 1. Process underlying the operation of a Φ factory.

The main results on antiproton EAs [$\bar{p}p$, $\bar{p}He$, $\bar{H} \equiv (\bar{p}e^+)$, etc.] were obtained on the LEAR (Low Energy Antiproton Ring) storage ring of the CERN accelerator complex, which was operated during 1984–1996. About 10^{10} antiprotons with a momentum $p = 105$ MeV/c and a spread in momenta $\Delta p/p \sim 10^{-3}$ were extracted from the ring approximately once an hour [17]. In this case, the time-average number of $\bar{p}$ stopping events in the targets was typically $\sim 10^4 - 10^5$ particles per second. A new facility — AD (Antiprotonic Decelerator) — has been constructed to replace LEAR, and a start has been made on the ATRAP, ATHENA, and ASACUSA experiments at the AD facility. Bunches of $\sim 5 \times 10^{13}$ protons are accelerated in a proton synchrotron to be directed onto a target once a minute. A secondary beam of antiprotons forms with an initial momentum of 3.5 GeV/c. Subsequently, this beam is slowed down in three stages ($3.5 \to 2 \to 0.3 \to 0.1$ GeV/c) by application of the electron cooling technique. The final antiproton beam has a momentum spread $\Delta p/p \sim 10^{-3}$, an energy of 5.8 MeV (0.1 GeV/c), and 5×10^7 particles per 200-ns long burst with a repetition rate of one burst per minute.

After this brief discussion of experimental facilities, we turn to the physics of exotic atoms itself.

2.2 Cascade processes in exotic atoms

The study of cascade EA deexcitation processes is of interest by itself. Moreover, this study is necessary for planning and interpreting the experiments staged to investigate the low-energy particle–nucleus interaction.

The principal cascade processes in EAs are Coulomb, radiative, and Auger transitions, Stark mixing, nuclear capture of X^- in excited EA states, and ion-molecular reactions involving an ionized EA being deexcited. Systematic calculations of the cascade process kinetics were performed only for the EAs of hydrogen isotopes ($Z = 1$) [31–40]. For $Z > 1$, only qualitative estimates are available.

2.2.1 Cascade processes in exotic atoms of hydrogen isotopes ($Z = 1$). The cascade processes for $Z = 1$ and $Z > 1$ are significantly different in character. For $Z = 1$, an EA in the states with principal quantum number $n \ll n_0 = \sqrt{m_X/m_e}$ has small dimensions $r_n = n^2/m_X \ll 1$ [from this point on, unless otherwise specified, formulas and values are given in atomic units (a.u.), in which $\hbar = m_e = e = 1$]. Moreover, an EA is electrically neutral, is therefore weakly scattered by the material atoms, and in this sense is similar to a neutron. Penetrating through electron shells, an EA finds itself periodically in a strong electric field existing inside the atoms. This field induces Stark transitions

$$(pX)_{nl} + H \to (pX)_{nl'} + H\,, \qquad l' \neq l\,, \tag{1}$$

thereby 'smearing' the EA states over the subspace of (n, l) Rydberg states with different l but similar n ('horizontal smearing'). Since the internal energy

$$\varepsilon_n = -\frac{\mu_X}{2n^2}\,, \qquad \mu_X^{-1} = m_X^{-1} + m_p^{-1} \tag{2}$$

does not change in the Stark transitions (1), they are characterized by large cross sections and are the fastest among the cascade processes. Therefore, the horizontal smearing is much faster than vertical transitions, with the effect that the hydrogen isotope EAs being deexcited quite often find themselves in the (n, s) states with an angular momentum $l = 0$. This circumstance is very important to hadronic atoms: in the (n, s) states, the rate of hadron capture by nuclei is very high (it may be thought of as being practically infinite). Hence follow two conclusions (the Day–Snow–Sucher effect [41]). First, the effective nuclear capture rate (introduced in Ref. [31]) in the hadronic atoms of hydrogen isotopes is high owing to the Stark mixing, and therefore only a small fraction of hadrons reaches the lower Rydberg states $n \sim 1$. That is why the X-ray K-series photon yields Y prove to be small, which are defined as the number of emitted photons per particle X brought to rest in the target. This compels the staging of experiments at low densities and, as a consequence, the build up of the target dimensions (which lowers the accuracy of measurements [13]) or the use of magnetic traps to increase the number of stopping events [42]. Second, the high rates of Stark transitions allow a definite conclusion that the captures of hadrons by nuclei occur in s-waves. The latter is of significance in studying the interaction of hadrons with nuclei, determining the spins and the parity of hadrons from experiments, etc.

Among vertical transitions are (everywhere $n' < n$):

the Auger transitions

$$(pX)_{nl} + H \to (pX)_{n'l'} + H^+ + e\,, \tag{3}$$

the Coulomb transitions

$$(pX)_{nl} + H \to (pX)_{n'l'} + H \tag{4}$$

and the radiative transitions

$$(pX)_{nl} \to (pX)_{n'l'} + \gamma \tag{5}$$

(for simplicity, an H atom is specified in expressions (3) and (4) in lieu of an H_2 molecule which actually experiences collisions). For large n, the radiative transitions are insignificant; they dominate in the lower states $n \sim 1$. In the processes (4), a part of the internal energy (2) of EAs goes into their kinetic energy E. The Stark transition rates [43–45] and hence the effective nuclear capture rates [39] essentially depend on E, and therefore the E-energy distribution function for EAs in the (n, l) states should be known to describe the cascade. Men'shikov [46] considered the kinetics of excited mesoatoms taking into account reaction (4) with a small variation of the internal state

$$\Delta n = n - n' = 1 \,. \tag{6}$$

The values obtained for the cross sections of Coulomb transitions were an order of magnitude lower than in Ref. [47], in which advantage was taken of the dipole approximation and the atomic basis for the muon wave functions (WFs), both inapplicable in this case. According to Ref. [46], assuming (6) for a density $\varphi = N/N_0 \sim 1$, where $N_0 = 4.25 \times 10^{22}$ cm^{-3} is the number of nuclei in a cubic centimeter of liquid hydrogen, approximately two thirds of mesoatoms are thermalized and one third have an energy $E \sim 0.5$ eV. This is far less than the value $E \sim \Delta\varepsilon = \varepsilon_n - \varepsilon_{n-1} \sim 10$ eV that could be expected. The reason is that the rate ($\lambda = Nv\sigma$) of elastic ($n = n'$) processes (4), which slow down the mesoatoms, exceeds the rate of inelastic transitions (6) by an order of magnitude or more. In particular, for $n \sim 5$ and a liquid hydrogen density ($\varphi = 1$) the following rates are found:

$$\begin{aligned} &\lambda_c \equiv \lambda\,(\Delta n = 1) \sim 3 \times 10^{11}\ \text{s}^{-1}\,, \\ &\lambda_{el} \equiv \lambda\,(\Delta n = 0) \sim 10^{13}\ \text{s}^{-1}\,, \\ &\lambda_A \sim 2 \times 10^{12}\ \text{s}^{-1}\,, \end{aligned} \tag{7}$$

where λ_A is the rate of Auger transitions. The rates given in Ref. [48] are of the same order of magnitude, with the Coulomb transitions calculated in greater detail. It is evident that the fraction f and the energy of fast atoms are determined by the competition between the Coulomb acceleration and the thermalization, i.e. by the λ_c/λ_{el} ratio (it is incorrectly stated in Ref. [48] that f depends only on λ_A/λ_{el} and concluded, on these grounds, that f is high in magnitude). So, according to Refs [46, 48] under the assumption (6), the fraction of fast atoms f should be small.

An ingenious method was used to measure the distribution of excited atoms ($p\pi$) in Refs [49, 50]. The time-of-flight method was employed to detect the neutrons arising from the $(p\pi) \to n + \pi^0$ reaction, which escaped from the target. In this connection we note that the majority of pions are, due to the Day–Snow–Sucher effect, captured in the excited states $n \sim 4-6$ and, say, the $n = 2$ state is reached by only $\sim 1\%$ of the pions. The neutrons emitted by immobile and fast EAs differ slightly in energy and therefore the times taken them to travel the path from the target to the detector are different. The distribution of the neutrons under detection over this time difference can easily be measured and unambiguously related to the energy distribution of the ($p\pi$) atoms. It was found that the energies of about a half of the atoms fall within the range between 0 and 1 eV, while the remaining atoms are accelerated to energies in the range from 1 to 70 eV. Schottmuller et al. [51] discovered ($p\pi$) atoms with energies up to 200 eV.

The reason of the discordance between the theory and the experiment disagree is that assumption (6) is wrong (see Ref. [39]). Since $n \gg 1$, both quantum and classical mechanics apply to the description of particle motion. Furthermore, a reliable quantum-mechanical calculation of reaction (4) can hardly be performed, whereas the trajectory problem is easily solved numerically. The masses of π^- and p are comparable, and therefore in every event of reaction (4) there occurs, as a rule, a significant change of the EA internal energy, like in a collision in a system of billiard balls:

$$|\Delta E| \sim |\Delta\varepsilon_n| \sim |\varepsilon_n| \,. \tag{8}$$

This conclusion was borne out by a detailed numerical computation [40]. It follows from expression (8) that for $n \gg 1$ the main role is played by the Coulomb transitions in which the principal quantum number changes significantly, viz.

$$|\Delta n| \sim n \gg 1 \,, \tag{9}$$

which is yet another reason why accomplishing quantum-mechanical calculations is highly problematic.

Faifman et al. [40] considered the upper states on the basis of classical mechanics. The 'fate' of every probe atom, beginning from its origin for $n = n_0$ to its death resulting from a nuclear capture or an X particle decay, was traced by the Monte Carlo method. The lower states ($n < n_q \sim 5$) were considered on the basis of quantum mechanics, which reduced to the solution of the Boltzmann equations containing the quantum-mechanical rates of the processes discussed in the foregoing. The right-hand sides of the Boltzmann equations contain the numbers of EAs that fall into the (n, l) states from the classical region $n > n_q$, which were obtained from the Monte Carlo calculation. This method received the name QCMC (Quantum Classical Monte-Carlo Code). It is characterized by a systematic error $1/n_q$ lying in the range between ~ 0.2 and ~ 0.04, which is quite sufficient for planning and analyzing experiments. At present, this is the only *ab initio* approach. All other cascade calculations reported thus far [31–38] include fit parameters, be it the factors which the cross sections of the processes (e.g., the Stark ones) should be multiplied by or the assumption

$$E \sim 1 \text{ eV} \tag{10}$$

about the kinetic energy of an EA. The unknown coefficients of the cross sections were determined by fitting the results of theoretical calculations to the extensive experimental data for pion atoms. However, it is by no means clear that the coefficient values found in this way can be employed for other particles X. Moreover, the distributions calculated in Refs [39, 40] signify that a typical energy value comprises

$$E \sim 100 \text{ eV} \,, \tag{11}$$

which is consistent with Refs [49, 50]. The K_α photon (the $2p \to 1s$ transition) yield Y for (K^-p) atoms, calculated in Ref. [40], agrees with the experiment of Ref. [52], while the results of Refs [34, 35] differ greatly from it. Interestingly, an energy $E \sim 1$ eV is in a sense a boundary [39, 40]. As an explanation, we note that the classical analog of Stark transitions is a deformation or, more precisely, a collision-induced change of the eccentricity and the orientation of the

Keplerian orbit along which a particle X moves in an EA. For $E \leqslant 1$ eV, there occurs a strong orbit deformation in every collision of the EA with an atom of the target material, namely, a mode of 'strong' Stark transitions [31]. For $E \geqslant 1$ eV, this deformation is small, and the Stark transitions acquire a similarity to random diffusive motion of EAs over the space of orbital angular momenta l. When they find themselves in the low-l range as a result of this motion, a nuclear capture occurs. This reasoning explains why the magnitudes of Y calculated under assumptions (10) and (11) differ significantly from each other.

In connection with the problem of muonic catalysis of nuclear fusion reactions (see Section 2.3), a rather detailed investigation is made of the cascade processes in a mixture of hydrogen isotopes [14–16, 20], in a DT mixture in particular. Here, an important role is played by the catching of muons from excited mesoatoms of deuterium to tritium [53]:

$$(d\mu)_n + t \rightarrow d + (t\mu)_n , \tag{12}$$

because this process is responsible for a significant reduction of the required tritium concentration. Its quantitative characteristic is the probability q_{1s} that a muon will remain a part of a $(d\mu)$ atom upon completion of the $(d\mu)_{n_0} \rightarrow (d\mu)_{1s}$ deexcitation process. If the $(d\mu)$ atoms are assumed to be thermalized, the calculated values of q_{1s} [33, 53] prove to be well below the experimental ones [54–60]. This discrepancy between theory and experiment, which has come to be known as *the problem of* q_{1s}, has not yet been eliminated. It is possible to point out two mechanisms involving an increase in q_{1s}: the acceleration of $(d\mu)$ atoms in the Coulomb transitions (4) (see Refs [36, 61–63]) and the shattering ('Coulomb explosion') of a diatomic molecule by a mesoatom as a result of its single or double Auger ionization [15] (this is a process of type (3), in which the mesoatom is $(d\mu)$ and H should be replaced with H_2, HD, DT, T_2, ...).

2.2.2 Case $Z > 1$. The Stark processes are insignificant for atoms with $Z > 1$, with the exception of light atoms, for example, helium (see below). The reason is that the interaction of a particle X with electrons, which are practically always present in such EAs, removes the Coulomb degeneracy in the orbital angular momentum. Reactions of type (1) become nonresonant and their cross sections drop.

External Auger processes (3) have a low probability for $Z > 1$ in comparison with the ejection of the intrinsic electrons:

$$\left[(XZ)_{nl}(N, e)\right] \rightarrow \left[(XZ)_{n'l'}(N-1, e)\right] + e , \tag{13}$$

where N is the number of electrons in the EA. The EA charge equals $q = e(Z - N - 1)$. Processes of type (13) lead to the formation of EAs with $q > 0$, i.e. ions. These ions polarize atoms to make up, as a result of ion-molecular reactions occurring nearly instantly (in $\sim 10^{-13} - 10^{-12}$ s), bound states — ion clusters. These processes are diverse, exceptionally interesting, but poorly studied. We will dwell on some specific examples.

Gorelkin and Smilga [64] noted that the dimensions of the lower muonic orbits of an EA which originates when μ^- lands on Ar or Ne are small in comparison with the electron ones. That is why the μ^- stopping events in these gases should result in the formation of an appreciable number of neutral EAs which have $N = Z - 1$ electrons orbiting a practically point-like charge $Z - 1$. Accordingly, these EAs are similar to fluorine ($_\mu$F) and chlorine ($_\mu$Cl) in electron shell structure and chemical properties. The magnetic moments of a muon and an unpaired electron present in these atoms interact to give rise to the precession of a muon spin with a frequency characteristic of a muonium (μ^+e^-). In the experiments of Refs [65, 66] utilizing a beam of spin-polarized muons, this precession was discovered on the basis of the MSR (muon spin relaxation) technique [7, 67]. In similar experiments [68] it was observed that the addition of xenon to argon was not attended with any changes in comparison with pure argon. However, the MSR signal corresponding to the ($_\mu$F) atom vanished on addition of xenon to neon. According to Ref. [69], XeF molecules are initially produced in the latter case (in what follows the index μ on fluorine is sometimes omitted). Similar NeF molecules do not exist and are therefore not produced. Next there occurs a dissociative attachment

$$XeF + e \rightarrow Xe + F^- \tag{14}$$

involving the secondary δ electrons that the muon has knocked out from atoms in its slowing-down. For pressures of ~ 40 bar typical for the above experiments, the potential energy of the thermalized δ electrons in the field of a track is high in comparison with their thermal energies, and therefore the regular drift in the electric field of a muon track prevails over chaotic diffusion which expels the electrons from the track. As a result, the δ electrons recombine with positive ions and the track gradually vanishes. Applying a sufficiently strong external electric field results in a significant increase of the lifetime of the charges in the target [70] because the electric field makes the positive and negative charges recede from each other.

Therefore, instead of ($_\mu$F) in experiments with a Ne|Xe mixture ($_\mu F^-$) ions are produced, in which the total electron spin is zero and hence the precession of a muon spin does not occur. Owing to the smallness of the binding energies, the XeCl and ArCl molecules are unstable at room temperatures, and so no changes were observed in the experiments involving Ar|Xe [69].

We note that this model is rather realistic despite its seeming complexity. Its most questionable link — the phenomenon of recombination of δ electrons on their own track — has long been known in radiation chemistry [71]. This phenomenon was independently discovered and put to use [72] in measuring the muons-to-^{3}He-nuclei attachment coefficient for the reactions of muonic catalysis in deuterium. In this experiment, the muons brought to rest in deuterium formed $dd\mu$ mesomolecules, in which DD fusion reactions occurred and fast ^{3}He nuclei originated with an energy of 0.8 MeV. It was necessary to determine the probability ω that a muon is captured by this nucleus to one of the bound states (sticking coefficient), i.e. the probability that a $\mu\,^3$He mesoion appears with a charge $+e$ rather than a ^{3}He nucleus with a charge $+2e$. Since the energies of these particles are the same, in a low-density gas, where tracks are broad and electrons do not recombine, they will produce the same number of ion pairs and will be indistinguishable, because the charge collected will be the same. However, the ^{3}He track is shorter and the ion number density in it is higher. It was discovered that a recombination in this track commenced for a deuterium pressure of ~ 100 bar, and therefore the electrical pulses obtained from the ^{3}He and mesoion tracks in the ionization chamber at the specified (and higher pressures) would be different, which allowed the measurement of the ω.

Ion-molecular reactions are characterized by the scale of length $\sim 10^{-7}$ cm and in this sense are macroscopic in comparison with the processes involving EAs, whose intrinsic scale of length is $\sim 10^{-11}$ cm. Nevertheless, the former have a significant effect on the rates of the latter in specific cases [73, 74]. The reason is that an EA finds its way, due to ion-molecular reactions, into that region of a cluster where the electron density is low or, conversely, is high. This changes the role of those microscopic mesoatomic processes whose rate is controlled by this electron density, for instance, the Auger transitions (13).

There is a contradiction of long standing which may be referred to as 'the muonic helium puzzle', in which an important role is played by ion-molecular reactions [75, 76]. Precision measurements of the atomic hydrogen spectrum have long been conducted with the aim of verifying quantum electrodynamics (QED). In this case, the main calculation errors are introduced by the correction to the electron energy levels, arising from the finite dimensions of a proton. A realistic way to determine this correction involves measuring the 2s- and 2p-energy level difference Δ in EAs $(p\mu)$ and $(\alpha\mu)$ [77 – 79]. The major contribution ($\sim 90\%$) to Δ is made by the effect of e^+e^- vacuum polarization, and $\sim 10\%$ by the corrections arising from the finite dimension of charge distributions in nuclei. There are several other, less significant, corrections which can be measured (the Lamb shift, etc.). That is why the measurements of EA spectra are of interest in themselves. The long-standing interest in these atoms is also related to the quest for the effects of weak neutral hadronic currents [80, 81] and, more recently, to the precision measurements of the characteristics of these currents [82]. To measure Δ in muonic helium, the target in the experiments of Refs [83 – 85] was irradiated by laser pulses with a wavelength λ close to the theoretical value of the resonance wavelength

$$\lambda_{\rm th} = 812.2 \pm 1.5 \text{ nm}$$

(see Ref. [86]). The laser radiation induced the $2s \to 2p$ transitions in $\mu\,{}^4$He, following which these EAs emitted X-ray photons arising from the K_α transition ($2p \to 1s$), which were detected. To separate the laser-induced K_α photons from those emitted in the course of cascade transitions, the laser pulse was initiated a sufficiently long time (~ 1 μs) — the delay time — after the incoming signal that a muon had flown into the target. In these experiments, a resonance was observed at the wavelength

$$\lambda = 811.7 \pm 1.5 \text{ nm} \qquad (15)$$

consistent with the theoretical value of $\lambda_{\rm th}$. Earlier [87, 88], for delay times $\geqslant 1$ μs the same authors observed electrons arising from the decay of muons, and X-ray photons arising from the K_α and two-photon $2s \to 1s$ transitions. They found that the time spectra of these particles (the frequency of the photon appearance as a function of the delay time t) were, for a helium pressure p from 7 to 50 bar, described with a good accuracy by a single exponential term, $\exp(-\lambda_0 t)$, where

$$\lambda_0 = \frac{1}{\tau_\mu} \approx 0.5 \times 10^6 \text{ s}^{-1}\,.$$

Whence the authors drew the conclusion that the lifetime of the metastable 2s state slightly depends on the pressure p; its decay is primarily dictated by muon decay, while the quenching rate $\lambda_{\rm Q}$ of the metastable 2s state is low.

Then contradictions began to accumulate. Carboni and Pitzurra [89], Mueller et al. [90], and Cohen and Bardsley [91] noticed that muonic helium loses the last electron in Auger processes (13) in the cascade to become an $(\alpha\mu)^+$ ion, where $\alpha \equiv {}^4$He. Owing to the adiabaticity of nuclear motion and the large difference between the ionization potentials of helium and hydrogen, this ion cannot capture an electron from other helium atoms, and so the authors assumed it to remain free. But then radiative transitions are induced: an $(\alpha\mu)^+_{2s}$ ion periodically finds itself in intraatomic electric fields which induce in it an admixture of the 2p state to give rise to the $2p \to 1s$ radiative transition. For $p \sim 50$ bar, the resultant rate of transition to the 1s state is $\sim 10^7$ s^{-1}, which contradicts the above conclusion of the smallness of $\lambda_{\rm Q}$. To resolve the contradiction, an assumption was made in Refs [88, 89] that an $(\alpha\mu)^+$ ion forms a cluster — an Atkins sphere [257]. The idea was that this ion occupies the central position in the cluster and the electric field at the $(\alpha\mu)^+$ ion vanishes owing to the symmetry, and hence the radiative transitions are no more induced. Cohen [92] and in greater detail Men'shikov et al. [93] showed that the above transitions in clusters are sped up rather than hindered. The reason is that the electric field at $(\alpha\mu)$ is zero only for the equilibrium position of the cluster nuclei. Nuclear vibrations, which are bound to occur even as $T \to 0$, give rise to an electric field that destroys the 2s states. So, with increasing pressure, the quenching rate $\lambda_{\rm Q}$ of the 2s state first grows linearly and later (for $p \geqslant 5$ bar) becomes constant [93]:

$$\lambda_{\rm Q} \sim 2 \times 10^7 \text{ s}^{-1}\,, \qquad (16)$$

which corresponds to quenching in the cluster produced. This dependence is consistent with the experiments [94, 95]. In the $p < 1$ bar range, one finds

$$\lambda_{\rm Q} = k_1 N + k_2 N^2\,, \qquad (17)$$

where $k_2 = (5.9 \pm 0.8) \times 10^{-32}$ cm^6 s^{-1} [94]. The second term in expression (17) describes the cluster formation in the reaction

$$(\alpha\mu)_{2s} + \text{He} + \text{He} \to \left[(\alpha\mu)\text{He}\right]^+ + \text{He}\,, \qquad (18)$$

since the magnitude of the k_2 reaction rate agrees with a figure of 6×10^{-32} cm^6 s^{-1} [96] measured for the reaction

$$\text{He}^+ + 2\text{He} \to \text{He}_2^+ + \text{He}\,.$$

All these results for $\lambda_{\rm Q}$ run counter to the conclusions reached in the experiments of Refs [87, 88]. The picture became still less clear when Hauser et al. [76] staged an experiment for a low pressure $p = 0.04$ bar, which was possible by the application of a magnetic trap for muons. According to expression (17), $\lambda_{\rm Q}$ should be low for the above pressures, and therefore a resonance should be observed when the experiments of Refs [83 – 85] are repeated with a laser of wavelength (15). However, resonances were discovered neither at a wavelength (15) nor in the immediate vicinity $811.4 < \lambda < 812$ nm. This brings up the question: which resonance did the Zavattini group observe [83 – 85]? One possible explanation is offered in the Conclusions.

The examples considered above show that the description of cascade transitions for $Z > 1$ is severely complicated by

ion-molecular and other chemical reactions. The details of a cascade depend in this case on the material molecular structure. Investigations into these phenomena make up a branch in their own right in the physics of EAs [5, 7, 9, 99] — meson chemistry — which will not be discussed here. Certain of the properties, however, are common to all materials. Unlike the case with $Z = 1$, EAs (or exotic molecules) for $Z > 1$ are thermalized because the cross section for the elastic scattering of these EAs from material atoms is large ($\sim 10^{-15}$ cm^2). This is so because such EAs are either neutrals, in which case they have an electron shell, or ions.

Most probable are radiative transitions (5) with the largest variation of n:

$$n' = \min = l' + 1 .$$

Auger transitions (3) are of significance in the higher levels, where they should be multiquantum ($\Delta n < -1$) according to the energy conservation law. Considering that the dipole transitions with $\Delta l = l' - l = -1$ are most probable in both cases [100], we conclude that $|\Delta n| \geqslant |\Delta l|$. Hence it follows that the cascade transitions in the lower levels of atoms with $Z > 1$ proceed primarily through the $l = n - 1$ circular states. This is yet another common property for $Z > 1$. For a purely radiative cascade, which takes place in the lower levels or in all the levels for a low-density material, this is easiest to verify by invoking classical electrodynamics [101, § 75].

A detailed calculation of the cascade processes in muonic and pionic helium [102] is important for the development of the theory of EAs with $Z > 1$. Numerical integration was performed of the equations of motion of a system comprising 30 helium atoms and one exotic ion $(X\alpha)^+$. The resultant value for the k_2 constant was an order of magnitude lower than the experimental one (17). It may be assumed that this is related to the numerical instabilities of a classical trajectory calculation that were sometimes observed in Ref. [40]. Considering the interest in exotic helium as a subject of investigation, it would be of value to abandon the approximations adopted in Ref. [102] in the subsequent computations. In particular, it is impermissible to neglect the transitions between the (n, l) states, arising from the rotation of the internuclear axis [33] (the fixed field approximation [31]). Nor is it possible to disregard the induced radiative transitions, which are of significance, as noted above.

2.3 Muonic atoms

The first to be discovered were muonic EAs [3], and the experiments performed on them were greatest in number. The lifetime of muonic atoms (MAs) is determined by the weak interaction and is therefore large (on the atomic scale) for all bound states of a muon. This property makes muons a good tool for studying nuclear properties (see the previously cited reviews). Measurements on the energy of the X-ray photons emitted in cascade transitions made it possible to find the shifts of MA energy levels, arising from the finite nuclear dimensions, and to determine the charge distribution in heavy nuclei (in light nuclei, experiments on electron scattering yield more precise results). The quadrupole moments of nonspherical nuclei were found from the hyperfine splitting of MA levels (see, e.g., Ref. [103]).

The interaction of a muon with internal nuclear degrees of freedom was studied in several experiments. Leon [104] predicted the effect of resonance excitation of nuclei by a cascading muon. The energies of specific transitions may prove to be close to the nuclear excitation energy. In this case, a muon makes a nonradiative transition to a lower energy level with a simultaneous excitation of the nucleus, and the latter transfers this excitation to an electron (internal conversion). Given another isotope of this nucleus, its excitation spectrum is quite different and the above resonance does not occur. This implies that the intensity of a given muonic transition in the cascade X-ray spectrum will be lower for the initial atom than for its isotope. This resonance effect was observed, for instance, in Ref. [105] for the ^{112}Cd and ^{114}Cd isotope pair.

Wheeler [106] discussed the possibility of a muon-induced fission reaction. By the first mechanism, a muon reaches the 1s state and is therefrom captured by the nucleus in $\sim 10^{-7}$ s due to the weak interaction. With a certain probability there occurs a simultaneous excitation of the nucleus, followed by its fission. By the second mechanism, this excitation occurs in the course of the muon cascade transitions. This phenomenon was discovered in Refs [107, 108] (an extensive list of references may be found in Ref. [109]).

The study on the phenomenon of muonic catalysis of nuclear fusion reactions, predicted in Refs [110, 111] and later discovered experimentally [112], has been pursued for 50 years. This phenomenon was comprehensively discussed in the scientific literature (see Refs [4, 14–16]), and we will take only a brief look at it. A muon brought to rest in a deuterium–tritium mixture (or in a ternary H|D|T mixture) experiences cascading and finally ends up as a constituent of muonic tμ atoms. These atoms collide with D_2 and DT molecules to form dtμ mesomolecules whose nuclei, within $\sim 10^{-12}$ s, enter into the DT synthesis reaction

$$\mathrm{dt}\mu \text{ —} \left| \begin{array}{ll} \longrightarrow {}^4\mathrm{He} + \mathrm{n} + \mu , & (19) \\ \longrightarrow \mu\, {}^4\mathrm{He} + \mathrm{n} . & (20) \end{array} \right.$$

This is one cycle of muonic catalysis, and it proceeds in a time $\tau_c \sim 10^{-8}$ s. A muon is released in reaction (19) to accomplish a new cycle. In reaction (20) which occurs with a probability $\omega_s \sim 0.005$ (the muon sticking coefficient), a muon is picked up by an α particle and dies as a constituent of an EA $\mu\,{}^4$He. The average number of DT fusion cycles catalyzed by a single muon is

$$X_c = (\omega_s + \lambda_0 \tau_c)^{-1} \sim 100 . \qquad (21)$$

The application of muonic catalysis to energy production is hardly possible, because the conditions required in this case are extremely rigorous and unacceptable from safety considerations:

$T \sim 600$ K, $p \sim 1000$ bar,

tritium mass $M_t \sim 1$ kg,

1-GeV proton beam, and $I \sim 10$ mA.

In our view, more realistic is the implementation of a research-oriented source of neutrons with an energy of 14 MeV and an intensity of $\sim 10^{14}$ neutrons per second, operating in less stringent conditions

$T \sim 400$ K, $p \sim 50$ bar,

$M_t \sim 0.1$ kg, and $I \sim 0.1$ mA.

It would not be out of place to add that, despite the optimism retained as regards the feasibility of using fusion reactions for energy production [113], fission-based energy production has hardly any alternative [114–119]. At present, investigations into muonic catalysis focus on the ternary

H|D|T mixture [18 – 21]. Improving muon beams [21] would supposedly allow staging experiments in new conditions, for instance, in a plasma [15] where the number of cycles of muonic catalysis is higher by an order of magnitude.

The quest for rare reactions involving muons makes up an important class of present-day experiments. It covers processes with lepton nonconservation [120]

$$\mu \to eee\,, \quad \mu \to e\gamma\,, \quad \mu A \to eA'\,. \tag{22}$$

Discovering these processes or establishing the upper bounds for their relative probabilities would allow a step beyond the limits of the standard electroweak model and the construction of a more sophisticated theory. Raising the intensity of a muon beam is vitally important for these experiments. Such projects have been proposed, for example, at the Moscow meson factory [121] and at the National High-Energy Physics Laboratory — KEK, Japan [122].

2.4 Hadronic atoms

The investigation of hadronic atoms (HAs) yields important information on the properties of a nucleus and hadrons themselves as well as the nature of their interaction with nucleons [6, 10 – 13, 122 – 124]. Energy measurements of the X-ray photons emitted in hadron transitions between the Rydberg states culminated in the determination of the masses and magnetic moments of negative kaons and antiprotons, which are the most precise to date [125 – 129]. Experiments with HAs allowed the determination of the spins and the parities of certain of the hadrons [7 – 10].

The products of the hadron reactions with neutrons and protons are different, and so the measurements of X-ray transition widths and branching ratios give an idea of the distributions of protons and neutrons in nuclei [130 – 132]. Owing to the Coulomb barrier, the proton density falls off at the periphery of a nucleus ('nuclear stratosphere') faster than the neutron density (neutron halo), which is confirmed by experiments. The absorption of hadrons in heavy nuclei occurs at precisely the periphery due to the action of two effects. The first one lies in the fact that the probability of a hadron penetration to the center of a nucleus is low owing to strong absorption by the surface. The second one arises due to the action of centrifugal forces significant for the circular states $l = n - 1$, in which hadrons primarily find themselves during cascading.

Experiments on HAs of hydrogen isotopes are of special value, for they yield direct information on the low-energy interaction of hadrons with nucleons, not complicated by multiparticle effects [123]. The measurements of X-ray energies yield the widths Γ and shifts ΔE of the 1s level of an HA, caused by the strong hadron – nucleus interaction. According to the theory [133, 134], these quantities are directly proportional respectively to the imaginary (a'') and real (a') parts of the scattering length a of hadrons by nucleons (more precisely, a specific linear combination of the scattering lengths a_I for the total isospin values $I = 0$ and $I = 1$). For a long time there existed a contradiction between the data on kaonic hydrogen (the kaonic hydrogen puzzle): the a' values determined from the scattering of K^- by p and from the ΔE measurements were opposite in sign [12, 13]. This contradiction was eliminated in Ref. [52] — it was presumably a consequence of the strong background in early experiments on kaonic hydrogen (this issue is discussed in Ref. [135]). The data of work [52] will be refined in the DEAR experiment on the DAΦNE facility [30]. Also planned are measurements of the admixture of virtual $S\bar{S}$ quark pairs to a proton, which significantly affects the interaction with kaons also incorporating strange quarks.

As the nuclear charge Z increases, the outer dimension of the lower 1s state of an HA becomes comparable with the nucleus dimension. On the face of it, the nuclear width of such a level should be large:

$$\Gamma \sim n_N\, v_H\, \sigma_{HN} \sim 10 \text{ MeV}\,,$$

where n_N is the nucleon number density, v_H is the hadron velocity in the nucleus, and σ_{HN} the total hadron – nucleon interaction cross section. In any event, Γ will be comparable with the spacing $\Delta\varepsilon$ between the neighboring levels. This implies the absence of deep bound states, because the hadron lifetime at these levels would be comparable with the orbital period. A numerical solution of the Klein – Gordon equation in which the pion – nucleus interaction was taken in the optical potential approximation showed, however (see Refs [136, 137]), that the 1s-level width in pionic atoms is small for any Z:

$$\frac{\Gamma}{\Delta\varepsilon} \sim 0.05\,.$$

The physical cause of the smallness of Γ is quite simple. It is known from optics [138] that a strongly absorbing material (with $\varepsilon'' \gg 1$) also exhibits a high reflectivity. Metals are an example. For the same reason, a pion is forced out from the nucleus, with the effect that the resultant absorption takes place only in a thin layer at the surface and drops sharply. This situation resembles the wave damping in a high-Q resonator.

Owing to nuclear absorption, only a small fraction of pions reaches the 1s state as a result of cascading. That is why a direct mechanism for the population of deep bound pion states was proposed to discover them (see Refs [137, 139]) — the charge exchange reaction

$$n \to p + \pi^-$$

occurring in the nuclear field; for instance, one observes

$$n + {}^{208}Pb \to (\pi^- {}^{208}Pb)_{2p} + p\,, \tag{23}$$

$$d + {}^{208}Pb \to (\pi^- {}^{208}Pb)_{2p} + {}^3He\,. \tag{24}$$

According to the calculations [140] performed in the momentum approximation, the probability that a pion is formed is highest for the 2p state in the nuclear field. Reaction (23) was studied [141] with a beam of neutrons with an energy $E = 408$ MeV, obtained at the TRIUMF accelerator in the reaction

$$p + {}^7Li \to n + (\text{anything})\,.$$

By the energy conservation law, a resonance should be observed for a proton energy

$$E_p = E_n - m_\pi c^2 + |\varepsilon_{2p}|\,,$$

where ε_{2p} is the pion binding energy in the nuclear field. However, it was not observed owing to a strong background. Eventually, deep pion states were discovered in studies of reaction (24) (see Ref. [142]).

In Section 2.2.2, 'the muonic helium puzzle' was discussed. It turns out that there are two more helium puzzles: the 'kaonic' and 'antiprotonic' ones. The latter is in fact the subject of our review (see Section 2.6 and further). Here, we will enlarge on 'the kaonic puzzle'.

The theoretical values of the widths Γ_{2p} of a kaon capture by nucleus and the 2p energy level shift ΔE_{2p} in a $(K^-{}^4He)$ atom, caused by the interaction with a nucleus, are as follows (in eV):

$$\Gamma_{2p} = 2\,, \quad \Delta E_{2p} = -0.2\ [143]\,;$$

$$\Gamma_{2p} = 3.3\,, \quad \Delta E_{2p} = -0.44\ [144]\,. \tag{25}$$

The calculations were carried out in the optical potential approximation. The averaged experimental data (in eV) are [143, 145, 146]

$$\Gamma_{2p} = 55 \pm 34\,, \quad \Delta E_{2p} = -43 \pm 8\,. \tag{26}$$

The disagreement between the data (25) and (26) is the heart of the 'kaonic puzzle'. Following paper [144], we estimate these values under the assumption that the main contribution to them is made by closely located hyperon resonances. These are $\Lambda(1405)$ and $\Sigma(1385)$ [147] whose total widths are 50 MeV and 35 MeV, respectively. The total mass of a kaon and a nucleon equals

$$m = m_K + m_N \approx 1430\ \text{MeV}\,,$$

i.e. the typical energy transferred in kaon–nucleon reactions is high ($\delta E \sim \Gamma \sim 40$ MeV), and a kaon can be assumed to react with every nucleon independently. The parity P of the system (K^-N) in the p state is $+1$, the isotopic spin $I = 0$ or $I = 1$, the strangeness $S = -1$, and the total angular momentum $J = 1/2$ or $J = 3/2$. The strong interaction conserves these quantities. A Λ hyperon does not suit in parity, and therefore the kaon capture occurs via the $\Sigma(1385)$ resonance with the quantum numbers

$$I = 1\,, \quad J = \frac{3}{2}\,, \quad P = 1\,, \quad S = -1\,.$$

To describe the decay of a $(K^-\alpha)$ EA in the 2p state, we take advantage of the Fano theory of resonance reactions [148, 149]. A kaon is absorbed by a nucleon to produce a Σ resonance, which either decays once again into a kaon and a nucleon (the elastic channel) or into $\Lambda + \pi$ (the inelastic channel). The system state vector is of the form

$$|\psi\rangle = C_0|\,\mathrm{EA}\,\rangle + C_1|\,\Sigma\,\rangle + \sum_{\mathbf{K}} C_{\mathbf{K}}|\,\mathbf{K}\,\rangle\,, \tag{27}$$

where $|\mathrm{EA}\rangle$, $|\,\Sigma\,\rangle$, and $|\,\mathbf{K}\,\rangle$ are the respective vectors of state of the $(K^-\alpha)$ atom, the Σ resonance, and the particles $\Lambda + \pi$ flying apart with a momentum $\mathbf{K}$ in the center-of-mass system (c.m.s.). All these states are not the eigenvectors of the total Hamiltonian, and therefore transitions occur between them. We assume that the reactions proceeding via the Σ resonance are most probable. Then, when projecting the equation of motion ($\hbar = 1$)

$$\mathrm{i}\,\frac{\partial|\,\psi\,\rangle}{\partial t} = \widehat{H}\,|\psi\rangle$$

onto the above-specified vectors of state, we may neglect the $(K^-N)-(\Lambda\pi)$ channel coupling and also the off-diagonal matrix elements $\langle\mathbf{K}'|H|\mathbf{K}\rangle$ (see Refs [148, 149]). We are led to the following equations for the probability amplitudes:

$$\begin{aligned}
&\mathrm{i}\dot{C}_0 = VC_1\,,\\
&\mathrm{i}\dot{C}_1 = VC_0 - \varepsilon C_1 + \sum_{\mathbf{K}} V_{\mathbf{K}} C_{\mathbf{K}}\,,\\
&\mathrm{i}\dot{C}_{\mathbf{K}} = V^*_{\mathbf{K}} C_1 + (-\Delta + T_K)a_{\mathbf{K}}\,.
\end{aligned} \tag{28}$$

Here, the following designations are used:

$$V = \langle\Sigma|\widehat{H}\,|\,\mathrm{EA}\rangle\,, \quad V_{\mathbf{K}} = \langle\,\Sigma|\widehat{H}\,|\,\mathbf{K}\,\rangle\,,$$

$$\Delta = (m_K + m_N - m_\Lambda - m_\pi)c^2 = 170\ \text{MeV}\,,$$

$$\varepsilon = (m_K + m_N - m_\Sigma)c^2 = 45\ \text{MeV}\,,$$

and T_K is the $\Lambda + \pi$ kinetic energy in the c.m.s. For a quasi-stationary state with an energy E, the amplitudes are proportional to $\exp(-\mathrm{i}Et)$. Then, from Eqns (28) there follows a dispersion relation

$$\frac{V^2}{E} - E - \varepsilon - \sum_{\mathbf{K}} \frac{V_K^2}{E + \Delta - T_K} = 0\,, \tag{29}$$

where $V_K^2 \equiv |V_{\mathbf{K}}|^2$. The energy of an unperturbed $(K^-\alpha)_{2p}$ atom is taken as zero. Assuming the widths of the states to be small:

$$E = \mathrm{Re}\,E - \frac{\mathrm{i}}{2}\,\Gamma \approx \mathrm{Re}\,E - \mathrm{i}0\,,$$

relationship (29) is rearranged to give

$$\frac{V^2}{E} - E - \bar{\varepsilon} - \frac{\mathrm{i}}{2}\,\Gamma = 0\,, \tag{30}$$

where Γ is the total width of a Σ resonance, and

$$\bar{\varepsilon} = \varepsilon + \delta\varepsilon\,, \qquad \delta\varepsilon = \sum_{\mathbf{K}} V_K^2\, P\!\left(\frac{1}{E + \Delta - T_K}\right)$$

is a correction to the Σ-resonance mass arising from virtual decays into $\Lambda\pi$. The root of Eqn (30) for high energies

$$E_2 \approx -\bar{\varepsilon} - \frac{\mathrm{i}}{2}\,\Gamma$$

describes the Σ resonance, and the root for low energies

$$E_1 \approx \frac{V^2}{\bar{\varepsilon} + (\mathrm{i}/2)\,\Gamma} \tag{31}$$

corresponds to $(K^-\alpha)_{2p}$.

Within the approximation of an optical potential $U(r)$ adopted in Refs [143, 144], the atomic energy in the first order of the perturbation theory is given by

$$E_1' \approx \int \varphi^2(r)\,U(r)\,\mathrm{d}^3 r \sim \varphi_0 J_0\,. \tag{32}$$

Here,

$$J_0 = \int U(r)\varphi(r)\,\mathrm{d}^3 r\,,$$

$$\varphi_0 \equiv \varphi(r_0) \sim \frac{1}{15}\,\frac{r_0}{a_K^{5/2}}$$

are the values of the kaon wave function (WF) $\varphi(\mathbf{r})$ at the boundary of a helium nucleus, $r = r_0 \approx 1.5$ fm, $a_K = 1/m_K$ a.u.

The matrix element V assumes the form

$$V = \int \phi(r)\widehat{H}\varphi(r)\,\mathrm{d}^3r \sim \int \phi(r)U(r)\varphi(r)\,\mathrm{d}^3r \sim \phi_0 J_0\,, \quad (33)$$

where $\phi_0 \sim V_0^{-1/2}$ is the characteristic value of the WF $\phi(r)$ of a Σ resonance, which is localized in the volume V_0 of a nucleus. From expressions (32) and (33) we obtain

$$\frac{V}{E_1'} \sim \frac{\varphi_0}{\phi_0} \sim 10\left(\frac{a_\mathrm{K}}{r_0}\right)^{5/2} \sim 5\times 10^4\,. \quad (34)$$

In view of the values (25), $E_1' \sim 1$ eV, and therefore $V \sim 5\times 10^4$ eV. Whence and from expression (31) we obtain

$$|\Delta E_{2\mathrm{p}}| \sim \Gamma_{2\mathrm{p}} \sim \frac{V^2}{\Gamma} \sim 100\ \mathrm{eV}\,,$$

which nicely agrees with data (26).

From expressions (31) and (34) it follows that

$$\frac{E_1}{E_1'} \sim \frac{|U_0|}{\Gamma} \sim 10\,, \quad (35)$$

where the estimate $|U_0| \sim 300$ eV for the $\mathrm{K}^- - {}^4\mathrm{He}$ optical potential was borrowed from Ref. [150].

The reason why the data (25) and (26) disagree becomes clear from the form of formula (35): the reason lies with the smallness of Γ. Therefore, the optical potential approximation does not take into account the resonance nature of the interaction between a kaon and nucleons, which arises due to the proximity of the energy E to the Σ resonance and the relative smallness of its width.

In work [144], the matrix elements V and V_K were assumed to be zero and account was taken of only the direct coupling between the channels (K N) and ($\Lambda\pi$). As regards the physical meaning, this is inconsistent with the Fano theory and corresponds to the nonresonant reaction $\mathrm{K}+\mathrm{N}\to\Lambda+\pi$ which, as shown above, has a low probability in comparison with the resonance one.

According to Refs [31, 34, 35, 40], the nuclear width $\Gamma_{2\mathrm{p}}$ of the 2p state in kaonic hydrogen $(\mathrm{K}^-\mathrm{p})_{2\mathrm{p}}$ is of the order of 5×10^{-4} eV. This follows both from the analysis of the measured fraction of nuclear captures happening in the p states [31] and from a comparison of the theoretical [34, 35, 40] and experimental [52] values of the X-ray K_α-photon yield Y. In our view, the smallness of a proton in comparison with a helium nucleus is, roughly speaking, the reason why $\Gamma_{2\mathrm{p}}$ for hydrogen is small in comparison with corresponding quantity for helium. In both atoms, the WF of a kaon decreases, owing to centrifugal forces, as it approaches the nucleus up to its boundary r_0. Inside the nucleus it remains approximately constant. Because the r_0' dimension for a proton is small, the matrix element V for kaonic hydrogen is much smaller than for helium.

Another plausible explanation for the anomalous width of $(\mathrm{K}^-\alpha)_{2\mathrm{p}}$ is as follows. Inside the helium nucleus, a kaon is rescattered by nucleons and therefore interacts with them not only in the p-wave, but also in the s-wave. In this case, the effect of smallness of the kaon WF at a nucleon, arising from the centrifugal forces, is absent. For $(\mathrm{K}^-\mathrm{p})_{2\mathrm{p}}$, the interaction takes place only in the p-wave. Because the effective proton dimension r_0' is small in comparison with the helium nucleus size r_0, the matrix element V for a proton is substantially lower [by a factor of $\sim (r_0/r_0')^3$] than for helium, and therefore

$$\frac{\Gamma_{2\mathrm{p}}(\mathrm{H})}{\Gamma_{2\mathrm{p}}(\mathrm{He})} \sim \left(\frac{r_0'}{r_0}\right)^6 \ll 1\,.$$

Both models rest on the assumption that the key role is played by the resonance kaon capture occurring in the direct kaon – nucleon interaction, when the kaon residence time inside the nucleus is of the order of the flight time. These mechanisms will be referred to as two-particle ones. However, this assumption leads to a contradiction. From the data for kaonic helium (26) and the two-particle mechanism it follows that the nuclear width of the 2p state in kaonic deuterium should be large (of the order of 10 eV). On the other hand, the width of the 2p state of kaonic deuterium was estimated at 0.004 eV [40] on the basis of the same mechanism, taking advantage of the measured width of the 1s state in kaonic protium [52]. The smallness of the width for deuterium implies that 'the kaonic helium puzzle' cannot be explained by the binary kaon – nucleons interaction — this is a multiparticle effect. The only plausible explanation is that the 'helium nucleus + kaon' system should have a narrow state with a low binding energy, the state being multiparticle in nature similar to neutron nuclear resonance [194]. In any case, this invites further investigation, for instance, measurements of the width of the 2p state in kaonic deuterium.

2.5 Experiments on antihydrogen

The simplest compound antinuclei were obtained by the L Lederman (antideuterium, 1965, USA) and Yu D Prokoshkin (antihelium-3, 1970, Protvino, Moscow region, Russia) groups. It was not until recently that it was possible to obtain and detect 11 atoms of antihydrogen $\overline{\mathrm{H}} = (\bar{\mathrm{p}}\mathrm{e}^+)$ [151] on the LEAR facility. At present, experiments to study the properties of antihydrogen are planned [122, 152, 153] or have been commenced [154, 155] in several laboratories. The schemes of these experiments are considered in detail below for the reader to gain an impression of the current state of the art in the experimental research.

The most important objectives of these experiments are the verification of the *CPT* invariance (which was first proposed in Ref. [156]) and the weak equivalence principle [157, 158]. To verify the *CPT* invariance (the physical significance of this symmetry is outlined in the Appendix, Section I), it is supposed to produce ~ 1000 $\overline{\mathrm{H}}$ atoms in a special magnetic trap and correlate their spectrum with that of hydrogen atoms. Comparing the $2\mathrm{s}_{1/2}\to 1\mathrm{s}_{1/2}$ transition energies would allow a verification of the equality among electron and positron charges with a precision of $\sim 10^{-11}$, and comparing the hyperfine splitting in the ground 1s state the equality among the magnetic moments of p and $\bar{\mathrm{p}}$ with a precision of $\sim 10^{-8}$. According to the Lüders – Pauli theorem [159], the equality between these quantities follows from the fulfillment of *CPT* invariance.

The atoms will be confined owing to their magnetic moments in an Ioffe plasma trap [161] type device [160]. At the center of such a trap is a minimum of the magnetic field H, and therefore the potential energy $U = M_\mathrm{B}H$ has a minimum for $\overline{\mathrm{H}}$ atoms with a positron spin opposed to the field. For $H \sim 1$ T, the typical temperature of the confined atoms is $T \sim U \sim 1$ K. To capture atoms in the trap and subsequently cool them, recourse will be made to the laser cooling technique [162 – 167] which in principle enables the tempera-

ture to be lowered to $\sim 10^{-3}$ K. These procedures were partly elaborated in Refs [168, 169]. The capture is facilitated due to the fact that $\overline{\mathrm{H}}$ atoms are produced in the region of a strong magnetic field [160]. To measure the frequency ω_0 of the $1s_{1/2} \to 2s_{1/2}$ transition in $\overline{\mathrm{H}}$ atoms, advantage will be taken of the method of nonlinear Doppler-free two-photon laser spectroscopy [171, 172], which was validly used to measure this frequency in H atoms [173] with an accuracy of $\sim 10^{-12}$. Conventional two-photon laser spectroscopy involves transitions arising in the second order of the perturbation theory in the interaction of a laser field $\mathbf{E}$ of frequency ω with an atom, $V = \mathbf{dE}(t)$. An atom in the 1s state absorbs a laser photon of frequency $\omega_1 = \omega \approx \omega_0/2$ and simultaneously executes a virtual dipole transition to one of the excited states. Whence it next makes a dipole transition to the 2s state, simultaneously absorbing a photon of frequency $\omega_2 = \omega \approx \omega_0/2$. In relation to the laser frequency ω, the resultant absorption refers to a resonance of width

$$\Delta\omega = \max(\Delta\omega_{2s}, \omega_D)\,, \tag{36}$$

where $\Delta\omega_{2s} = 7\ \mathrm{s}^{-1}$ is the natural width of the 2s level, and

$$\Delta\omega_{2s} \sim \frac{v_T}{c}\,\omega_0$$

is the Doppler width. In the experiments of Ref. [173], measurements were taken of the number of atoms transferred to the 2s state per unit time. Under external fields, an admixture of the 2p state is induced in them, with the result that they drop back to the 1s state with the emission of a photon to be recorded.

The Doppler width is very large even for $T \sim 1$ K: $\Delta\omega_D/\omega_0 \sim 10^{-6}$. A way out of the impasse is opened up by Doppler-free spectroscopy [171, 172]. A laser beam passes forward through a gas along the x-axis (beam 1) and, on reflection from a mirror, returns to pass through the gas for the second time (beam 2). Therefore, the gas resides in the field of a standing laser wave. To analyze the resultant absorption, it is best to pass to the rest frame of an atom. In the rest frame of an atom with a velocity v_z, beam 1 has a frequency $\omega_1 \approx \omega - kv_z$, and beam 2 a frequency $\omega_2 \approx \omega + kv_z$, where $k = 2\pi c/\omega$ is the wave vector. In the virtual transition from the 1s state of the atom, photon 1 is absorbed from the beam 1, and in the reverse transition to the 2s state, photon 2. As a consequence, the Doppler shift linear in v_z is compensated for and the width $\Delta\omega_{2s}$ is determined by the quadratic Doppler effect:

$$\frac{\Delta\omega}{\omega_0} = \frac{\Delta\omega_D}{\omega_0} \sim \left(\frac{v_T}{c}\right)^2,$$

which is $\sim 10^{-12}$ for $T \sim 1$ K. The width of a transition in which both photons are absorbed from one and the same beam is determined by a value of v_T/c as before, and therefore the resultant absorption curve exhibits a narrow resonance against a broad background. It is evident that the laser cooling of the atoms entrapped would allow a significant improvement of ω measurements.

The production of $\overline{\mathrm{H}}$ atoms in an Ioffe trap is in essence the final stage of the ATRAP and ATHENA experiments. It is preceded by several preliminary stages some of which have already been elaborated [174, 175]. The antiprotons and the positrons required for the production of $\overline{\mathrm{H}}$ atoms are accumulated in two coaxial Penning traps [176–179]. A magnetic field is induced along the common axis of the traps, which is nearly uniform inside each of them. At the ends of each trap are two electrodes in the form of paraboloids of rotation. A voltage is applied to them, which is required for electrostatic blocking of the particles under confinement. Drilled along the common axis of the electrodes are the openings required for the injection of particles into the trap. The electric field lines run from these electrodes to a annular electrode at a voltage of opposite sign, which surrounds the trap. A bunch of antiprotons with an initial energy of 5.8 MeV is first decelerated in a material layer to energies less than 3 keV and then captured in the region with a nonstationary electric potential (for details, see Refs [180, 181]). Following the bunch cooling by electrons, proposed in the projects, some of the antiprotons find themselves in the Penning trap. Next, owing to the ohmic relaxation of the Foucault currents induced by the antiprotons in the trap electrodes [182, 183], the antiprotons are cooled down to the electrode temperature (liquid helium) in a time of ~ 100 s. Here an interesting, in our view, problem arises which concerns the development of collective cyclotron instabilities of the antiprotons in a trap, thus reducing the relaxation time (speculation on this possibility may be found in Ref. [183]). The relaxation process is in this case similar to the superradiance at the cyclotron frequency [184], which is conceivably the principal energy loss mechanism in tokamaks. Analogous procedures are accomplished on positrons, which are proposed to be obtained from β sources. In the last experiment [174] carried out prior to the shutdown of the LEAR facility, about 10^6 particles were accumulated in both traps.

Eventually, the $\bar{\mathrm{p}}$ and e^+ stored in the coaxial Penning traps are brought into the contact with each other by varying the voltages of the parabolic electrodes. In the contact region, the production of $\overline{\mathrm{H}}$ atoms by recombination occurs. Specifically, the following mechanisms are considered [185]:

stimulated radiative recombination

$$\mathrm{e}^+ + \bar{\mathrm{p}} + N\hbar\omega \to \overline{\mathrm{H}}_n + (N+1)\hbar\omega\,, \tag{37}$$

and three-body recombination

$$\bar{\mathrm{p}} + \mathrm{e}^+ + \mathrm{e}^+ \to \overline{\mathrm{H}}^* + \mathrm{e}^+\,,$$

$$\overline{\mathrm{H}}^* + \mathrm{e}^+ \to \overline{\mathrm{H}} + \mathrm{e}^+\,. \tag{38}$$

In the recombination process (37), n denotes the principal quantum number of the level on which the laser-stimulated positron landing is accomplished. In process (38), the former reaction governs the initial capture of e^+ to a state of $\overline{\mathrm{H}}$ with the binding energy $|\varepsilon| \sim T$. The latter describes the result of multiple collisions of $\overline{\mathrm{H}}^*$ with positrons, with the effect that the atom reaches the low-n states to find itself in the 1s state after a radiative transition.

Following works [186–188], we will analyze processes (37) and (38) in conditions typical of the $\bar{\mathrm{p}}$ and e^+ recombination region in the ATRAP and ATHENA experiments:

$$n_e = 10^8\ \mathrm{s}^{-3}, \quad T = 4.2\ \mathrm{K}\,, \quad H = 3\ \mathrm{T}. \tag{39}$$

Here, n_e is the number density of e^+.

The radius of the Larmor orbit of e^+ (from this point on $\hbar = m_e = e = 1$) is of the order of

$$r_H \sim \frac{v_T}{\omega_H} \sim 500\,, \tag{40}$$

where v_T is the thermal velocity of e^+, and $\omega_H = eH/(m_e c)$ is the positron cyclotron frequency. The radius (40) is small in comparison with the Thomson radius:

$$r_H \ll R_T, \quad R_T = \frac{e^2}{T} \sim 0.7 \times 10^5 . \tag{41}$$

This implies that the positrons are magnetized and move as if along stretched strings. We direct the z-axis along **H**. The potential energy of a positron in a 'string' passing at a distance ρ from $\bar{p}$ is given by

$$U = -\frac{1}{r} = -\frac{1}{\sqrt{\rho^2 + z^2}} . \tag{42}$$

Only the positrons inside the Thomson sphere ($r < R_T$) can recombine with an antiproton, because their potential energy is of the order of the kinetic one ($|U| \sim T$). The number of these positrons is of the order of

$$N^* \sim \frac{4}{3}\pi R_T^3 n_e . \tag{43}$$

In the first stage of recombination, the mechanism of 'replacement collisions' operates [186]. A positron moving in the potential well (42) relaxes in collisions with other positrons and is brought to the bottom ($z = 0$) with a characteristic rate (the reciprocal of the relaxation time)

$$\lambda_{GN} \sim \pi \rho^2 n_e v_T . \tag{44}$$

Replacement collisions occur with the same frequency: a positron residing in a bound state in the 'string' with a parameter ρ is knocked out by another positron moving along the 'string' with the parameter $\rho' \sim \rho$, the incident positron finding itself in the bound state.

According to expression (44), the characteristic value of ρ decreases according to the law

$$\dot{\rho} = -\lambda_{GN}\rho .$$

Hence it is evident that recombination moderates for small ρ. In this region ($\rho \sim \rho_c$), the drift mechanism is 'engaged' [187]. The positrons flying past at long distances ($\rho' \leqslant r_D$)) act on the trapped positron with their electric fields $E \sim 1/\rho'^2$. During the collision time $\tau \sim \rho'/v_T$, it drifts with a velocity

$$v_D = \frac{c(\mathbf{E} \times \mathbf{H})}{H^2}$$

and moves through a distance $\delta\boldsymbol{\rho} \sim \mathbf{v}_D \tau$. Since the $\delta\boldsymbol{\rho}$ quantities are random and small ($|\delta\boldsymbol{\rho}| \ll \rho$), the motion of a trapped positron in $\boldsymbol{\rho}$ is inherently diffusive with a diffusion coefficient

$$D_T = \sqrt{\frac{\pi}{2T}}\,\frac{n_e c^2 \Lambda^2}{H^2} ,$$

where $\Lambda = \ln(T n_e^{-1/3}) \sim 2$ is the Coulomb logarithm of an $e^+\bar{p}$ plasma. A positron is attracted to an antiproton with a force $F = -1/\rho^2$ and therefore drifts to the latter with a velocity $v_D = b_\perp F$, where $b_\perp = D_T/T$ is the mobility.

With the inclusion of the two mechanisms considered, the distance of the recombining positron to the antiproton decreases from $\rho \sim R_T$ to $\rho = 0$ according to the law [188]

$$\dot{\rho} = -\lambda_{GN}\rho - b_\perp \frac{1}{\rho^2} . \tag{45}$$

Hence we obtain the recombination time

$$\tau_r = \int_0^{R_T} \frac{d\rho}{\beta n_e v_T \rho^3 + b_\perp/\rho^2} , \tag{46}$$

where $\beta \sim 1$. From expressions (45) and (46) we find

$$\rho_c = \left(\frac{b_\perp}{\beta n_e v_T}\right)^{1/5} \sim 0.8 \times 10^4 , \tag{47}$$

$$\tau_r \sim \frac{\rho_c^3}{b_\perp} , \tag{48}$$

the main contribution to τ_r being made by distances $\rho \sim \rho_c$. This is just the limiting, slowest (bottle-neck) stage of collisional recombination (38) (see Ref. [188]). The recombination rate $\lambda_{\overline{H}} \sim N^*/\tau_r$ is estimated as

$$\lambda_{\overline{H}} \sim 4\pi b_\perp n_e \left(\frac{R_T}{\rho_c}\right)^3 , \tag{49}$$

where the first factor stands for the rate obtained in Ref. [187]. The rate (49) is $(R_T/\rho_c)^3 \sim 10^3$ times higher than that given in Ref. [187], and by the same factor lower than that arrived at in Ref. [186]. Under the condition (39), it is assessed that

$$\lambda_{\overline{H}} \sim 2 \times 10^4 \ \mathrm{s}^{-1} . \tag{50}$$

We emphasize that the three-body recombination considered above results in the production of antihydrogen in the 1s state. If an $\overline{H}$ atom escapes from the plasma prior to the completion of recombination, it will be ionized by the electric fields of the Penning traps and the resultant e^+ and $\bar{p}$ will return to the plasma. Hence follows a condition imposed on the dimension of the recombination region (plasma):

$$L > \frac{v_a}{\lambda_{\overline{H}}} \sim 0.5 \ \mathrm{cm} , \tag{51}$$

where $v_a = \sqrt{2T/m_p}$ is the atomic thermal velocity.

The theory of three-body recombination (38) outlined here (see Refs [186–188]) breaks down for small ρ:

$$\rho < \rho_0 = \omega_H^{-2/3} \sim 2 \times 10^3 .$$

For these distances, the Coulomb force $1/r^2$ is strong in comparison with the Lorentz force Hv/c, and therefore the effect of magnetized plasma is absent and the positron cyclotron motion around the magnetic field lines gives way to motion along Keplerian elliptic orbits around protons. Under the action of the magnetic field, these orbits rotate as a whole with a Larmor frequency $\omega_L = \omega_H/2$, which for $\rho < \rho_0$ is low in comparison with the frequency of positron revolution along the Keplerian orbits.

The orbit dimension $r \sim \rho_0$ corresponds to the principal quantum numbers $n \sim 30$. Inelastic collisions of positrons with $\overline{H}$ atoms, accompanied by variations of n, are unlikely. The subsequent deexcitation of such $\overline{H}$ atoms takes place in two stages. At first, as a result of the Stark processes

$$\overline{H}_{nl} + e^+ \to \overline{H}_{nl'} + e^+ ,$$

the states with low orbital angular momenta l are reached. Next radiative transitions occur from these states directly to

the low-n levels. The rate of such transitions is of the order of

$$\Gamma_\gamma \sim \Gamma_{np} \approx \Gamma_{2p}\, n^{-3} \sim 2 \times 10^4\ \mathrm{s}^{-1}\,,$$

where $\Gamma_{2p} = 0.6 \times 10^9\ \mathrm{s}^{-1}$ is the $2p \to 1s$ transition rate. One can see from expressions (49) and (50) that the limiting stage of process (38) for $n_e > 10^8\ \mathrm{cm}^{-3}$ is the above radiative transitions

$$\lambda_{\overline{H}} \approx \Gamma_\gamma \sim 10^4\ \mathrm{s}^{-1}, \quad n > 10^8\ \mathrm{cm}^{-3}. \tag{52}$$

For $n_e < 10^8\,\mathrm{cm}^{-3}$, formula (49) is appropriate. With this in mind, for an estimate we next assume that $\Gamma_\gamma = \infty$. This implies that the $\overline{H}$ atoms known to have reached the low-l states instantaneously abandon a level n. In this formulation, the problem of a cascade transitions for $\rho < \rho_0$ becomes completely similar to the calculation of the effective rate of hadron capture by nucleus in the level n during cascading in hadronic atoms [39] (see also Section 2.2). The electric field of the positrons that travel along magnetic 'strings' with $\rho \leqslant r_D$ cause a small variation of the eccentricity and a rotation of the Keplerian orbit. These variations are random, and therefore a diffusion of the recombining positron over the l subspace occurs (for a fixed n). A zero boundary condition for $l = l_0$, where $l_0 \sim 1$, should be imposed on the corresponding diffusion equation. The effective rate of radiative deexcitation, Γ_D, of the level n is equal to the magnitude of diffusive flux in the l 'variable' for $l = l_0$:

$$\Gamma_D = \frac{3n^2 n_e \Lambda^2}{\Lambda_1}\sqrt{\frac{2\pi}{T}},$$

where $\Lambda = \ln(r_D v_T/n)$, $\Lambda_1 = \ln n$. Under the conditions (39) and for $n \sim 30$, one obtains

$$\Gamma_D \sim 3 \times 10^6\ \mathrm{s}^{-1}\,,$$

i.e. the diffusion to the low-l values is a fast stage. Hence follows expression (52).

To our knowledge, the most comprehensive consideration of the mechanism of stimulated recombination (37) is given in Ref. [189]. Let the laser-stimulated positron landing be performed from a state with an energy E to some state $|\,\mathrm{f}\rangle$ of an $\overline{H}$ atom with an ionization potential I. In the first order of the perturbation theory in the positron interaction $V = \mathbf{rE}(t)$ with the laser field $\mathbf{E} = \mathbf{E}_0 \cos(\omega t)$, the number of atoms produced in the $|\,\mathrm{f}\rangle$ state per unit time is given by the expression

$$J_\mathrm{f} = N_{\bar{p}}\, \lambda_\mathrm{r}\, n(E)\,. \tag{53}$$

Here, $N_{\bar{p}}$ is the number of free antiprotons in the plasma, $n(E)$ is the occupation number for the positron states with an energy E, and

$$\lambda_\mathrm{r} = \frac{4\pi^2 S}{c}\, F(E)\,, \quad F(E) = \rho(E)|z_{E\mathrm{f}}|^2\,, \tag{54}$$

where S is the energy flux density of the laser beam, $\rho(E)$ is the density of positron states per unit volume, and $z_{E\mathrm{f}}$ is the matrix element of the z coordinate of a positron (the z-axis is aligned with $\mathbf{E}_0$). Two possibilities were considered in Ref. [189]: positron landing from a continuous ($E > 0$) and discrete ($E < 0$) spectra. For $E > 0$, the asymptotic (as $r \to \infty$) behavior of the wave function of the initial positron state is $|\,\mathbf{p}\,\rangle \to \exp(\mathrm{i}\mathbf{pr})$, and

$$|z_{E\mathrm{f}}|^2 \equiv \int \left|\langle \mathbf{p}\,|\,z\,|f\rangle\right|^2 \frac{\mathrm{d}\Omega_\mathbf{p}}{4\pi}\,,$$

$$\rho(E) = \frac{p}{2\pi^2}\,, \quad p = \sqrt{2E}\,, \quad E = \omega - I\,,$$

$$n(E) = \left(\frac{2\pi}{T}\right)^{3/2} \exp\left\{\frac{-p^2}{2T}\right\} n_e$$

(the positron spin does not change and is therefore not taken into account).

For the temperature (39), the de Broglie wavelength of a positron is long ($\sim 10^3$ a.u.) and therefore in the initial positron state $|\,\mathbf{p}\rangle$ it would suffice to retain the s-wave and pass to the limit $p \to 0$:

$$|\,\mathbf{p}\rangle \to |\,p, \mathrm{s}\rangle \approx \sqrt{\frac{\pi}{pr}}\, J_1(\sqrt{8r})\,. \tag{55}$$

Due to the dipole selection rule, the positron landing will occur primarily to the state

$$|\,\mathrm{f}\rangle = |\,\mathrm{n}\,,\ l = 1,\ \mathrm{m} = 0\rangle$$

with an angular momentum $l = 1$ and its projection $m = 0$ onto the z-axis.

The same laser field will ionize the resultant atoms with a rate $\lambda_\mathrm{i} = \lambda_\mathrm{r}$ via the inverse transitions $|\,\mathrm{f}\rangle \to |\mathbf{p}\rangle$. Finally, with a rate λ_γ, a stabilization of the atoms occurs in the spontaneous radiative transitions to lower lying states. Next they escape from the plasma, which is in progress for a longer time period $\sim L/v_a$. The number of atoms produced per unit time equals

$$J_{\overline{H}} = \lambda_{\overline{H}} N_{\bar{p}}, \qquad \lambda_{\overline{H}} = \lambda n(E)\,, \tag{56}$$

where

$$\frac{1}{\lambda} = \frac{1}{\lambda_\mathrm{i}} + \frac{1}{\lambda_\gamma}\,,$$

$$\lambda_\mathrm{i} \approx \frac{4\pi^2 S}{c}\, F(0)\,.$$

It follows from expression (55) that $F(E) \to F(0) \neq 0$ as $E \to 0$, and therefore $F(E)$ in expressions (53) and (54) can be replaced with

$$F(0) = \frac{2}{3}Q^2\,, \qquad Q = \int_0^\infty r^{5/2} J_1(\sqrt{8r}) R(r)\,\mathrm{d}r\,,$$

where $R(r)$ is the radial WF of the state $|f\rangle$ normalized by the condition

$$\int_0^\infty r^2 R^2(r)\,\mathrm{d}r = 1\,.$$

In this form, formula (56) describes a positron landing from a state with E of arbitrary sign. The states with $E < 0$ are populated in the collisions (38).

According to the Monte Carlo calculation of Ref. [191], the quantum-state occupation number $n(E)$ increases approximately by the law $\exp(|E|/T)$ with decreasing E,

attains a maximum for $E = E_s = -3.8\,T$, and decreases further. That is why, according to Ref. [189] [see formula (56)], when the laser is tuned to the frequency

$$\omega = I + E = I - |E_s|\,,$$

one would expect an increase in $J_{\overline{H}}$ by a factor of $n(E_s)/n(0) = \exp(3.8) = 45$ in comparison with a landing from the $E = 0$ state.

In the foregoing calculation of a laser-induced positron landing and also in Ref. [191], the effect of the magnetic field was disregarded. The main contribution to Q is made by the r values of the order of the orbit dimension for the $|f\rangle$ state ($r \sim 2n^2$). Since $r < \rho_0$, the effect of magnetic field on the laser-induced landing to the states with $n < 30$ can be neglected.

By way of example let us consider the laser-induced positron landing to the 2p state, for which

$$\lambda_\gamma = 0.6 \times 10^9\ \text{s}^{-1}\,,\quad \frac{\lambda_i}{\lambda_\gamma} = \frac{S}{S_0}\,,\quad S_0 = 25\ \text{MW cm}^{-2}\,.$$

For $S \geqslant S_0$, according to formula (56), saturation is attained and the rate of $\overline{H}$ atom production reaches its maximum

$$\lambda_{\overline{H}} \approx \lambda_\gamma n(E)\,. \tag{57}$$

For $E = 0$, one finds $\lambda_{\overline{H}} \approx 3\ \text{s}^{-1}$, while for a positron landing from the $E = E_s = -3.8\,T$ states, $\lambda_{\overline{H}} = 140\ \text{s}^{-1}$. Whence and from expression (50) it is evident that process (38) is more effective than process (37), which is true for $n_e > 10^6\ \text{cm}^{-3}$. What is more, in the case of laser-induced recombination there remains the following indeterminate question which calls for additional investigation. It has been known (see the review [190]) that under conditions

$$S > S_D = \frac{2 \times 10^{10}}{n^8}\ \text{W cm}^{-2}\,,\quad \omega \ll I = \frac{1}{2n^2} \tag{58}$$

a rapid ionization of an atom residing in the nth Rydberg state occurs, the ionization being inherently stochastic and diffusive. On the other hand, the laser field was not included in the calculation of Ref. [191], and therefore the question arises of whether the Rydberg states with $E \sim E_s$ are stable. There exist two arguments in favor of the stability of these states and hence the validity of the calculated results [189]. First, there is a satisfactory agreement between the experiment of Ref. [192] on laser-induced electron landing on protons in a facility with a proton beam cooling by electrons and a calculation of the number of resultant atoms, performed using the above scheme. Second, for the states with $E \sim E_s$, instead of the second condition entering Eqn (58) we have the opposite: $\omega \gg |E_s|$. In Section 9, the weakly bound states are shown to be long-lived in this case.

The magnitude of S required for the laser-induced landing to the 2p state is high ($\sim 10^2\ \text{MW cm}^{-2}$) for the lasers available at a frequency $\omega \sim 3.5$ eV. That is why the direct process $|E \sim E_s\rangle \to |2p\rangle$ can be accomplished only in a pulsed laser operation. But then the effective landing rate $\lambda \sim \lambda_{\overline{H}}\overline{W}/W$ will be too low due to the smallness of the ratio between the average laser power $\overline{W}$ and the peak power $W = S \cdot \sigma$ (σ is the cross section area of the laser beam). To obviate this difficulty, Wolf [189] proposed to accomplish the positron landing in two steps:

(a) $|E \sim E_s\rangle \to |n = 11\rangle$;

(b) $|n = 11\rangle \to |2p\rangle$.

Transition (a) is effected by a CO_2 laser, while transition (b) by a $\lambda = 377$ nm wavelength laser. For the magnitudes $S_a \sim 60\ \text{kW cm}^{-2}$ and $S_b \sim 250\ \text{W cm}^{-2}$, saturation is achieved respectively for the former (CO_2) and the latter lasers, and the $\overline{H}$ atom production rate attains the magnitude (57), i.e. $\sim 100\ \text{s}^{-1}$. According to expression (58), for $n = 11$, $S_D = 0.1\ \text{kW cm}^{-2}$, and therefore this scheme is impracticable owing to the fast diffusive ionization of the intermediate level ($n = 11$).

The saturation of the nth level sets in for

$$S = S_0 = 25\left(\frac{2}{n}\right)^3\ \text{MW cm}^{-2}\,.$$

Whence and from expression (58) it follows that for $n \geqslant 3$ $S_D > S_0$, i.e. none of the levels can be used as an intermediate one for landing the positron to the 2p state.

All these arguments cast doubt on the feasibility of implementation of laser radiation-induced recombination of positrons and antiprotons (37). At the same time, $\overline{H}$ atoms are produced fast enough by three-body recombination (38), which gives confidence in the feasibility of the experiments on antihydrogen, discussed above. However, considering their complexity, several authors (see, for instance, papers [152, 153, 193] and references cited therein) proposed to produce and study $\overline{H}$ atoms with combined antiproton and positron beams. A discussion of this vast field of research is beyond the scope of our review.

2.6 Metastability of exotic helium. The Condo model

So, negatively charged hadrons π^-, K^-, $\bar{p}$, Σ^-, ... produce exotic atoms within a time of $\sim 10^{-12}$ s following deceleration in practically any material. The duration of cascade transitions in exotic atoms is the same to an order of magnitude [12]. Consequently, the hadrons are captured by nuclei within $\sim 10^{-11} - 10^{-12}$ s after entry into the target. Experiments [195, 196] with pions have shown that helium targets are an exception: $\sim 99\%$ of pions are captured within $\sim 10^{-12}$ s, but $\sim 1\%$ decay as free particles ($\pi^- \to \mu^- + \nu_\mu$) within a standard time period of $\sim 10^{-8}$ s. This metastability effect is general in nature and has also been discovered for other particles: K^- [197 – 199], Σ^- [200, 201], and $\bar{p}$ [202]. The main results obtained on the investigations of this effect, which are being pursued in several laboratories, will be considered in the subsequent sections of our review.

A qualitative explanation of the metastability effect [203], detailed in Ref. [204], has come to be known as the Condo model or the 'atomcule' model. According to this model, on the deceleration of $\bar{p}$ (for definiteness, in the subsequent discussion antiprotons will be dealt with, even though all the conclusions are valid for other particles, too) a neutral atomcule ($\bar{p}\alpha e$) forms by the reaction

$$\bar{p} + \text{He} \to (\bar{p}\alpha e)_{nl} + e\,, \tag{59}$$

which will hereafter be referred to as *the direct production mechanism of antiproton helium*. Here (n, l) are the principal and orbital quantum numbers of the antiproton state (their initial values $l_0 \sim n_0 \sim \sqrt{m_p/m_e} \sim 40$). A small fraction of the antiprotons $f_M \sim 1/n_0 \sim 0.03$ find themselves in nearly circular orbits $n - l \ll n$. For these orbits, the acceleration experienced by $\bar{p}$ for a given total (internal) energy ε_n is minimal, and therefore the radiative transition rates for the processes

$$(\bar{p}\alpha e)_{nl} \to (\bar{p}\alpha e)_{n'l'} + \gamma,\qquad n' < n$$

are low ($\Gamma_\gamma \sim 10^6\ \mathrm{s}^{-1}$). The Auger transitions

$$(\bar{\mathrm{p}}\alpha\mathrm{e})_{nl} \to (\bar{\mathrm{p}}\alpha)_{n'l'} + \mathrm{e}\,, \qquad n' < n$$

are suppressed ($\Gamma_\mathrm{A} \ll \Gamma_\gamma$) owing to the high magnitude of the angular momentum ($\Delta l \sim 5$) which should be imparted to the escaping electron by heavy particles (the $\Delta l \sim 1$ transitions are energy-forbidden). The interaction between $\bar{\mathrm{p}}$ and e removes the Coulomb degeneracy of states in l and produces an energy level splitting of the order of

$$\Delta E = E_{n,l+1} - E_{nl} \sim 0.3\ \mathrm{eV},$$

and therefore the Stark transitions

$$(\bar{\mathrm{p}}\alpha\mathrm{e})_{nl} + \mathrm{He} \to (\bar{\mathrm{p}}\alpha\mathrm{e})_{nl'} + \mathrm{He} \tag{60}$$

prove to be suppressed, too. Another reason why the Stark processes are unlikely lies with the Pauli repulsion of an atomcule from helium atoms: an atomcule is similar to hydrogen atoms H in chemical properties [204]. Since the He orbitals are occupied, H and He repel each other.

So, the Condo model explains why metastability exists in helium and gives a correct estimate of f_M. But it leaves unexplained why the metastability of antiprotons is missing from other materials. Moreover, the majority of experiments performed in recent years cannot be explained in the context of this model. The objective of our paper is to review the experimental facts and the existing theoretical models and also to go into details of the 'ioncule' model proposed on a qualitative level in Refs [205, 206]. The latter model is contemplated for verification as one of the experimental tasks (the ASACUSA project) dedicated to the study of atom-molecular processes involving antiprotons, whose execution commenced in 2000 [207, 208].

3. Direct production mechanism of antiproton helium

The following reactions can be brought about as a result of an antiproton collision with a helium atom:

$$\bar{\mathrm{p}} + \mathrm{He} \left\{ \begin{array}{ll} \longrightarrow \bar{\mathrm{p}} + \mathrm{He}\,, & (61)\\ \longrightarrow \bar{\mathrm{p}} + \mathrm{He}^*\,, & (62)\\ \longrightarrow (\bar{\mathrm{p}}\alpha\mathrm{e}) + \mathrm{e}\,, & (63)\\ \longrightarrow (\bar{\mathrm{p}}\alpha) + \mathrm{e} + \mathrm{e}\,, & (64)\\ \longrightarrow \bar{\mathrm{p}} + (\alpha\mathrm{e})^* + \mathrm{e}\,, & (65)\\ \longrightarrow \bar{\mathrm{p}} + \alpha + \mathrm{e} + \mathrm{e}\,. & (66) \end{array} \right.$$

Here, reaction (61) is an elastic scattering, reaction (62) an inelastic one, (63) the direct mechanism of reaction (59), (64) a direct $(\bar{\mathrm{p}}\alpha)$ ion formation, and (65) and (66) the events of single and double ionization of helium. A light particle can carry away the energy but not the momentum of a heavy particle, and therefore reactions (63) and (64) are possible only for relatively low energies of $\bar{\mathrm{p}}$:

$$E \leqslant I_\mathrm{He} = 24.6\ \mathrm{eV}\,.$$

Reaction (64) [like reaction (63) involving an excited atomcule electron] is adiabatically unlikely and can therefore be neglected. The available experimental data for the total cross section σ_i of reactions (63)–(66) are given in Fig. 2 (curve *1*).

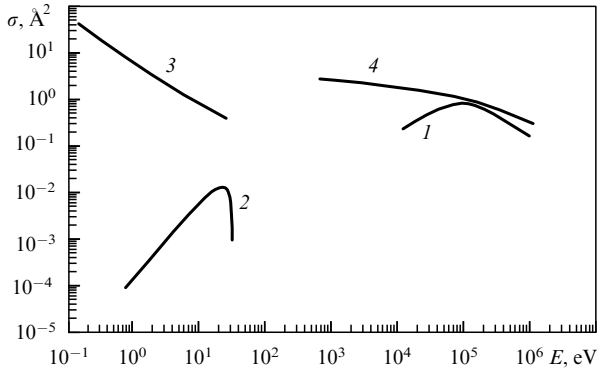

Figure 2. Cross sections of several processes involving antiprotons in relation to their energy E: (*1*) experiments of Refs [207, 209] for the total cross section of reactions (63) — (66); (*2*) our calculation for reaction (63); (*3*) the calculation of Ref. [212]; (*4*) the theory and the experiment of Refs [207, 209] for the total cross section of reactions (69) and (70).

It would be instructive to compare reactions (61)–(66) with similar ones for hydrogen:

$$\bar{\mathrm{p}} + \mathrm{H} \left\{ \begin{array}{ll} \longrightarrow \bar{\mathrm{p}} + \mathrm{H}\,, & (67)\\ \longrightarrow \bar{\mathrm{p}} + \mathrm{H}^*\,, & (68)\\ \longrightarrow (\bar{\mathrm{p}}\mathrm{p}) + \mathrm{e}\,, & (69)\\ \longrightarrow \bar{\mathrm{p}} + \mathrm{p} + \mathrm{e}\,. & (70) \end{array} \right.$$

A comparison of curves *1* and *4* in Fig. 2 reveals a significant difference between the measured cross sections σ_i for hydrogen [reactions (69) and (70)] and helium. The reason is that, for a distance $R = R_\mathrm{FT} = 0.64$ a.u. (the Fermi–Teller radius) between the heavy particles $\bar{\mathrm{p}}$ and p, the energy level of the electronic ground state in reactions (67)–(70) crosses the continuum boundary, and bound electron states are non-existent for $R < R_\mathrm{FT}$. An arbitrarily slow antiproton 'forces out' the electron from a hydrogen atom ('adiabatic ionization'), and therefore the cross section σ_i for hydrogen is high.

For an energy $E < I_\mathrm{He}$, only reaction (63) is possible of all the ionization channels: on expending an energy $\sim I_\mathrm{He}$ to force out the electron, the antiproton can no more recede to infinity and forms a bound state with He^+. For helium, adiabatic ionization is impossible, and therefore σ_i is small (curve *2* in Fig. 2; see the Appendix, Section II). The reason is that in this case for $R \to 0$, an H^- ion forms with an ionization potential $I = 0.75$ eV, i.e. no crossing of the continuum boundary occurs. In a typical collision, the minimal distance between $\bar{\mathrm{p}}$ and α is of order $R \sim R_0 \sim 0.5$ a.u., the ionization potential of a weakly bound electron is $I \sim 2$ eV (Fig. 11, see below), and the velocity of nuclear motion $v \sim 0.025$ a.u. For the Massey parameter (see, for instance, Refs [210, 211]) we obtain the following estimate

$$\xi \sim \frac{IR}{v} \sim 3\,.$$

The ionization probability will be $W \sim \exp(-\xi) \sim 0.05$ and the cross section

$$\sigma \sim \pi R_0^2 W \sim 10^{-18}\ \mathrm{cm}^2\,,$$

which is confirmed by a detailed calculation (Appendix, Section II). The reason for the smallness of σ_i is evident: for

a slow nuclear motion, the probability that the electron transits from a bound state to the continuum is low.

When calculating σ_i in the low-energy range, the main difficulty is associated with the proper choice of a correct numerical procedure for evaluating the integrals of rapidly oscillating functions. We took advantage of a standard procedure which involved partitioning the integration domain into intervals contained between the integrand zeros with subsequent summation of the contributions of these intervals. The accuracy of this procedure was verified employing analytically calculable examples with parameters close to ours. In the calculation of σ_i in Ref. [212] (curve *3* in Fig. 2), the following assumptions were made, which are partly incorrect:

(a) the electronic terms of the $\bar{p} + He$ and $\bar{p} + He^+$ systems calculated in Ref. [213], which were also used in our calculation, were replaced with approximate analytical expressions;

(b) these expressions were analytically continued to the complex R domain;

(c) the point of crossing of these electronic terms was found in the complex R domain;

(d) to calculate σ_i, advantage was taken of an analytical formula which is no better than exponentially accurate in the case of adiabatic nuclear motion (as are many approximate analytical formulas for transition probabilities known in the physics of atomic collisions [210, 211, 283 – 285]).

Beck et al. [214] also arrived at very large magnitudes of the cross sections of reactions (59). However, they were calculated on the basis of classical mechanics for all the particles. Evidently, this is not the way to describe the motion of a weakly bound electron that executes a quantum transition to the continuum.

The inference that σ_i is small is borne out by experimental data on metastability quenching by impurities (see Section 6): if it is assumed that antiproton helium is produced by the mechanism (59), the cross sections for the metastability quenching prove to be 3 – 4 orders of magnitude lower than the experimental ones.

4. Production of antiproton helium by recombination mechanism. The 'ioncule'

Since, as noted above, reactions (59), (63) can be neglected, only the elastic collisions (61) remain significant for antiproton energies $E < I_{He}$. After several such collisions, an antiproton becomes thermalized ($E \sim I_{He} \to E \sim T$) and then recombines in a three-body collision

$$\bar{p} + He + He \to (\bar{p}\alpha ee)_{|\varepsilon|} + He\,. \tag{71}$$

Here $\varepsilon \sim -T$ is the initial antiproton binding energy in the resultant negative ion $(\bar{p}\alpha ee)$ which will be referred to as an ioncule by analogy with an 'atomcule.'

Subsequently, due to a gradual deexcitation

$$(\bar{p}\alpha ee)_{|\varepsilon|} + He \to (\bar{p}\alpha ee)_{|\varepsilon'|} + He\,, \quad |\varepsilon'| > |\varepsilon|\,, \tag{72}$$

the binding energy rises to the values $|\varepsilon| \sim |\varepsilon_0| \sim 10$ eV in a time of $\sim 10^{-9} - 10^{-10}$ s, while the distance between $\bar{p}$ and α shortens to

$$R \sim 0.5 - 1 \text{ a.u.} \tag{73}$$

For the R values specified above, an antiproton 'conceals itself' inside the electron shell. The Pauli repulsion of electrons from the neighboring helium atoms comes into effect, and the inelastic processes (72) and (60) are practically terminated, metastability setting in for circular states.

The rate of recombination (71), (72) can be estimated assuming that $m_p \ll m_\alpha$ (Appendix, Section III), where m_p and m_α are the masses of $\bar{p}$ and the nucleus of a helium atom, respectively. In this case, the energy ε changes by a small value in one collision (72) and the diffusive motion over the levels $|\varepsilon| \sim T$ comes to be the limiting (the longest) recombination stage. On the basis of the multiphoton recombination theory [215] (see also Ref. [216]), we obtain an estimate for the resultant rate of recombination (71), (72):

$$\lambda_r = \frac{3^{1/2}\pi^3\alpha^{5/4}N^2 m_p^{1/2}}{2^{5/4}T^{3/4}m_\alpha}\,. \tag{74}$$

Here, $\alpha = 1.4$ a.u. is the helium polarizability, and N the atomic helium number density (the number of atoms per unit volume). So, antiproton helium is an ioncule $(\bar{p}\alpha ee)$ rather than an atomcule $(\bar{p}\alpha e)$, as implied by the Condo model. It is shown below that this new model gives a better fit to the available experimental data.

5. Why is metastability inherent only in helium?

According to the Condo model, the metastability of antiprotons in helium is explained by the Pauli repulsion of an atomcule from helium atoms (see Section 2.6). The electron shells of other rare-gas atoms are also completely filled, and therefore in this case, too, the Pauli repulsion occurs and the metastability should be present. Numerous investigations have shown, however, that it is absent from all materials with the exception of helium (see the reviews [233, 234]).

This fact is naturally explained in the context of the ioncule model. As $\bar{p}$ approaches He, a $(\bar{p}He)$ system forms similar to an H^- ion. Analogously, when $\bar{p}$ approaches Ne, Ar, Kr, and Xe atoms, ions result akin to F^-, Cl^-, Br^-, and I^- negative ions, respectively. The metastable antiproton states are not destroyed in collisions only when these 'ioncules' are repelled from the medium atoms.

Due to the low binding energy, the external electron of these 'ioncules' interacts with rare-gas atoms approximately as a free electron with a low kinetic energy [235]. This interaction exhibits two opposite effects: the Pauli repulsion and the polarization attraction. The result of their competition is determined by the sign of the slow electron – atom scattering length. One can see from Table 1 that an ioncule exhibits repulsion only in the case of helium (Fig. 3). In the remaining cases, immediately after the production of an ioncule (for instance, $\bar{p} + Xe \to I^-$) in which the antiproton is in a metastable orbit, a fast decay of this state occurs in collisions with atoms $(I^- + Xe)$ by the mechanism of an induced Auger transition, considered in the following section.

6. Quenching of metastability by impurities. Comparison with experiments

Immediately the metastability of antiprotons in helium was discovered [202], a start was made on the comprehensive investigation of this phenomenon [220, 233, 234, 238 – 242], which is still in progress [207]. Early studies were concerned with the integral time spectra of antiproton annihilation products [delayed annihilation time (DAT) spectra]: measurements were taken of the detection time t of the pions

Table 1. Polarizability α and the scattering length a of slow electrons by rare-gas atoms [235–237].

Atom	He	Ne	Ar	Kr	Xe
α, a.u.	1.4	2.7	11.1	16.7	27
a, a.u.	1.14	0.2	−1.6	−3.2	−5.8

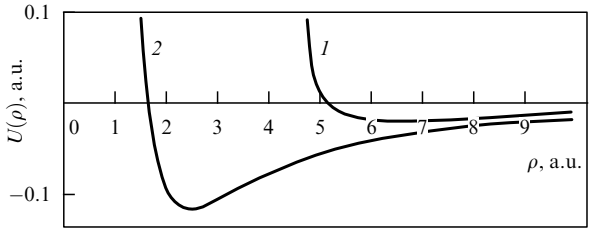

Figure 3. Qualitative dependences of the potential energy of the interaction between a rare-gas atom and its corresponding ioncule on the distance ρ between them: (*1*) He + ($\bar{p}$He); (*2*) Xe + ($\bar{p}$Xe).

originating in the annihilation of antiprotons, which elapsed from the $\bar{p}$ stopping in the target, and histograms were plotted of the number of pions emerging in different intervals of time. More recently, advantage was taken of a laser-spectroscopy technique: the signal that $\bar{p}$ had been brought to rest triggered a short laser pulse. When the laser frequency Ω was at resonance with one of the antiproton transitions from a metastable atomcule state to a short-lived one ($\Omega \sim \omega$), a peak appeared in the DAT spectra, which corresponded to the $\bar{p}$ annihilation occurring after the transition to this short-lived state. All these experiments were carried out both in pure helium and helium with atomic (rare gases) and molecular (H_2, N_2, O_2) admixtures. The helium number density in the target N was varied over a broad range

$$2 \times 10^{20} < N < 2 \times 10^{22} \text{ cm}^{-3}.$$

Let us calculate the cross section σ_q for the quenching of the metastable states of antiproton helium in collisions with rare-gas atoms.

According to the Hellmann–Feynman theorem [243, 244], for a distance ρ between an ioncule and an impurity atom Z, in the neighborhood of the core of the ioncule (which is an atomcule) there exists an electric field

$$\mathcal{E} = -\frac{\mathrm{d}U(\rho)}{\mathrm{d}\rho}\,.$$

This field perturbs the antiproton motion and mixes the metastable (n, l) state with the short-lived (n, $l-1$) state closest in energy, whose decay rate will be denoted as Γ_A (the principal channel of decay of short-lived states is the Auger transition in an atomcule):

$$\psi_{nl} \to \psi_{nl} + \alpha\psi_{n,l-1}\,, \quad \alpha = \frac{V_{21}}{\Delta E}\,, \tag{75}$$

where V_{21} is the off-diagonal matrix element of the $V = -\mathbf{Ed}$ operator, taken for these states, $\mathbf{d}$ is the dipole moment operator for the 'atomcule,' and

$$\Delta E = E_{nl} - E_{n,l-1} \sim 0.3 \text{ eV}\,.$$

According to expressions (75), the Auger transition rate in an atomcule takes the form

$$\Gamma(\rho) = \Gamma_A \alpha^2(\rho)\,.$$

Hence, on interchanging the order of integration with respect to ρ and the impact parameter b [210, 245], in view of the relationship

$$\mathrm{d}t = \frac{\mathrm{d}\rho}{\sqrt{v^2(1 - b^2/\rho^2) - 2U/\mu_0}}$$

we obtain [205]

$$\begin{aligned}\sigma_q &= \int_0^\infty 2\pi b\,\mathrm{d}b \int_{-\infty}^{\infty} \Gamma\big(\rho(t)\big)\,\mathrm{d}t \\ &= \frac{4\pi\Gamma_A d^2}{3v(\Delta E)^2}\int_{\rho_0}^{\infty} \rho^2 \left(\frac{\mathrm{d}U}{\mathrm{d}\rho}\right)^2 \mathrm{d}\rho\,.\end{aligned} \tag{76}$$

Here, $\mu_0 = MM_Z/(M + M_Z)$, $M = m_p + m_\alpha$, v is the collision velocity of the ioncule with an impurity atom Z (of mass M_Z), and ρ_0 the distance of closest approach (see Fig. 3) in their central collision ($b = 0$). To calculate the transition matrix element d, advantage will be taken of the hydrogenlike wave function approximation for the relative motion of $\bar{p}$ and α [219, 246]:

$$\begin{aligned}d^2 &= \frac{1}{2l+1}\sum_{m=-l}^{l} \big|\langle n, l-1, m\,|z|\,n, l, m\rangle\big|^2 \\ &= \frac{3}{2}\left(\frac{n}{q\mu}\right)^2 \frac{l^2(n^2 - l^2)}{(4l^2 - 1)}\,,\end{aligned} \tag{77}$$

where $\mu = m_p m_\alpha/M$, m is the projection of the antiproton orbital angular momentum onto the z-axis (i.e. the ρ-axis), and $q \approx 1.5$ is the effective charge in the field of which $\bar{p}$ moves in the atomcule. The averaging over m was performed in expression (77). The antiproton binding energy and the radius of its circular orbit in the hydrogen-like approximation are defined by the formulas

$$\varepsilon = -\frac{q^2}{2\mu n^2}\,, \quad R = \frac{n^2}{q\mu}\,. \tag{78}$$

Prevailing in the energy $U(\rho)$ for short ρ is the Pauli repulsion, the same as in the H + Z system, and prevailing for long ρ is the $H^- + Z$ polarization attraction

$$U(\rho) \approx A\exp(-\eta\rho) - \frac{\alpha}{2\rho^4}\,. \tag{79}$$

The values of σ_q for the ($n = 37$, $l = 34$) state of antiproton helium and rare gases as impurities, calculated in the framework of the ion model by formula (76), are given in Table 2 (the last line). The A, η, and α parameters required for the calculation were borrowed from Refs [235–237], and the values of Γ_A from Refs [247, 248]. Given in the penultimate line of Table 2 are the σ_q values for the atomcule-based Condo model. In this case, the polarization attraction should be replaced with the van der Waals attraction, resulting in a potential well substantially shallower than that of expression (79):

$$U(\rho) \approx A\exp(-\eta\rho) - \frac{C}{\rho^6}\,. \tag{80}$$

Table 2. Measured [249] and calculated cross sections σ_q for metastability quenching by impurities Z.

Impurity Z	N_2	H_2	O_2	He
σ_q, cm^2 (experiment)	1×10^{-17}	2×10^{-16}	2×10^{-15}	1×10^{-22}
σ_q, cm^2 ('atomcule', theory)	$<10^{-17}$	$<10^{-17}$	$<10^{-16}$	2×10^{-24}
σ_q, cm^2 ('ioncule', theory)	$\sim10^{-17}$	$\sim10^{-16}-10^{-15}$	$\sim5\times10^{-15}$	1×10^{-22}
Impurity Z	Ne	Ar	Kr	Xe
σ_q, cm^2 (experiment)	1×10^{-20}	4×10^{-20}	$0{,}5\times10^{-18}$	3×10^{-18}
σ_q, cm^2 ('atomcule', theory)	1×10^{-24}	3×10^{-24}	7×10^{-22}	1.5×10^{-20}
σ_q, cm^2 ('ioncule', theory)	0.3×10^{-20}	6×10^{-20}	1×10^{-18}	3×10^{-18}

The electric field $\mathcal{E}=-U'(\rho)$ for potential (80) is much weaker than for potential (79), and therefore the σ_q values resulting for the atomcule model are substantially lower than the experimental ones [249]. The data of Table 2 may be regarded as a direct evidence that there exists a long-range polarization 'tail' in the interaction of antiproton helium with rare gases, i.e. confirmation of the ioncule model.

For pure helium (Z = He), the collisional quenching mechanism prevails for low densities ($N<10^{21}\text{cm}^{-3}$). For high densities, the cluster mechanism becomes the principal one (see Section 7).

Due to the existence of splitting ΔE between the (n, l) and $(n, l-1)$ states, the direct quenching mechanism (60) is characterized by an exponentially small cross section, and therefore the mechanism of induced Auger transitions considered here is the principal one [33, 205] [in Ref. [33], the mechanism (60) and that considered at this point were denoted respectively as collisional and induced Stark transitions]. The conclusion that the induced mechanism prevails for the atomcule model was also drawn in Ref. [250]. We note, however, that the calculation was performed for an unrealistic potential $U(\rho)=B/\rho^2$, and that the Hellmann–Feynman theorem was not invoked for the electric field $\mathcal{E}$. According to paper [250], for experimental temperatures $T\sim10-300$ K of interest, the σ_q values obtained within the atomcule model are substantially lower than the observed ones, which is consistent with Table 2. A conclusion was drawn in Ref. [250] that the mechanism of induced transitions for the atomcule model explains the experimental values for pure helium (Z = He), which necessitates bringing an atomcule within a distance $\rho\approx1.5$ a.u. from a He atom. However, according to formula (80), for these separations $U(\rho)\sim+5$ eV. It is evident that atoms capable of overcoming so strong a repulsion are hardly present for the temperatures specified above. That is why the calculation by Korenman [250] is in fact demonstration that the atomcule model fails to explain the data on metastability quenching, which is consistent with our conclusions.

In the case of molecular impurities (Z = N_2, H_2, O_2), our attention is engaged primarily by the large magnitudes of σ_q observed for H_2 and O_2 [241] (see Table 2). These data suggest (especially those for O_2) that the quenching occurs in collisions with large impact parameters ($b\sim10$ a.u.). At these distances, the electric field of molecules is the field of their quadrupole moment Q, which decays with distance ρ by a power law. First we consider the atomcule model.

For the separations specified above ($b\geqslant5-10$ a.u.), the relative motion of an atomcule and Z can be treated as rectilinear and uniform. Process (60) is extremely unlikely because the Massey parameter for the process reaches $\xi\sim10^2$. The probability of the induced Auger transition is of order

$$W\sim\frac{b}{v}\,\Gamma_A\left(\frac{Qd}{b^4\Delta E}\right)^2$$

and for $b=5$ and $b=10$ amounts to 10^{-7} and 10^{-9}, respectively. Therefore, quenching in rectilinear trajectories is impossible and, to account for the experiments, antiproton helium is to be captured by Z molecules for large impact parameters. Then one may set

$$\sigma_q=\sigma_c W_q\,, \tag{81}$$

where σ_c is the capture cross section, and W_q is the probability of metastability quenching in the subsequent approach of the particles within small distances ρ in between.

Figure 4 gives the σ_c values for an atomcule captured by the molecules Z = N_2, H_2, and O_2. The calculation was performed using the Monte Carlo technique with classical trajectories for the particles α, $\bar{p}$, and Z. For α and $\bar{p}$, advantage was taken of the interaction potential from Ref. [213]. The particles were assumed to initially move with respect to each other in a circular path of radius $R=0.6$ a.u. The Z–atomcule interaction was taken in the dipole approximation: $V=\mathbf{ER}$. The electric field $\mathbf{E}$ of a molecule was made up of two components: the quadrupole term (for the N_2, H_2, and O_2 molecules whose quadrupole moments are equal to $Q=1.13$, 0.48, and 0.29 a.u. according to Refs [236, 237]) and the 'short-range' one $\mathcal{E}_S=\exp(-2\rho)(1+2\rho+2\rho^2)/\rho^2$ [219]. The molecule was treated as a rigid classical rotator with a Boltzmann distribution over angular momentum and with a moment of inertia $I=\mu_0R_0^2$, where μ_0 is the reduced mass of its nuclei, and R_0 is the equilibrium internuclear distance in the

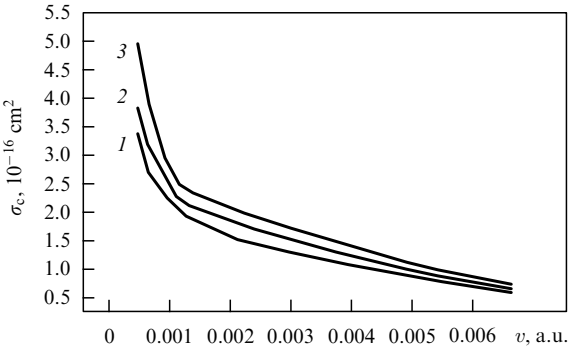

Figure 4. Capture cross section of an atomcule ($\bar{p}\alpha e$) by a molecule in the case of a circular antiproton orbit of radius $R=0.6$ a.u. Curves *1*, *2*, and *3* represent collisions with the N_2, H_2, and O_2 molecules, respectively; v is the molecule–atomcule collision velocity.

molecule. The calculation showed that the capture occurs primarily owing to the dipole–quadrupole interaction: on 'removing' the field $\mathcal{E}_S$, the σ_c magnitudes changed only slightly. The relatively small values of σ_c are attributable to the fast antiproton revolution in an atomcule.

According to Fig. 4, the values of $\sigma_c \sim 2 \times 10^{-16}$ cm^2 are typical of experimental conditions. One can see from Table 2 that the experimental σ_q values for O_2 are higher by an order of magnitude. It is shown below that $W_q \ll 1$ for N_2 and H_2, and that $W_q \sim 1$ for O_2. That is why a sharp discordance is also seen for the N_2 and H_2 molecules. Consequently, the atomcule model fails to explain the experiment by Hori et al. [249], which receives a natural explanation in the context of the ioncule model.

A charged ioncule polarizes a molecule, resulting in large capture cross sections

$$\sigma_c = \frac{2\pi}{v}\sqrt{\frac{\alpha}{\mu_0}} \approx 10^{-14}\ \text{cm}^2\ , \qquad (82)$$

where α is the molecular polarizability, and μ_0 is the reduced mass of the Z molecule and the ioncule. After the capture event, the ioncule approaches the molecule and interacts with the latter via its 'core' — the atomcule, for the dimension of the orbit of a weakly bound electron is rather large. Therefore, the case in point is an 'H + molecule' type interaction.

An HN_2 radical does not exist [251, 252] and, consequently, the magnitudes of W_q and σ_q for the $Z = N_2$ case are small owing to the repulsion between H and N_2.

In the case of H_2, the quenching occurs by the exchange reaction $H + H_2 \rightarrow H_2 + H$, which has a potential barrier $U_0 \approx 0.2$ eV [253, 254] and hence $W_q \ll 1$ (naturally, we are dealing with the minimal potential barrier). When the atomcule dipole moment $d \sim n(n_1 - n_2)/\mu$, where n_1 and n_2 are the parabolic quantum numbers [219], is taken into account, the barrier lowers in the following way

$$U \approx U_0 - d\mathcal{E}_M\ ,$$

where $\mathcal{E}_M$ is the electric field strength of the molecule. Hence we conclude that the magnitudes of W_q and σ_q for $Z = H_2$ should increase with n, which is consistent with the experiments [240].

Finally, in the case $Z = O_2$, there exists a strongly bound HO_2 radical with a dissociation energy of about 2 eV, which plays an important part in the chain reaction in the detonating (electrolytic) gas [251, 252]. After the capture event, the particles approaching each other will consequently be accelerated to a kinetic energy of ~ 2 eV. This latter energy will go into the vibrational and rotational degrees of freedom of the intermediate long-lived ($\sim 10^{-10}$ s [254]) complex of HO_2^* type, wherein the antiproton annihilation will occur within $\sim 10^{-12}$ s. The complex production goes without inference from a potential barrier, and therefore $W_q \sim 1$ while the quenching cross section is large and independent of n in accordance with Refs [240, 241].

Therefore, the ioncule model agrees well with the experiments on the antiproton metastability quenching by atomic and molecular impurities.

7. Metastability of antiprotons in pure helium. The bubble model

The measurements of the integral time spectra of antiproton annihilation (the DAT spectra) in pure helium showed [233, 234, 242] that the average lifetime of metastable states depends only slightly on the helium number density N: in going from a gas to a liquid state, it shortens by only $\sim 30\%$. As noted in these experiments, the increase in helium density is associated with the occurrence of a fast exponent in the DAT spectra. Invoking the techniques of resonance laser spectroscopy made it possible to elucidate its nature [249]. It turned out that increasing N has no effect on the lifetime τ of the majority of metastable (n, l) states (Fig. 5). However, there exist states, for instance, (37, 34) (Fig. 6), for which τ steeply decreases with N, the rate of their decay $\lambda = 1/\tau$ being a nonlinear function of N (Fig. 7). It is precisely these (n, l) states that are responsible for the fast exponent entering the DAT spectra.

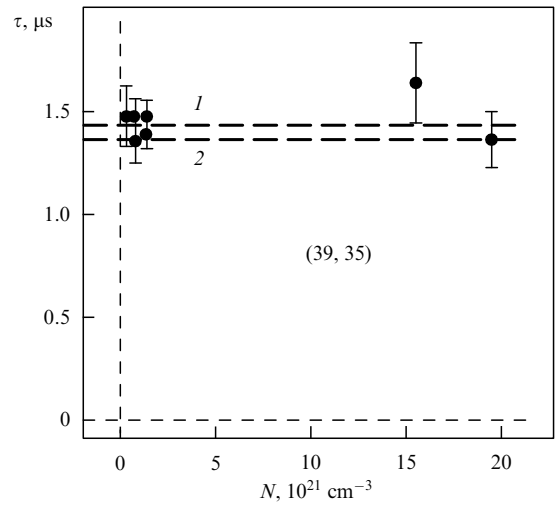

Figure 5. Lifetime τ of the metastable (39, 35) state as a function of the helium number density [249]. Lines *1* and *2* depict the radiative and total (with the inclusion of Auger transitions) lifetimes, respectively.

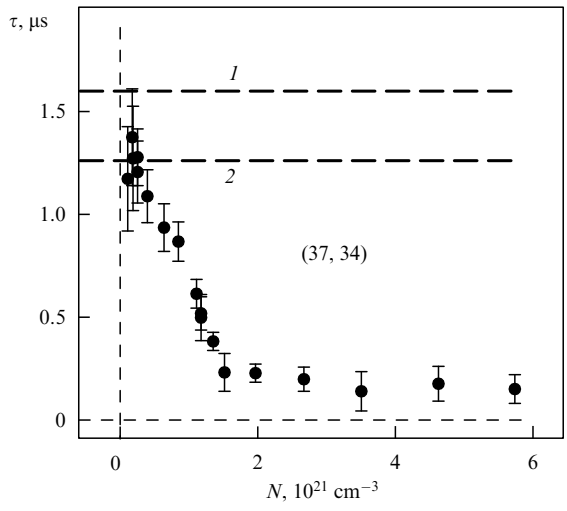

Figure 6. Lifetime τ of the metastable (37, 34) state as a function of the helium number density [249]. Lines *1* and *2* depict the radiative and total (with the inclusion of Auger transitions) lifetimes, respectively.

In our opinion, comparing Figs 6 and 8 furnishes insights into the nature of these phenomena. Figure 8 gives the results of measurements of electron mobility μ in helium. One can see that the onset of a sharp decrease of absolutely dissimilar

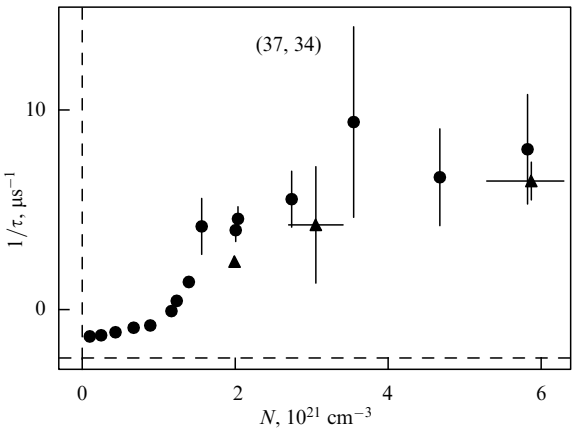

Figure 7. Decay rate $1/\tau$ (reciprocal of the lifetime) of the (37, 34) state as a function of the helium number density [249].

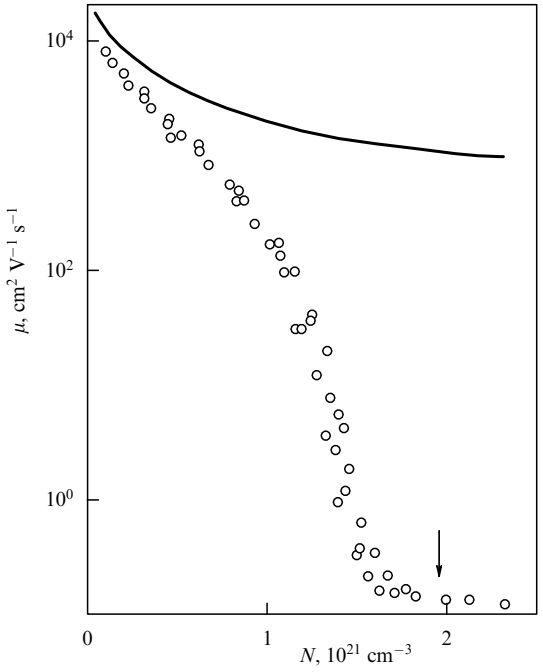

Figure 8. Electron mobility μ in gaseous helium for a temperature $T = 4.2$ K as a function of the helium number density [255]. The calculated value of the critical helium number density N_c [256, 257] is marked by an arrow. The curve represents the result of calculations in the context of the kinetic mobility theory.

quantities (τ and μ) occurs for one and the same critical helium number density $N = N_c$ (Fig. 9), which suggests that these phenomena are similar in nature. For $N > N_c$, free (or nearly free, weakly bound, as in the case of an ioncule) electrons in helium push, owing to the Pauli repulsion, helium atoms apart to form bubbles and become localized inside them, resulting in a drastic reduction of the mobility μ. For $N < N_c$, a free electron in helium is delocalized, the bubbles are absent, and the mobility is high.

For a free electron, the bubble radius r_0 is found from the condition that the quantum pressure

$$p_q = -\frac{1}{4\pi r_0^2}\,\frac{dE_{1s}}{dr_0}\,, \tag{83}$$

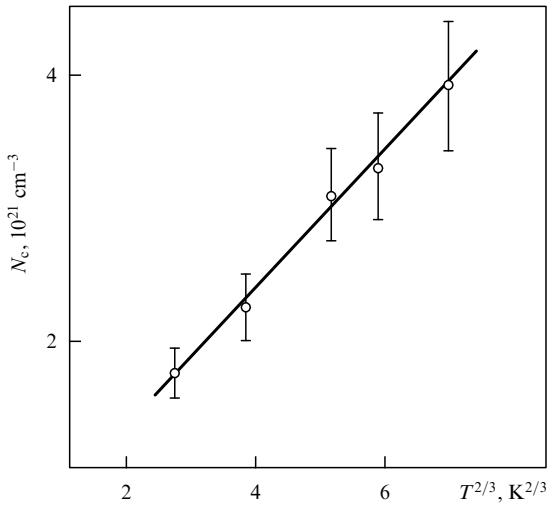

Figure 9. Critical helium number density N_c as a function of the temperature [258]. The straight line corresponds to the theoretical evaluation [256, 257].

$$E_{1s} = \frac{\pi^2\hbar^2}{2m_e r_0^2}\,, \tag{84}$$

be equal to the sum of the capillary pressure, $p_\sigma = 2\sigma/r_0$, and external pressure p [256, 257]:

$$p_q = p + p_\sigma\,, \tag{85}$$

where $\sigma = 0.36$ cgs is the surface tension of helium. For $p = 0$, from expressions (83) – (85) we obtain

$$r_0 = \left(\frac{\pi\hbar^2}{8m_e\sigma}\right)^{1/4} \equiv r_в = 17\ \text{Å}\,.$$

In this case, $p_\sigma = 4$ bar.

The formation of charged bubbles is also observed in neon and hydrogen [259 – 263], i.e. a weak Pauli repulsion occurs in the process. As explained in Section 5, the metastability of antiprotons is nonexistent in these materials due to a fast quenching. In hydrogen, the Fermi – Teller mechanism (see Section 3) is responsible for the production of neutral ($\bar{p}p$) atoms which rapidly annihilate ($\sim 10^{-12}$ s) due to the Stark transitions [31, 41]. In neon, the circular orbits of antiprotons collapse as a result of induced Auger transitions which are fast owing to the smallness of the ρ_0 parameter (see Fig. 3). In the scientific literature, no mention has been made of the bubbles in the remaining rare gases. They may not indeed exist, for the corresponding scattering lengths a are negative (see Table 1), i.e. an electron is attracted to these atoms.

Formula (84) for the electron energy level was obtained within the approximation of an infinitely high potential well at the bubble boundary ($U_0 = +\infty$). According to experiments, the actual height of the potential barrier penetrated by an electron which finds its way into liquid helium comes out to

$$U_0 = 1.3 \pm 0.4\ \text{eV}\ \ [264]\,,$$
$$U_0 = 1.02 \pm 0.08\ \text{eV}\ \ [265]\,. \tag{86}$$

According to these experiments, electrons with an energy lower than U_0 are completely reflected from the helium

surface. The theory by Budrick [266] based on the Fermi pseudopotential [219] gives

$$U_0 = \frac{2\pi\hbar^2 a}{m_e} N. \tag{87}$$

In particular, for a liquid-helium density, $U_0 = 1.09$ eV according to formula (87) and Table 1.

Therefore, the origination of bubbles in helium is a well-established fact, and so it would appear reasonable that the experimentally examined behavior of antiproton metastability would be accounted for by the production of these bubbles. We analyze here one of the possible scenarios. A thermal antiproton recombines with one of the helium atoms (see Section 4) to form an ioncule. As the antiproton orbit radius R decreases in the course of the relaxation (72), the binding energy of the weakly bound electron lowers. The electron cloud 'swells' and a vacuum bubble is produced with an ioncule at the center (Fig. 10). The Auger processes

$$(\bar{p}\alpha ee)_{nl} = (\bar{p}\alpha e)_{n'l'} + e \tag{88}$$

in the lower electronic 1s state are strongly moderated because of the increase in electron ionization energy by U_0 (to knock out an electron, it should be torn loose from the atomcule entirely and should overcome the repulsion from helium atoms). That is why (see also Section 8) the electronic excitation of an ioncule in dense helium does not take place and it is produced in the ground 1s state.

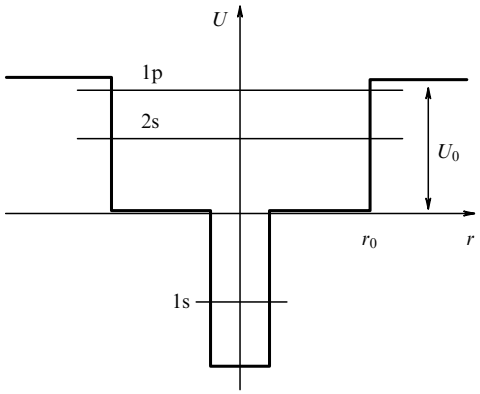

Figure 10. Electron potential energy in an ioncule formed in dense helium ($N > N_c$). Depicted are the ground (1s) and several excited electronic states.

The equilibrium bubble radius r_0 depends on the electronic state, much like the equilibrium internuclear distance in a diatomic molecule. The electron excitation raises the quantum pressure p_q to increase r_0. In this connection we note that the existence of excited electron states in a bubble has been proved in Ref. [267], where observations were made of the electromagnetic transitions between them, pertaining to the infrared spectral region.

The bubble radius r_0 also depends on the helium pressure p. To illustrate, for the 1s state with $I = 2.2$ eV, which corresponds to $R = 0.8$ a.u. (Fig. 11), r_0 is equal to 10.6, 10.4, 8.5, and 6.5 a.u. for liquid-helium pressures of 0, 3, 100, and 1000 bar, respectively. The calculation was performed in the approximation of zero radius potentials (ZRP) [226] with recourse to formulas (83) and (85).

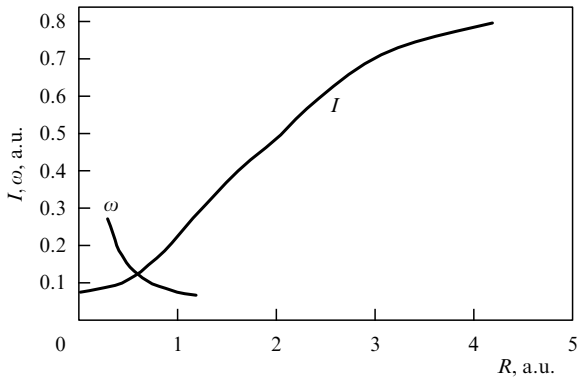

Figure 11. Ionization potential I of an isolated ioncule and the frequency ω of its revolution for a circular antiproton orbit of radius R (the electronic ground state).

We now turn to the explanation of experimental data on the basis of the facts outlined. Let an ioncule and a bubble form at $t = 0$, the electron residing in the 1s state (see Fig. 10).

The energy $\Delta E = E_{1p} - E_{1s}$ of the $1s \to 1p$ dipole electron transition in a bubble is, as a rule, significantly different from the energy $\Delta\varepsilon = \varepsilon_{nl} - \varepsilon_{n-1,l-1}$ of dipole antiproton transitions in an atomcule from the metastable (n, l) state to the rapidly decaying $(n-1, l-1)$ state (the decay rate of the latter will be denoted as Γ_A). In this case, the bubble formation will have no effect on the lifetime of the (n, l) state, which corresponds to Fig. 5. Some of the states may accidentally prove to be at resonance [for instance, the state (37, 34)]: $\Delta E \approx \Delta\varepsilon$. Then, there arises a substantial admixture of the $(n-1, l-1)$ state to the (n, l) state, accompanied by the induced Auger decay of metastability (see Fig. 6) with a rate

$$\Gamma = \frac{V^2\Gamma_A}{V^2 + \delta E^2/4}. \tag{89}$$

Here, $V \sim 0.1 R\gamma^{3/2} r_0^{-1/2} \sim 0.05$ eV is the off-diagonal matrix element of the dipole interaction operator of the atomcule with the weakly bound electron, $\delta E \approx \Delta E - \Delta\varepsilon$ (in the estimate for V given above, account was taken of the screening of the dipole moment of the atomcule by its electron [268]). Owing to the smallness of V, the case $|\delta E| \gg V$ is most likely, for which we obtain from formula (89):

$$\Gamma = \left(\frac{2V}{\delta E}\right)^2 \Gamma_A. \tag{90}$$

According to Fig. 7, one arrives at the estimate for $\Gamma \sim 10^7\ s^{-1}$, with $\Gamma_A = 2.4 \times 10^8\ s^{-1}$ for the $(n-1, l-1) = (36, 33)$ state [247]. Thus it follows from formula (90) that $|\delta E| \sim 5\ V \sim 0.2$ eV. Therefore, according to this rough estimate, the fraction of the (37, 34) type states whose decay rate is density-dependent (see Fig. 7) amounts to $5\ V/\Delta E \sim 0.3$.

Here we have examined the $1s \to 1p$ electronic transitions occurring for a fixed bubble radius r_0. The actual picture of the processes involved may prove to be more complex. When an electron transits to the 1p state, the quantum pressure increases and the bubble begins to expand. The bubble potential energy U_α for the $\alpha = 1s$ and $\alpha = 1p$ electronic states is given in Fig. 12. The bubble radial motion is

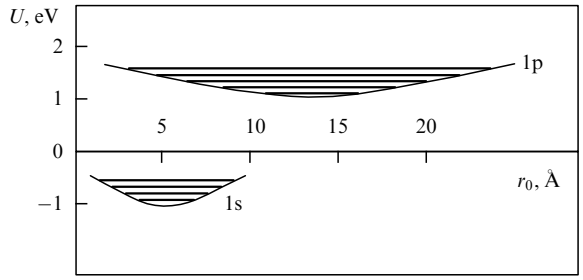

Figure 12. Bubble potential energy (qualitatively) $U(R) = E_\alpha(r_0) + 4\pi r_0^2\sigma$ as a function of its radius r_0 for the $\alpha = 1s$ and $\alpha = 1p$ electronic states.

characterized by a mass $M_в$ of the order of several atomic helium masses: it is estimated from the kinetic energy of liquid helium, appearing in the variation of r_0. A vibrational spectrum (see Fig. 12) with a frequency $\omega_в \sim 10^{12}$ s^{-1} corresponds to this motion.

The atomcule and the electron make up a 'fast' subsystem, while the bubble makes up a 'slow' one. We separate fast and slow variables by the Born–Oppenheimer method to conclude that the energy of the fast subsystem for a fixed r_0 is defined as

$$\varepsilon_{\alpha\beta}(r_0) = U_\alpha(r_0) + \varepsilon_\beta\,,$$

where ε_β is the energy of the atomcule in the $\beta = (n, l)$ and $\beta = (n-1, l-1)$ states. There are two fast-subsystem states close in energy:

$$\mathrm{L} = [\alpha = 1s\,,\ \beta = (n, l)]$$

and

$$\mathrm{S} = [\alpha = 1p\,,\ \beta = (n-1, l-1)]\,.$$

The corresponding electronic terms $\varepsilon_\mathrm{L}(r_0)$ and $\varepsilon_\mathrm{S}(r_0)$ appear as in Fig. 13, with the difference that the upper 1p term should be lowered by a value of $\Delta\varepsilon$. Then, taking into account the interaction of the atomcule dipole moment with the weakly bound electron, we obtain a quasi-crossing of terms of two types (Figs 13 and 14).

In the case of the (37, 34) state, to which Fig. 13 corresponds, there occurs a fast predissociation, with the irreversible production of a large-radius (~ 17 Å) bubble

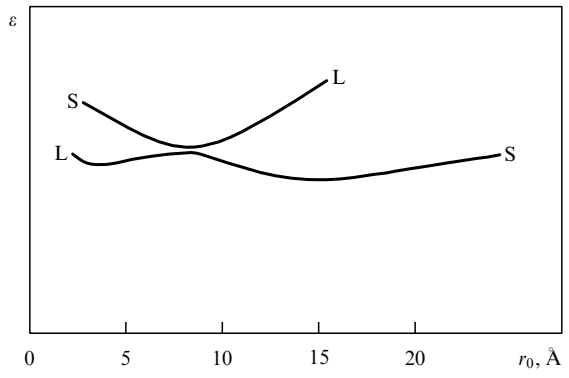

Figure 13. Qualitative picture of the electronic terms of an ioncule in a bubble for the resonance (37, 34) state.

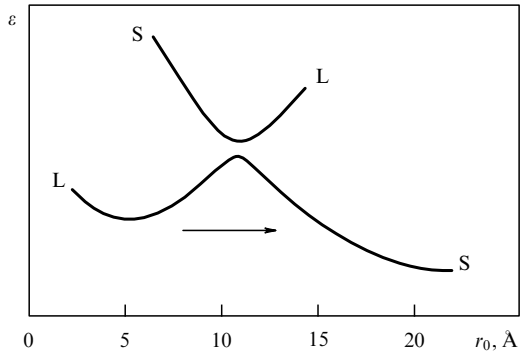

Figure 14. Qualitative picture of the electronic terms of an ioncule in a bubble for nonresonance (39, 35) type states. The unlikely tunnel transition of a bubble to the state with an excited electron and a short-lived atomcule is indicated by an arrow.

with an electron in the 1p state and an atomcule in the short-lived $(n-1,\ l-1)$ state, following the emission of several acoustic phonons in a time of 10^{-11} s [267]. As for the (39, 35) state shown in Fig. 14, the predissociation can occur only as a result of a bubble tunnel transition and is therefore unlikely.

An ioncule produced in dense helium has a quasi-continuum of excited electronic states. It is different in character from the quasi-continuum of Efimov states in an isolated ioncule (see Section 8). We first consider the excited s state of an electron localized in a bubble, with the number of nodes of the radial wave function equal to $K-1$ $(K = 1, 2, 3, ...)$. Then, instead of formula (84) we have

$$E_K = \frac{\pi^2\hbar^2 K^2}{2m_e r_0^2} \tag{91}$$

and, for the bubble radius at $p = 0$, from expressions (83) and (85) we obtain

$$r_0 = r_в\sqrt{K}\,, \tag{92}$$

which, together with formula (91), give

$$E_K = E_в K, \quad E_в = \frac{\pi^{3/2}2^{1/2}\hbar\sqrt{\sigma}}{\sqrt{m}} = 0.15\ \mathrm{eV}\,.$$

Equating E_K to U_0, we conclude that there exist bound states with $K \leqslant 6$. The limiting bubble radius is attained for $K = 6$ and, according to relationship (92), measures

$$r_m = 40\ \text{Å}\,. \tag{93}$$

We may estimate the total number of electronic states, including those with a nonzero orbital angular momentum $(L \neq 0)$, as the number of states in a spherical potential well of radius r_m and height U_0 [219]:

$$N_\mathrm{S} = \frac{2^{3/2}}{9\pi}\, r_m^3 U_0^{3/2} \approx 500\,. \tag{94}$$

Since $N_\mathrm{S} \gg 1$ and the typical quantum numbers are large, we arrive at the estimates

$$L \sim \sqrt{2U_0}r_m \sim 30\,, \quad K \sim 5\,, \tag{95}$$

where **L** is the electron orbital angular momentum relative to the bubble center, thus the electron in an excited state moves

like a classical particle inside the bubble, along rectilinear trajectories and experiencing elastic reflections from the bubble walls. The atomcule moves similarly to the electron and is also reflected from the helium walls (we are reminded that it is similar to a hydrogen atom in chemical properties and is therefore repelled from the helium walls).

If a weakly bound electron finds itself in this quasi-continuum, which may occur as a result of nonadiabatic transitions from the 1p state, the principal mechanism of metastability quenching proves to be the Stark process

$$e + (\bar{p}\alpha e)_{nl} \rightarrow e + (\bar{p}\alpha e)_{n,l-1}\,, \tag{96}$$

operating with a rate of $\sim 10^{10}$ s^{-1}. The electron and the atomcule confined in the bubble sometimes collides with one another, and the processes (96) proceed.

The radiative $(1p \rightarrow 1s)$ and $(1p \rightarrow 2s)$ transition rates for the electron in a bubble are of the order of 10^6 s^{-1}, and therefore these transitions may also prove to be significant. For instance, an antiproton deexcitation cascade via an electron bridge is a possibility: the antiproton transfers the energy to the weakly bound electron which radiates it to return to the initial state. It is also evident that relaxation processes involving the emission of phonons may also play an important role.

One can see that several explanations for experimental data are possible in the context of the bubble model. In our view, however, there is little point in going now into details because the data are insufficient and indirect. Additional and more direct experiments are called for (see Section 10).

8. Electronic states of an ioncule for low helium densities

An atomcule possesses a dipole moment

$$\mathbf{d} \approx -\mathbf{R} \tag{97}$$

and therefore, apart from the ground bound electronic state which goes into the state of an H^- ion as $R \rightarrow 0$, there exist excited bound states (Fig. 15). An immobile dipole composed of charges $Z_1 = +1$ and $Z_2 = -1$ possesses, for $d > d_0 \approx R_{FT} = 0.64$ a.u. (i.e. $R > R_{FT}$), an infinite number of bound states [217] (a quasi-continuum), which are forced out into the continuum in portions having an infinite number of levels in each with a decrease in R.

In our case, instead of a point charge $Z = +1$ there is a He^+ ion with a deeper potential well than that of a point charge. That is why one bound H^--like state persists as R is reduced to $R = 0$. Others are forced out into the continuum as before. As this takes place, the corresponding critical values R_c at which infinite portions of the bound states are forced out into the continuum decrease in comparison with R_c for a point charge. In the limit $R \rightarrow \infty$, all these states go over into the ground and excited states of a helium atom.

Due to the rotation of an atomcule, all these states become quasi-stationary, because the Auger process (88) involving

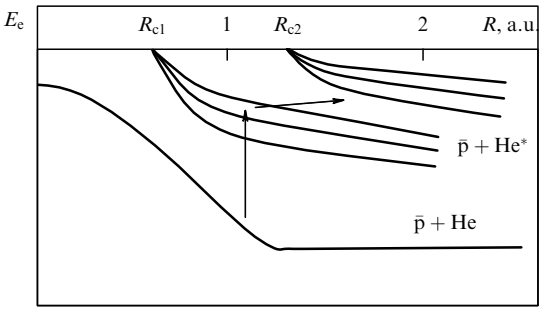

Figure 15. Electronic terms of an ioncule $(\bar{p}\alpha ee)$. The arrows indicate the Auger transitions to the quasi-continuum of Efimov states and also the subsequent transitions to other states in the quasi-continuum.

the ejection of a weakly bound electron is made possible under the action of Coriolis and centrifugal forces. The rate $\Gamma_A^{(g)}$ of the Auger transition (88) is calculated in the Appendix (Section IV) for the ground electronic state of the ioncule and the nearly circular antiproton orbits that hold the greatest interest; its dependence on R is given in Table 3. The excited states are also considered in the Appendix (Section V).

The rate of process (88) steeply rises with a decrease in the ioncule ionization potential I, hence the explanation for the character of its dependence on R. It follows that the electron excitation

$$(\bar{p}\alpha ee) \rightarrow (\bar{p}\alpha ee)^* \tag{98}$$

will, in the course of antiproton orbit diminution accompanying (72), be more likely than the ionization processes (88), because in the latter case the energy transferred from the nuclei to the electron will be higher. The excited state spectrum is rather dense (Appendix, Section V), and therefore it may be treated as continuous when estimating the excitation rate (98). A similar example is the excitation of an atom to the quasi-continuum of Rydberg states [100, 218] or the photorecombination to these states [230]. Consequently, the excitation rate $\Gamma_{ex}(R)$ can be estimated using the formula for $\Gamma_A^{(g)}$ from the Appendix (Section IV), by taking the separation between the ground state and the nearest excited energy level as the ionization potential $I(R)$. The probability that an ioncule will remain in the ground electronic state during its deexcitation (72) is estimated by the formula

$$W_0 \sim \exp(-B), \quad B = \int_0^\infty \frac{\Gamma_{ex}(R)\,dR}{\dot{R}}\,,$$

where

$$\dot{R} = \frac{|\dot{\varepsilon}|}{d\varepsilon(R)/dR}\,,$$

and $\dot{\varepsilon}$ is the average rate of variation of the ioncule internal energy $\varepsilon(R) \approx -1/(2R)$ due to processes (72). On the strength

Table 3. $(\bar{p}\alpha ee) \rightarrow (\bar{p}\alpha e) + e$ Auger decay rates for an ioncule in the ground electronic state for circular antiproton orbits (R is the distance between $\bar{p}$ and α).

R, a.u.	0.2	0.3	0.4	0.5	0.6	0.7	0.8	0.9
$\Gamma_A^{(g)}$, s^{-1}	5×10^{14}	3×10^{14}	2×10^{14}	1×10^{14}	2×10^{11}	8×10^9	1×10^6	6

of the Appendix (Sections III and IV) we conclude that in liquid helium $B \sim 10$. Since B is inversely proportional to N, then $W_0 \approx 0$ for all densities. The direct excitation (98) occurs primarily as a result of two- and three-photon transitions ($m_1 \geqslant 2$; see the Appendix, Section IV). Following the direct deexcitation, single-photon and diffusive transitions (see the review [190]) are made inside the quasi-continuum, with the result that the weakly bound electron finds itself in the long-lived states (see the Appendix, Section V) with an ionization potential

$$I_{ex} \sim 0.1 \text{ eV}, \tag{99}$$

an electron cloud dimension

$$r \sim \frac{1}{\sqrt{I_{ex}}} \sim 20 \text{ a.u.}, \tag{100}$$

and sufficiently large quantum numbers

$$l_{ex} \sim n_{ex} \geqslant 2. \tag{101}$$

In summary of this section we note that, since variational calculations (like in Ref. [213]) overrate the energy [219], the true values of the ioncule ionization potential I exceed those given in Fig. 11. It is known from quantum-chemical computations (see, for instance, Ref. [254]) that the error in electronic energy evaluations may be as high as ~ 1 eV and is especially high in the domain of electronic structure transformation with $R \sim 1-2$ a.u. If, in our case, I is raised by ~ 1 eV, the ground electronic state of the ioncule becomes long-lived ($\tau > 10^{-6}$ s) and the transitions to the quasi-continuum become unlikely. Simultaneously, the low as it is probability of the direct mechanism (59) drastically decreases still further. It is evident that the predictions of the ioncule model heavily depend on the accuracy of calculations of I, but on the whole the 'scenario' remains invariable.

9. Basic ioncule properties. Comparison of the model with laser-spectroscopy data

As shown earlier, the resultant ioncule consists of a core — an atomcule with the dimensions (73) 'embedded' in the cloud of a weakly bound electron with the parameters (99) – (101). The lifetime τ_i of an ioncule in excited electronic states (Appendix, Section V) is high in comparison with the observed lifetime τ_m of antiproton metastability [202]:

$$\tau_i \gg \tau_m \sim 10^{-6} \text{ s}. \tag{102}$$

In the subsequent discussion we therefore assume that $\tau_i = \infty$.

Let us estimate the shifts of antiproton transition frequencies ω in an atomcule caused by its interaction with a weakly bound electron, i.e. the difference $\Delta\omega$ between the frequencies ω in an atomcule and an ioncule. By its physical meaning, ω is the frequency of antiproton revolution around a helium nucleus. Since $\omega \gg I_{ex}$, then according to the Born – Oppenheimer approximation we first need to calculate the corrections to the energy levels of an atomcule residing in the electric field $\mathbf{E} = \mathbf{r}/r^3$ of an immobile electron [219]:

$$E^{(2)} = \sum_n \frac{|V_{n0}|^2}{E_0 - E_n} \sim \frac{R^2 I_{ex}^2}{\omega} f^2 S^2. \tag{103}$$

Here, $\hat{V} = f\,\mathbf{RE}$, $f \sim 0.5$ is the factor that takes into account the screening [268] of the antiproton by the electron of the atomcule [in lieu of formula (97) we then have $\mathbf{d} = -f\,\mathbf{R}$], and $S \sim 0.5$ is the overlap integral of the radial wave functions of the atomcule. In expression (103), use was made of the estimate $1/r^2 \sim I_{ex}$ and account was taken of the fact that the main contribution to $E^{(2)}$ is made by the atomcule transitions to the states with the same number of zeroes of the radial wave function:

$$v_n = v_0, \qquad v = n - l - 1.$$

The effective potential energy of radial motion of an atomcule is of the form

$$U_{ef}(R) = U(R) + \frac{l(l+1)}{2\mu R^2} \approx \frac{1}{2}\mu\omega^2 (R - R_0)^2,$$

where $U(R)$ is the potential energy of the atomcule [213], $l = n - 1$ (for a circular state), and R_0 is the equilibrium radius of the circular orbit. We calculate $\Delta\omega$ for the dipole transition $\Delta l = 1$, $\Delta n = 1$ ($\Delta v = 0$). Let R_0 refer to the initial state. Then, for the final state one finds

$$U_{ef}(R) \approx \frac{1}{2}\mu\omega^2 (R - R_0)^2 + \frac{l\,\Delta l}{\mu R^2} \approx \frac{1}{2}\mu\omega^2 (R - R_0')^2.$$

Whence

$$\Delta R = R_0' - R_0 \sim \frac{l\,\Delta l}{\mu^2\omega^2 R_0^3} \sim \frac{n}{\mu^2\omega^2 R_0^3} \sim \frac{1}{\mu\omega R_0}. \tag{104}$$

Here, account was taken of the relationships

$$l \approx \mu R_0 v \sim n, \quad \omega \sim \frac{v}{R_0} \sim \frac{n}{\mu R_0^2},$$

where v is the relative velocity of $\bar{p}$ and α.

For a typical value of $\omega \sim 2$ eV, from expressions (103) and (104) we obtain

$$\frac{\Delta\omega}{\omega} \sim \frac{I_{ex}^2 R\,\Delta R}{\omega^2} f^2 S^2 \sim \frac{I_{ex}^2 f^2 S^2}{\mu\omega^3} \sim 10^{-5} - 10^{-6}. \tag{105}$$

This figure is of the order of the relative discrepancy between the experimental [220] and theoretical [221 – 225] values of antiproton transition frequencies ω. Hence it follows that in the laser-spectroscopy experiments [220] antiproton transitions in an ioncule were observed.

To conclude, in this section we show that 'ioncules' survived the laser action in the experiments by Yamazaki et al. [220].

To do this we first consider the electronic ground state of an ioncule (which is not populated in reality — see Section 8). The wave function of a weakly bound electron is written down in the approximation of a zero radius potential (ZRP) (see Ref. [226]):

$$\psi_0(\mathbf{r}) = \sqrt{\frac{\gamma}{2\pi}} \frac{\exp(-\gamma r)}{r}, \quad \frac{\gamma^2}{2} = I. \tag{106}$$

In this case, the atomcule potential is replaced with the boundary condition

$$\lim_{r \to 0} \left[\frac{1}{r\psi} \frac{\mathrm{d}}{\mathrm{d}r}(r\psi)\right] = -\gamma. \tag{107}$$

Then, the rate of the ioncule ionization in the field $E = E_0 \cos(\Omega t)$ becomes [226]

$$\lambda_i^{(g)} = \frac{2^{5/2}\gamma E_0^2}{3\Omega^{5/2}} . \quad (108)$$

The excited states (99) – (101) obey the strong inequality

$$\Omega \gg I_{ex} \quad (109)$$

(in Ref. [220], advantage was taken of a resonant field $\Omega \approx \omega \sim 2$ eV). In this case, when moving in its orbit (if recourse is made to the classical analogy), an electron experiences small-amplitude oscillations ($\sim E_0/\omega^2$) under the action of the laser field. On the average, its energy does not change, i.e. ionization does not occur. It does take place in the rare cases that the electron comes close to the nucleus [227 – 232]. From this follows an estimate for the rate of laser ionization of an ioncule in an excited electronic state:

$$\lambda_i^{(ex)} \sim \lambda_i^{(g)} g , \quad (110)$$

where the factor $g = \psi_{ex}^2(0)/\psi_0^2(0) \leqslant 10^{-4}$ is evaluated in the Appendix (Section V).

In Ref. [220], use was made of the laser field with the intensity $E_0 \sim 4\times 10^3$ V cm^{-1}. From expressions (108) and (110) we then obtain

$$\lambda_i^{(g)} \sim 2 \times 10^7 \text{ s}^{-1} , \quad \lambda_i^{(ex)} \leqslant 10^3 \text{ s}^{-1} . \quad (111)$$

Consequently, the ground-state 'ioncules' in Ref. [220], if any were present, would have been fully ionized to become 'atomcules' in a time τ_m from inequality (102), whereas nothing happens to excited ioncules.

10. Conclusions

Experiments on exotic atoms (EAs) provide valuable information on the properties of particles and nuclei. They allow highly accurate verification of the following subjects of inquiry:

— quantum electrodynamics;

— the standard electroweak model (and its generalization in the experimental quest of rare decays);

— the chiral perturbation theory (the phenomenological theory of nuclear forces at low energies);

— theoretical models of atomic and molecular processes involving EAs;

— theoretical calculations of few-body systems;

— *CPT* invariance;

— the equivalence principle for antimatter.

Certain of the findings in the physics of EAs have come to underlie fields of practical importance:

— meson chemistry (the study of the kinetics of chemical processes involving atoms and molecules 'labelled' by muons and pions, analysis of materials properties, etc.);

— the muon spin relaxation method (the investigation of local magnetic fields in materials, which is of significance, for instance, for HTSC physics).

Research-oriented intense 14-MeV neutron sources can be devised on the basis of the muonic catalysis phenomenon.

Early in the review we drew a general picture of EA research. Then, we considered in detail certain of the lines of research and specific problems that still remain unsolved and provided plausible answers to them. Among these are:

— the problem of the anomalous width of the 2p state of kaonic helium;

— the problem of antihydrogen atom production in *CPT*-invariance verification experiments;

— 'the muonic helium puzzle' (see Section 2.2.2 and the end of this section).

The greater part of our review is concerned with the problem of exotic helium metastable states.

The phenomenon of the metastability inherent to heavy particles ($\bar{p}, \pi^-, \mu^-, K^-, ...$) in matter, discovered 40 years ago [195 – 202], is being studied intensively in several laboratories [207, 220, 233, 234]. The Condo model [203, 204], which underlies the theory of this phenomenon, calls for refinement. The point is that the model does not agree with experiments on metastability quenching by impurities and also with the data for pure helium: the observed quenching cross sections and rates are considerably above those calculated in the context of a neutral 'atomcule' ($\bar{p}\alpha e$) model. In Refs [205, 206] and in our review the 'ioncule' model is discussed, which retains Condo's principal statement justifying the metastability on the basis of circular orbits. In lieu of the atomcule, we consider a negatively charged ioncule ($\bar{p}\alpha ee$).

We now summarize the main implications of this ion model (for definiteness, antiprotons will be referred to).

(1) The deceleration of $\bar{p}$ in helium persists down to thermal energies $\varepsilon \sim T$.

(2) On reaching $\varepsilon \sim T$, a 'primary ioncule' with $\varepsilon \sim -T$ originates in a three-body collision (71).

(3) The multistep recombination (72) produces an ioncule ($\bar{p}\alpha ee$) with some distance (73) between the $\bar{p}$ and α and the electron in a weakly bound excited state (99) – (101).

(4) The time (102) of Auger ionization (88) of the ioncule is long, which allows it to be considered as stable in the course of experiments.

(5) The difference (105) in the antiproton transition frequencies ω characteristic of an atomcule and an ioncule to an order of magnitude coincides with the discrepancy between the observed and calculated values of ω for the atomcule. It seems likely that this will not allow the acquisition of new information on the electromagnetic nature of an antiproton from spectroscopic experiments with antiproton helium (which is discussed in Refs [207, 222, 269]).

(6) The large observed cross sections for metastability quenching by impurities in helium suggest that there exists a long-range interaction between antiproton helium and an impurity atom or molecule, which is absent in the case of an atomcule ($\bar{p}\alpha e$) and is present in the case of an ioncule ($\bar{p}\alpha ee$). Therefore, experiments with impurities count in favor of the ioncule model.

(7) The ioncule model provides a natural explanation why the metastability exists only in helium.

(8) An outcome of the ioncule model is the bubble model, which provides a qualitative explanation for the metastability features in pure helium of arbitrary density.

Let us discuss the experiments in which the ioncule model could be verified.

The first experiment is to be staged with kaonic helium. For a helium number density $N > N_1 = 5 \times 10^{20}$ cm^{-3}, $\lambda_r > 1/\tau_K$ according to formula (74), where $\tau_K = 1.2\times 10^{-8}$ s is the K^--meson lifetime. That is why the time spectrum of the particles resulting from the capture of kaons

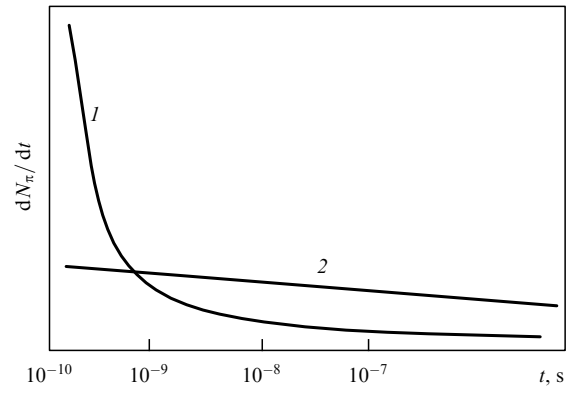

Figure 16. Qualitative shape of the time spectra of the products formed by the nuclear capture of negative kaons in helium: (*1*) $N \gg N_1$; (*2*) $N \ll N_1$; $N_1 = 5 \times 10^{20}$ cm^{-3}.

by nuclei should show up as curve *1* in Fig. 16. Kaonic helium atoms are produced in this case, with the result that most of the kaons disappear in a time of $\sim 10^{-10}$ s, and a small fraction of the kaons ($\sim 2\%$) decay as free particles in circular Condo orbits in a time τ_K. With a decrease in density (curve *2*), λ_r becomes small and kaons decay in a time τ_K in flight, without producing the atoms. This experiment is intended to verify the recombination mechanism of production of exotic helium (see Section 4). Formula (74) and the magnitude of N_1 should be refined in subsequent calculations. The experiment with kaons is preferable to that with stable antiprotons, because at low helium densities the direct mechanism (59) acquires a significance (its rate is linear in the helium number density N). For kaons, the transition from curve *1* to curve *2* with decreasing helium number density N takes place in a relatively narrow interval.

The conception of another experiment is illustrated in Fig. 17. Antiprotons are brought to rest in a helium target with a number density of $\sim 5 \times 10^{21}$ cm^{-3} containing an admixture of oxygen (O_2) with a number density of $\sim 5 \times 10^{16}$ cm^{-3}. In these conditions, the 'ioncules' bearing antiprotons in metastable states are rapidly disrupted in collisions with oxygen molecules (see Table 2), which is described by curve *1*. Curve *2* shows antiproton stopping events followed by a laser pulse after a time of $\sim 10^{-6}$ s, like in

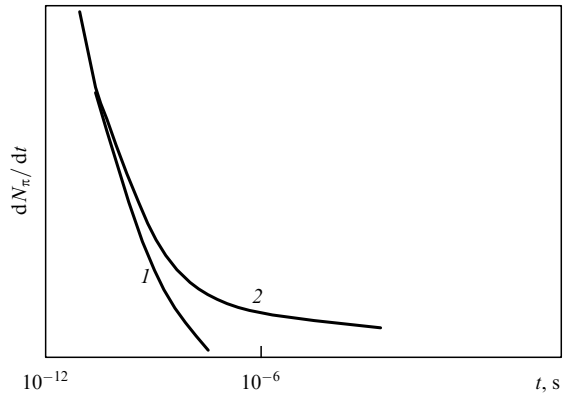

Figure 17. Time spectra (qualitative curves) of antiproton annihilation products (DAT spectra) in helium containing an admixture of oxygen: (*1*) ordinary $\bar{p}$ stopping events in helium; (*2*) $\bar{p}$ stopping events followed by a laser pulse disrupting 'ioncules'.

the experiments by Ketzer et al. [270]. Under the action of this pulse, the 'ioncules' lose the weakly bound electrons to turn into 'atomcules'. The quenching cross section drops by nearly two orders of magnitude (see Table 2), and the metastability is regained. The laser parameters estimated from expression (110) are as follows: a pulse duration of $\sim 10^{-8}$ s, a frequency of ~ 0.1 eV (CO_2 laser), and a power flux density $S \sim 10^5$ W cm^{-2}.

The third experiment is intended to verify the bubble model. If the pressure of liquid helium is raised to several tens of bars, the bubble radii will become significantly smaller and the 2s and 2p levels (see Fig. 10) will shift upwards by ~ 0.3 eV. The (37, 34) state will move away from the resonance with electron transitions (see Section 7) to acquire metastability: instead of the dependence given in Fig. 6, we will obtain a dependence similar to that in Fig. 5. It would also be of importance to measure the cross section of the process (59) in experiments with slow antiprotons.

We now turn to the discussion of the muonic helium problem posed in Section 2.2.2. This problem is easily solved if it is assumed that the resonance observed in Refs [83–85] corresponds not to the $2s \to 2p$ transition, but to the transition from a metastable circular ($l = n - 1$) or nearly circular Condo state to a rapidly decaying one, which is completely similar to the previously discussed resonance transitions in antiproton helium, discovered by the Yamazaki group [239].

According to the estimate (74) (in which the replacement $m_p \to m_\mu$ should be made), at room temperature, as was the case with all previously discussed experiments with muonic helium, the rate of ioncule production by the recombination mechanism (71) is given by (in s^{-1})

$$\lambda_r = (2 \times 10^6)\, p^2\,, \tag{112}$$

where p is the helium pressure (in bars). We showed in Sections 3 and 4 that a muon first thermalizes and only later ends up in a bound state. The type of the state depends on the helium pressure p: an ioncule for high pressures, and an atomcule for low ones. In fact, when approaching the next helium atom, a thermalized muon polarizes it and is thereby accelerated to an energy of ~ 1 eV. Reference to Fig. 2 shows that the cross section for atomcule production by the direct mechanism (59) is of the order of $\sigma_d \sim 10^{-18}$ cm^2, and therefore the atomcule production rate is estimated as

$$\lambda_d \sim 10^7 p\,. \tag{113}$$

From expressions (112) and (113) it may be concluded that 'ioncules' are produced for $p > p_c \approx 5$ bar. At first, the highly excited states $|\varepsilon| \sim T$ are populated; attained later, as a result of the processes (72), are the levels

$$n \sim n_0 = \sqrt{\frac{m_\mu}{m_e}}$$

with the orbit dimension (73). For $p < p_c$, the three-body ioncule production mechanism (71) becomes unlikely. At these pressures 'atomcules' are produced immediately in the $n \sim n_0$ states [97, 98, 214]. The spacing of the neighboring energy levels in the 'atomcules' (μHe) comprises

$$\omega \approx \frac{m_\mu}{n^3}\,.$$

The binding energies in such states of (μHe) and ($\bar{p}$He) are approximately equal and close to I_{He}, and therefore

$$\frac{\omega_\mu}{\omega_p} \sim \frac{n_0^p}{n_0^\mu} \sim \sqrt{\frac{m_p}{m_\mu}} \sim 3\,.$$

It follows that $\omega \sim 5$ eV for muonic 'atomcules' (μHe).

Hence we conclude that the $\Delta E \approx 1.6$ eV resonance observed in Refs [83–85] corresponds to highly excited states with $n \sim 20$, i.e. to 'ioncules'. That is why for low pressures $p \ll p_c$, when 'ioncules' are not produced, the resonance should not be observed, which agrees with Ref. [76]. The time spectra of the form $\exp(-\lambda_0 t)$ observed in Refs [87, 88] closely correspond to the DAT spectra recorded for other particles [195–202] and describe the decay of metastable Condo states in muonic 'ioncules' (μHe). Therefore, the metastable Condo states for muons in helium were originally observed in the experiments of Refs [87, 88]. Like for antiprotons [233, 234], the lifetime of these states manifested in the time spectra depend only slightly on the helium pressure. As for the 2s states, in the experiments of Refs [87, 88] they did not make a contribution to the microsecond regions of the time spectrum, because these states are short-lived at high pressures.

In Refs [94, 95], measurements were made on the time spectra of the K_α photons corresponding to the $2p \to 1s$ transition in muonic helium. As the time delay, values of

$$\tau = t(K_\alpha) - t(L) \tag{114}$$

were plotted on the abscissa, where $t(K_\alpha)$ and $t(L)$ were the detection times of the K_α and L photons originating within the same time gates (i.e. emitted by one and the same muon). This signifies that τ is counted from the point in time $t(L)$ at which an L photon was emitted, i.e. a muonic helium transited to the $n = 2$ state. The atoms that find themselves in the 2p state emit a prompt K_α photon. The atoms that find themselves in the metastable (at low pressures) 2s states emit, owing to the induced radiative transitions $2s \to 2p \to 1s$, photons after a much longer time (~ 1 μs). These atoms were responsible for the metastable 'tail' in the time spectra indicated [94, 95].

The delay time of a muon in the Condo states makes a contribution both to $t(K_\alpha)$ and to $t(L)$, and is therefore not involved in the time τ.

Therefore, in the experiments of Refs [83–85, 87, 88] and [94, 95] observations were made of absolutely different metastable states of muonic helium, and therein lies the source of apparent contradictions discussed in Section 2.2.2. It follows that the search for the genuine $2s \to 2p$ resonance, which is supposed to be within ±3 meV from the theoretical value (15), is still a topical problem.

In summary, we wish to express our deep appreciation to T Yamazaki, W Breunlich, L I Ponomarev, V S Lisitsa, V B Belyaev, L Simons, and M P Faĭfman for their helpful discussions.

11. Appendix

I. *CPT* invariance

The *CPT* theorem was established in Ref. [159]. The following hypotheses were assumed:

(1) space-time, particles, and fields are Lorentz-invariant;

(2) particles and fields are described by certain of the representations of the Lorentz group;

(3) the property of interaction locality is fulfilled, i.e. the Lagrangian density at a given point is composed of the fields taken at the same point.

Under these assumptions, the following property of the transition S matrix is established:

$$\widehat{U^+} S \widehat{U} = \widehat{S^+}, \quad \widehat{U} = \widehat{C}\widehat{P}\widehat{T}. \tag{I.1}$$

Hence it follows that the probability amplitude and the $|a\rangle \to |b\rangle$ transition probability obey the relationships

$$\langle b|S|a\rangle = \left(\langle \bar{a}|S|\bar{b}\rangle\right)^*,$$

$$W_{ab} = \left|\langle b|S|a\rangle\right|^2 = \left|\langle \bar{a}|S|\bar{b}\rangle\right|^2 = W_{\bar{a}\bar{b}}\,. \tag{I.2}$$

Here, $|\bar{a}\rangle = \widehat{U}|a\rangle$. It follows from the properties of the $\widehat{U}$ operator, which are demonstrated for particles of any spin, that the state $|\bar{a}\rangle$ is obtained from $|a\rangle$ by replacing all the particles with the antiparticles and reversing all the momenta. The particle helicities are not changed.

A property similar to Eqn (I.1) is established for the energy-momentum tensor, the electric current four-vector, etc. It follows from the consideration of the matrix elements of these quantities that the masses and lifetimes of particles and antiparticles are equal, while the charges and the magnetic moments are opposite. The proof can be found in Refs [286, 287]; technically, it is not complicated. Following primarily Refs [288, 289], we explain the physical meaning of the *CPT* symmetry and at the same time discuss the related physical phenomena.

We commence with a rotational transformation. From the space isotropy considerations we know that, if there is a cat M looking to the North, there also exists a cat M' looking to the South (following E Schrödinger, we will pursue thought experiments with these animals). The latter is obtained by rotating the former. We can state it in different terms. In the frame of reference $K = (x, y, z)$, the first cat resides in a quite specific way. By rotating this frame of reference, we obtain a new one: $K' = (x', y', z')$. By isotropy, K and K' are equivalent, and therefore there exists a cat M' that resides in a similar way in K'. In other words, if there is an equation to describe cats, then it possesses the property of isotropy. One of its solutions is the M cat. By applying a rotational transformation to M, we obtain M', which also satisfies the equation.

Now let us consider the reflection transformation. The K' frame, in which $x' = -x$, $y' = y$, and $z' = z$, is obtained from K by reflecting the coordinate axes in the (y, z) plane. The M' cat is located relative to the K' frame as is the M cat relative to the K frame and the former is obtained under a mirror reflection of the M cat in the (y, z) plane. The M' cat cannot be obtained from M by rotation, for its heart is located on the right-hand side. It is not evident that such cats do exist, at least they are scarce (in this connection we note an intriguing review [290], in which an attempt was made to trace the relation between the left–right symmetry violation in macrouniverse and microworld physics). It is easily verified that reflecting two axes ($x' = -x$, $y' = -y$, $z' = z$) produces a cat M' with a left-sided heart, which is obtained by rotating the M cat by 180° about the z-axis. It is evident from these examples that a reflection of an even number of axes is equivalent to rotation. An odd number of reflections results in objects not always occurring in nature. The reflection of three spatial axes (three mirror reflections)

$$x' = -x\,, \qquad y' = -y\,, \qquad z' = -z$$

is the inversion transformation P. A neutrino originating in the decay $\pi^+ \to \mu^+ + \nu_\mu$ is similar to a left-threaded screw: its spin is in opposition to its momentum ($\lambda = -1$ helicity). The inversion of a left-threaded screw and a $\lambda = -1$ neutrino results in a right-threaded screw and a right neutrino ($\lambda = +1$), respectively. Experiments show that such neutrinos are not found in nature, which is the cause of the parity violation in weak interactions. However, there exist antineutrinos with $\lambda = +1$, and therefore the laws of nature were assumed to be CP-invariant to retain the equivalence of particles and antiparticles [291 – 293]. According to this assumption, if there exists a cat M, then there exists a reflected anticat $\overline{M}$ (for simplicity, the inversion is sometimes replaced with a mirror reflection, because the two remaining reflections come to be equivalent to a rotation which is, by virtue of space isotropy, immaterial to the solution of the problem of whether the cats exist).

Experiments with kaons revealed a violation of the CP invariance [294] (at present, similar experiments on B mesons are being conducted and contemplated [295], including experiments at the B factories discussed in the Introduction). A consequence of this violation is, for instance, the fact that the rates of decay of one and the same particle into a group of particles and a group of their antiparticles

$$K_{\rm L}^0 \to {\rm e}^- + \pi^+ + \tilde{\nu}_{\rm e}\,, \quad K_{\rm L}^0 \to {\rm e}^+ + \pi^- + \nu_{\rm e}\,, \tag{I.3}$$

are slightly different from each other (by $\sim 0.6\%$) [286, 287]. Using this line of reasoning, A D Sakharov [296] advanced a hypothesis for the mechanism of Universe baryonic asymmetry (the observed overwhelming prevalence of matter over antimatter), which was subsequently treated in greater detail in Refs [297 – 299]. According to this mechanism, early in the expansion of the Universe, the nonstationarity of the metric was responsible for the production of superheavy bosons from vacuum [300, 301], which are involved in the Grand Unified Theories (GUT). Due to the CP invariance violation (and the baryon charge nonconservation inherent in the GUT), a trifle more matter than antimatter is produced in their subsequent decays. Next, owing to the annihilation of matter and antimatter, a huge quantity of photons originates and there remains an excess small fraction of the matter, which is consistent with present-day observations.

It seems as if the CP invariance violation signified the disappearance of symmetry between matter and antimatter, but this is wrong. The CPT invariance is the 'last stronghold' of this symmetry, and its violation has not been discovered up to the present. To each point of the Minkowski space corresponds a light cone (Fig. 18). The M cat follows trajectory *1*, and the inverted $\overline{M} = \widehat{C}\widehat{P}M$ anticat (the one with a right-sided heart) follows trajectory 2. Its future resides in the upper light cone. The points B, L, and D in the world lines denote the cats' births, lives, and deaths. CP invariance violation implies that the organism of the $\overline{M}$ cat is different from that of the M cat in some respect, for instance, its pulse rate may be lower. Similarly, the products of reactions (I.3) (which fly within the upper light cone) are slightly different, with the effect that the rates of these decays are also somewhat distinguished.

We now consider the inversion transformation $K \to K'$ of the Minkowski space:

$$x' = -x\,, \quad y' = -y\,, \quad z' = -z\,, \quad t' = -t\,, \tag{I.4}$$

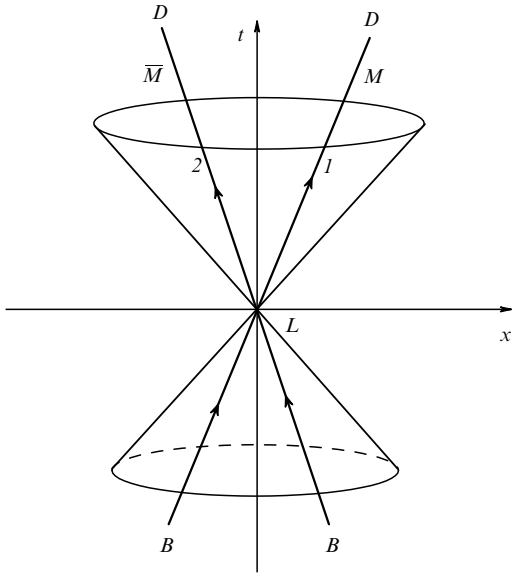

Figure 18. World lines of the cats M and $\overline{M} = \widehat{C}\widehat{P}M$.

which is also referred to as a 'weak' reflection, or the PT transformation. The idea of subsequent reasoning is that an even number (four) of reflections (I.4) come to be equivalent to a rotation. The PT transformation applied to the M cat is therefore surmised to give a genuinely existing M' cat.

The first three transformations in the set (I.4) produce an inverted (right-hearted) cat, while the last one produces a cat moving back in time (Fig. 19). From the viewpoint of an observer stationed in the K frame, the $\overline{M}$ cat lives like in a movie shown in reverse. At point D, the $\overline{M}$ cat is collected from dust and regains its soul. Next it grows younger to disappear into the womb of its mother at point B. As an explanation, we recall that considered here and in earlier text were active transformations, whereby the particles of the M cat took up new positions prescribed by the transformation, and in this way the new M' cat was 'assembled'. The same

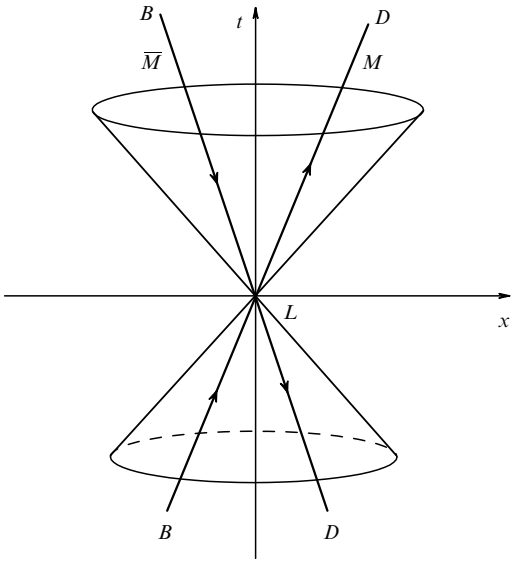

Figure 19. World lines of the cats M and $\overline{M} = \widehat{C}\widehat{P}\widehat{T}M$.

was performed on the coordinate axes to construct the K' frame. The M' cat is located and moves in the K' frame just as the M cat does in the K frame. In particular, its future corresponds to increasing t'. In this connection we note that the upper and lower cavities of the light cone are initially equivalent. For a given object, the future corresponds to that direction along its world line whereby it goes over from less to more likely events. For instance, a stone falling into water is a less likely state. A stone lying at the bottom of a river, whose energy went into the thermal motion of the molecules of the calming water, is a more likely state possessing a higher entropy.

In reality, the $\overline{M}$ cat is an unclosed system and can live in the above way on condition that either it is completely isolated from the ambient world or the entire Universe is subjected to the transformation (I.4). In practical situations, there always exists at least a weak action on $\overline{M}$ from the side of the ambient world (for instance, an observation, i.e. photon scattering). Owing to the exponential recession of molecular trajectories [302, § 33, 34], i.e. the Lyapunov instability of this motion, this external action is responsible for a total collapse of the above sequence of events: instead of D, L, B for the $\overline{M}$ cat, the D, L, D sequence would result (we do not discuss the annihilation of the $\overline{M}$ cat, regarding it as a weak surface effect or implying a confinement in magnetic traps, etc.). Reverting to the example with water, this corresponds to imparting an upward-directed velocity to the stone. Owing to dissipation, it will never escape from the water (everything would occur in the required reverse order only if the velocities of all the molecules of the water, the stone, the air, etc. were reversed at $t = 0$). After the above relaxation, the future of the $\overline{M}$ anticat and the stone (i.e. the most probable states) will belong to the upper cavity of the light cone corresponding to a rise in the total entropy of the Universe and, hence, to the direction of the world time t (the so-called 'time arrow').

We now explain why the $\overline{M}$ anticat is depicted in Fig. 19. In the space inversion $\widehat{P}$, out of a particle with an energy ε and momentum $\mathbf{p}$ there results another particle with an energy ε and momentum $-\mathbf{p}$. Similarly, the weak reflection (I.4) produces a particle with an energy $E = -\varepsilon < 0$ and a momentum $\mathbf{P} = -\mathbf{p}$ [because $(E, \mathbf{P})$ is a four-vector]. A body with a negative energy is absolutely unstable. In collisions with other bodies and in the emission of light, it loses energy in an uncontrollable way to occupy progressively lower energy levels. According to observations, such bodies that serve as inexhaustible energy sources do not exist in nature. Hence, the result of the weak reflection was a body M' not occurring in nature. We came across this effect earlier, when we obtained a right-threaded neutrino. In both cases, the reasons were similar: both transformations do not amount to rotation. More precisely, the active transformation (I.4) cannot be carried out on a physical object in a continuous way. If a body is accelerated, its world line may arbitrarily closely approach the upper light cone (see Fig. 19) but never would cross it. That is why this world line cannot be continuously transformed to the negative t-semiaxis, as is required in the active transformation (I.4).

To understand what resulted from the transformation (I.4), let us consider the motion of a body M' along the x-axis by taking advantage of Zeno's expedient. The body leaves point $x = x_1$ and arrives at point $x = x_2$ $(x_2 > x_1)$, i.e. for $t = t_1$ it vanishes at point x_1 to appear at point x_2 for $t = t_2 > t_1$. Moreover, let it have a charge $q_0 > 0$. The energy and charge variations at point x_1 are given by

$$\Delta E_1 = E_\mathrm{f} - E_\mathrm{i} = 0 - E = \varepsilon > 0\,,$$

$$\Delta q_1 = -q_0 < 0\,, \tag{I.5}$$

respectively. Similarly, at point x_2 we obtain

$$\Delta E_2 = -\varepsilon < 0\,, \quad \Delta q_2 = q_0 > 0\,. \tag{I.6}$$

Therefore, the energy lowered at point $x = x_2$ and heightened at point $x = x_1$, and quite the reverse with the charge. Instead of a nonexistent body M' with $E < 0$, we consider another real body $\overline{M}$ with a positive energy $E = \varepsilon > 0$ and a charge $\bar{q}$. It follows from expressions (I.5) and (I.6) that the new body moves as in Fig. 19. For $t > t_2$ and $t < t_1$, it does not exist. It is in existence only on the interval $t_1 < t < t_2$. The body $\overline{M}$ appears at the point $x = x_2$ at the point in time $t = t_2$, moves back in time to the point $x = x_1$ at which it disappears at the point in time $t = t_1$. The charge of this new body is $\bar{q} = -q_0$, i.e. the M cat produces the $\overline{M}$ anticat. Only for this character of motion and charge of the $\overline{M}$ body is it possible to reconcile the energy positiveness requirement for the $\overline{M}$ body with the energy and charge variations (I.5) and (I.6) at points x_1 and x_2. We see that the extermination of the M body with a negative energy is the production of $\overline{M}$ with a positive energy and an opposite charge.

Therefore, the transformation (I.4) in the Minkowski space with a signature $(+, -, -, -)$ is actually not a rotation. That is why, in order to obtain an existent body (or a new solution to the 'equation describing cats'), the PT transformation should be complemented by the charge C transformation which replaces particles by antiparticles. We note that the PT transformation is a rotation in Euclidean space with a signature $(+, +, +, +)$, and therefore antiparticles do not live in such a space. Hence it follows that the existence of antiparticles is a direct consequence of the fact that our space refers to the Minkowski type space.

Let us summarize the aforesaid. The CPT transformation of the M body has produced a new body $\overline{M}$.

(1) The $\overline{M}$ body is produced from M as a result of inversion $\widehat{P}$ of all its parts (the right-threaded screws are replaced with the left-threaded ones) and subsequent substitution of antiparticles for particles.

(2) The $\overline{M}$ body possesses an opposite momentum and moves backwards in time.

(3) The parts of $\overline{M}$ body execute the same relative motion as in M, and therefore the particle and antiparticle masses are equal (and the charges are opposite).

These three statements elucidate the significance of the quantum-mechanical relationship (I.2).

If a body $\overline{M}$ consisting of antimatter is subjected to a CPT transformation, the result is an inverted body M of matter moving back in time. Hence it is evident that the symmetry between matter and antimatter is conserved.

As to the backward motion in time, we emphasize once again that in the foregoing we were dealing with the symmetry properties of a Lagrangian and the mutual consistency between possible motions and solutions of quantum-field equations: if there exists some solution, on application of a CPT transformation to this solution there results a state that obeys the quantum-field equations once again and can be produced in experiments.

II. Calculation of the cross section for the direct production of antiproton helium

The calculation of the cross section σ_i will be performed in the context of the adiabatic perturbation theory (APT) [210, 211, 235, 245]. Since the characteristic orbital angular momentum of the nuclei in reaction (59) is large (~ 50) and the potential energy of their interaction is lower than the characteristic kinetic energy (~ 10 eV), $\bar{p}$ will be assumed to move along a rectilinear trajectory $\mathbf{R} = \mathbf{b} + \mathbf{v}t$ and the helium atom to be at rest at the origin. Nuclei move slowly ($v \sim 0.02$ a.u.) in comparison with electrons, and therefore the calculation should be performed in the adiabatic basis of electron wave functions (WFs). The ionization (59) takes place primarily for small impact parameters $b \leqslant 1$ (see Fig. 20), when the ionization potential $I = \gamma^2/2$ is smallest (see Fig. 11) and the condition

$$\gamma R \ll 1 \tag{II.1}$$

is fulfilled, which allows use of the ZRP approximation (106), (107) for the WF of the weakly bound electron, with $\gamma = \gamma(R) = \sqrt{2I(R)}$ in this case. The WF of the continuum spectrum takes the form [226]

$$\psi_{\mathbf{p}}(\mathbf{r}, t) = \exp(\mathrm{i}\mathbf{pr}) + f\frac{\exp(\mathrm{i}pr)}{r}\,, \quad f = -\frac{1}{\gamma + \mathrm{i}p}\,.$$

In the approximation adopted we thereby take into account the so-called radial transitions and disregard the Coriolis ones [211], which is acceptable in the range (II.1).

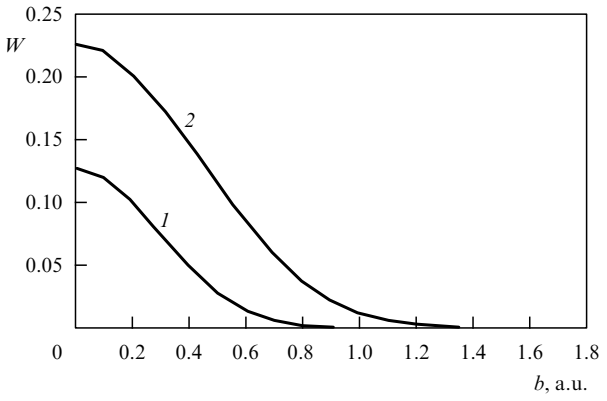

Figure 20. Probability W of ionization process (59) as a function of the impact parameter b in collisions of an antiproton with a helium atom: (*1*) collision velocity $v = 0.035$ a.u.; (*2*) $v = 0.1$ a.u.

We expand the WF of the weakly bound electron in the specified adiabatic basis $[\psi_0(\mathbf{r}, t),\ \psi_{\mathbf{p}}(\mathbf{r}, t)]$:

$$\psi(\mathbf{r}, t) = C_0(t)\psi_0(r)\exp\left(\mathrm{i}\phi_0(t)\right) + \int C_{\mathbf{p}}(t)\psi_{\mathbf{p}}(\mathbf{r}, t)\exp\left(\frac{-\mathrm{i}tp^2}{2}\right)\mathrm{d}\Gamma\,,$$

where

$$\mathrm{d}\Gamma = \frac{\mathrm{d}^3p}{(2\pi)^3}\,, \quad \phi_0(t) = \int_0^t I\big(R(t')\big)\,\mathrm{d}t'\,.$$

Whence and from the Schrödinger equation for $\psi(\mathbf{r}, t)$ we obtain the system of equations for the scattering amplitudes

$$\dot{C}_0 = -\int C_{\mathbf{p}} V_{\mathbf{p}} \exp(-\mathrm{i}\phi)\,\mathrm{d}\Gamma\,,$$

$$\dot{C}_{\mathbf{p}} = C_0 V_{\mathbf{p}}^* \exp(\mathrm{i}\phi) - \int V_{\mathbf{pp}'} C_{\mathbf{p}'}\,\mathrm{d}\Gamma'\,. \tag{II.2}$$

Here, the following designations are used:

$$\phi = \frac{1}{2}\int_0^t (p^2 + \gamma^2)\,\mathrm{d}t'\,,$$

$$V_{\mathbf{p}} = \left\langle 0 \left| \frac{\partial}{\partial t} \right| \mathbf{p} \right\rangle = \frac{2\sqrt{2\pi\gamma}\,\dot{\gamma}}{(\gamma^2 + p^2)(\gamma + \mathrm{i}p)}\,,$$

$$V_{\mathbf{pp}'} = \left\langle p \left| \frac{\partial}{\partial t} \right| \mathbf{p}' \right\rangle.$$

In the APT approximation we put $C_0 = 1$ and $C_{\mathbf{p}'} = 0$ in the second equation of the system (II.2), which gives the ionization probability and the cross section for process (59):

$$\sigma_i = \int_0^\infty 2\pi b W(b)\,\mathrm{d}b\,,$$

$$W(b) = \int |f(p, b)|^2\,\mathrm{d}\Gamma\,,$$

$$f(p, b) = \int_{-\infty}^{\infty} V_{\mathbf{p}}^* \exp(\mathrm{i}\phi)\,\mathrm{d}t\,.$$

To calculate the $f(p, b)$ integral of a rapidly oscillating function, recourse was made to a conventional technique described briefly in Section 3. One can see from Fig. 20 that the APT validity condition $W(b) \ll 1$ is fulfilled for collision velocities $v \sim 0.02$ a.u. typical of process (59). The cross section is represented by curve *2* in Fig. 2. With consideration of the $\bar{p}$–He interaction, the magnitude of the cross section should be increased by $\sim 50\%$. However, the ultimate conclusion that process (59) is insignificant retains its validity.

III. Rate of antiproton helium production by the recombination mechanism (71), (72)

By the multiphoton recombination theory [215, 216], one has

$$\lambda_r \sim \frac{4\pi}{3}\, r_T^3\, \frac{N}{\tau_T}\,, \qquad \tau_T \sim \frac{T^2}{D}\,. \tag{III.1}$$

Here, r_T is the Thomson radius determined from the relationship $|U(r_T)| = T$, $U(R) = -\alpha/(2r^4)$ is the polarization potential of the interaction between $\bar{p}$ and He, next

$$D = \frac{m_p^2 TN}{2m_\alpha}\langle v^3 \sigma_t(v)\rangle \approx \frac{3\sqrt{3\alpha}\,\pi^2 T^2 N m_p^{1/2}}{2^{5/2} m_\alpha} \tag{III.2}$$

is the coefficient of antiproton diffusion over the levels $|\varepsilon| \sim T$, v is the antiproton velocity, and

$$\sigma_t \approx \frac{\pi^2\sqrt{3\alpha}}{2^{3/2}\, m_p^{1/2} v}$$

is the transport cross section for the scattering of $\bar{p}$ by a helium atom in the polarization interaction approximation. A consequence of formulas (III.1) and (III.2) is the estimate (74).This finding can also be obtained from simpler con-

siderations [205]. The probability that $\bar{p}$ resides within the Thomson sphere surrounding some helium atom is of the order of $\omega_T \sim r_T^3 N$. Other helium atoms hit this sphere with a frequency $\nu \sim r_T^2 v_T N$. If $\bar{p}$ and He were equal in mass, $\bar{p}$ would, at every such impact, gain or lose an energy $\sim T$ and, consequently, $\lambda_r \sim v\omega_T$. In actuality $m_{\bar{p}} < m_\alpha$, and therefore the energy extracted is lower to give rise to an additional factor $m_{\bar{p}}/m_\alpha$.

IV. Rate of Auger ionization (88) of an ioncule in the ground electronic state

We calculate the rate $\Gamma_A^{(g)}$ for the $l = n - 1$ circular states, which hold the greatest interest, in the classical trajectory approximation for the nuclear motion. Within this approximation, $\bar{p}$ and an α particle orbit their common center of mass in circular trajectories with the radii

$$r_p = \alpha R\,, \quad r_\alpha = \beta R\,,$$

where $\alpha = m_\alpha/M$, $\beta = m_p/M$, and $M = m_\alpha + m_p$.

We go over to the frame of reference K' rotating with an angular velocity ω about the z-axis together with the nuclei. We direct the x-axis of the K' frame along the radius vector $\mathbf{R}$, then $\bar{p}$ and α will lie at the points in the x-axis with the coordinates

$$\mathbf{r}_p \equiv \mathbf{R}_a = (r_p, 0, 0)\,, \quad \mathbf{r}_\alpha \equiv \mathbf{R}_b = (-r_\alpha, 0, 0)\,.$$

The motion of a weakly bound electron in K' is described by the time-independent Hamiltonian

$$\hat{H} = \hat{T} + U(\mathbf{r}, \mathbf{R}) + V(\mathbf{r})\,, \tag{IV.1}$$

where $\hat{T} = -\Delta_r/2$, and $U(\mathbf{r}, \mathbf{R})$ is the interaction potential energy between an electron and an atomcule ($\bar{p}\alpha e$). The ionization (88) of a weakly bound electron takes place under the action of centrifugal and Coriolis forces, which are described by the operator [45, 211, 230]

$$V(\mathbf{r}) = \omega \hat{l}_z\,. \tag{IV.2}$$

Owing to the neutrality of an atomcule, its interaction ($U \sim -1/r^4$) with the outcoming electron is short-range ($\lim r^2|U| = 0$ for $r \to \infty$), and therefore the following formula is appropriate [271]:

$$\Gamma_A = \int 2\pi\delta(E_f - E_i)|V_{fi}|^2\, dv_f\,. \tag{IV.3}$$

It coincides in form with the formula derived within the framework of the perturbation theory, but in actuality is not of this kind (its physical significance and some of its applications are discussed, for instance, in Refs [15, 272, 273]; its implications are compared with experiment in Refs [274–276]). The Hamiltonian (IV.1) can be represented in two forms

$$\hat{H} = \hat{H}_i + \hat{V}_i = \hat{H}_f + \hat{V}_f\,, \tag{IV.4}$$

where

$$\hat{H}_i = \hat{T} + U\,, \quad \hat{V}_i = V\,, \quad \hat{H}_f = \hat{T} + \hat{V}\,, \quad \hat{V}_f = U\,.$$

In formula (IV.3), it was designated that

$$V_{fi} = \langle f|\hat{V}_i|i\rangle = \langle f|\hat{V}_f|i\rangle\,, \tag{IV.5}$$

where $|i\rangle$, $E_i = -\gamma^2/2 = -I$ and $|f\rangle$, E_f are the eigenvectors and the eigenenergies of the Hamiltonians H_i and H_f, respectively.

For $U(\mathbf{r}, \mathbf{R})$, in this work advantage was taken of a separable potential of the form [226]

$$U = \lambda_a|\varphi_a\rangle\langle\varphi_a| - \lambda_b|\varphi_b\rangle\langle\varphi_b|\,, \tag{IV.6}$$

where

$$a \equiv \bar{p}\,, \quad b \equiv \alpha\,, \quad 4\pi\lambda_a = 1.9341989\,, \quad 4\pi\lambda_b = 3.4606589\,,$$

$$\varphi_a \equiv \varphi(\mathbf{r}_a)\,, \quad \mathbf{r}_a = \mathbf{r} - \mathbf{R}_a\,,$$

$$\varphi_b \equiv \varphi(\mathbf{r}_b)\,, \quad \mathbf{r}_b = \mathbf{r} - \mathbf{R}_b\,,$$

$$\varphi(r) = \frac{\exp(-r)}{r}\,.$$

The first term in expression (IV.6) describes the electron repulsion from $\bar{p}$, and the second one the attraction to an α particle. The constants λ_a and λ_b were selected in such a way as to show the best correlation with the ioncule ionization potential I in the most significant interval $0 \leqslant R \leqslant 1.5$ (see Fig. 11). The potential (IV.6) allows an analytical calculation of Γ_A to be made. Its advantage, for instance, in comparison with zero-radius potentials lies in the fact that the latter gives rise to a nonphysical electron bound state whose energy tends to $-\infty$ as $R \to 0$ [217, 226].

The calculation of Γ_A is significantly facilitated in the momentum representation for $|i\rangle$ and $|f\rangle$. The result is of the form

$$\Gamma_A = \sum_{m=-m_1}^{-\infty} \Gamma_m\,, \quad \Gamma_m = 4\pi \int_0^{p_0} Q^2\, dp_z\,, \tag{IV.7}$$

where $p_0 = \sqrt{-\gamma^2 - 2\omega m}$, $m_1 = 1 + [I/\omega]$, and $[...]$ is the integral part of a number. Next, one has

$$Q = AJ_{|m|}(q\alpha R) + (-1)^m BJ_{|m|}(q\beta R)\,,$$

where J is the Bessel function, and $q = \sqrt{p_0^2 - p_z^2}$. The coefficients A and B appear in the expression for the WF of the electron bound state:

$$\psi_i = Ag(r_a) + Bg(r_b)\,,$$

where

$$g(r) = \left[\exp(-\gamma r) - \exp(-r)\right] r^{-1}\,.$$

They are found from the homogeneous system of equations

$$\left(I_{aa} + \frac{1 - \gamma^2}{2\lambda_a}\right) A + I_{ab}B = 0\,,$$

$$I_{ab}A + \left(I_{aa} - \frac{1 - \gamma^2}{2\lambda_b}\right) B = 0 \tag{IV.8}$$

and the normalization condition $\int \psi_i^2\, d^3r = 1$. The ionization potential $I = \gamma^2/2$ is determined from the condition that the determinant of the system (IV.8) is zero.

In the coordinate representation, the WF of the final state is of the form

$$\psi_f(\mathbf{r}) = \sqrt{\frac{q_\perp}{2}} \exp(im\varphi + ip_z z) J_{|m|}(q_\perp \rho)\,, \tag{IV.9}$$

where

$$q_\perp = \sqrt{2\left(E_\mathrm{f} - \omega m - \frac{p_z^2}{2}\right)},$$

ρ is the distance to the z-axis (the polar coordinate), φ is the angle between $\boldsymbol{\rho}$ and the x-axis, and m and p_z are the projections of the angular momentum and the momentum of the outcoming electron on the z-axis. In the momentum representation, the WF of $|\mathrm{f}\rangle$ becomes simpler:

$$\psi_\mathrm{f}(\mathbf{K}) = 2\pi^2\sqrt{q_\perp}\,\delta(K_z - p_z) \times \exp(\mathrm{i}m\phi)\,\delta\left(\frac{1}{2}K_\perp^2 - \frac{1}{2}p_z - E_\mathrm{f} + \omega m\right), \quad \text{(IV.10)}$$

where ϕ is the angle between the x-axis and the projection $\mathbf{K}_\perp$ of the $\mathbf{K}$ vector on the (x, y) plane.

The normalization conditions for WFs (IV.9), (IV.10) correspond to one particle in the normalization volume; a cylinder of radius ρ_0 and height L_z coaxial with the z-axis is convenient to use for the volume. Since $L_z \to \infty$, $\rho_0 \to \infty$, it may assumed that the following boundary conditions are fulfilled:

$$\varphi_\mathrm{f}(\rho = \rho_0) = 0\,, \quad \psi_\mathrm{f}(z + L_z) = \psi_\mathrm{f}(z)\,.$$

Then, the summation over the final states in expression (IV.3) takes the form

$$\int \mathrm{d}\nu_\mathrm{f} \ldots = \sum_m \int_{-\infty}^{\infty} \frac{\mathrm{d}p_z}{2\pi} \int_0^\infty \frac{\mathrm{d}q_\perp}{\pi} \ldots$$

In the laboratory frame of reference, the electron is embedded in a periodically varying field of a rotating atomcule, which can be expanded into Fourier harmonics:

$$U(\mathbf{r}, t) = \sum_{m=-\infty}^{\infty} \exp(\mathrm{i}\omega_m t) V_m(\mathbf{r})\,, \quad \text{(IV.11)}$$

where $\omega_m = \omega m$. The harmonic numbered m produces the ionization of an ioncule with a rate Γ_m (m stands for a quantum transition), which explains the physical significance of formula (IV.7).

The $\Gamma_\mathrm{A}^{(\mathrm{g})}$ values collected in Table 3 should be regarded as an estimate to an order of magnitude. The reason is that the outcoming electron moves in the field of the atomcule dipole, which does not satisfy the condition for the short-range character of interaction, required for the validity of formula (IV.3). The inaccuracies in $\Gamma_\mathrm{A}^{(\mathrm{g})}$ are larger for long R, when the Auger width is low. We note that a similar error should be involved in the Auger widths of the atomcule given in Ref. [247], in which recourse was made to a formula similar to expression (IV.3). In the case of the Auger ionization of an atomcule, the knocked-on electron moves in the Coulomb field of the $(\bar{\mathrm{p}}\alpha)$ ion.

V. Excited electronic states of an ioncule

We first consider the rotating frame of reference, like in Section IV.

In a weakly bound state, the electron binding energy is of the order of the electron – atomcule interaction energy ε:

$$|\varepsilon| \sim |U| \sim \frac{R}{r^2}\,. \quad \text{(V.1)}$$

Hence it follows that the characteristic dimension of the electron orbit is

$$r \sim R^{1/2}|\varepsilon|^{-1/2}\,, \quad \text{(V.2)}$$

and the probability that the electron finds itself in the vicinity of the atomcule is estimated as follows

$$g \sim \left(\frac{R}{r}\right)^3 \sim \left(R|\varepsilon|\right)^{3/2}. \quad \text{(V.3)}$$

When the electron is acted upon by the $m \neq 0$ components in the expansion (IV.11), ionization occurs. By analogy with relationships (109) and (110), the decay rate of an excited ioncule in a state with $|\varepsilon| \ll \omega$ is estimated by the expression

$$\Gamma_\mathrm{A}^{(\mathrm{ex})} \sim \Gamma_\mathrm{A}^{(\mathrm{g})} g\,. \quad \text{(V.4)}$$

Therefore, the lifetimes of the states with large quantum numbers (101) turn out to be long because of the smallness of the square of the wave function at the zero point. This is evident from formulas (IV.3) and (IV.5): in the integrand of the matrix element V_fi, the WF ψ_i of the excited electronic state oscillates rapidly. The Γ_A rate is therefore low, the singularity region $r \sim R$ of the potential energy making the main contribution to the rate.

The binding energy of an electron in the field of a dipole is expressed in terms of its quantum numbers by the formula [217, 279]

$$\varepsilon \sim -I \exp\left(-\frac{2\pi n_\mathrm{r}}{\sigma}\right), \quad \text{(V.5)}$$

where $I = \gamma^2/2$ is the ionization potential of the ground ($n_\mathrm{r} = 0$) state, $n_\mathrm{r} = 0, 1, 2, \ldots$ is the radial quantum number, and $\sigma = \sqrt{2(R - R_\mathrm{c})}$. The characteristic dimension of the electron cloud is given by

$$r_n \sim \frac{1}{\gamma} \exp\left(\frac{\pi n_\mathrm{r}}{\sigma}\right). \quad \text{(V.6)}$$

Expressions (V.1) and (V.2) follow from formulas (V.5) and (V.6), as does the estimate

$$g \sim \exp\left(-\frac{3\pi n_\mathrm{r}}{\sigma}\right). \quad \text{(V.7)}$$

Formulas (V.5) – (V.7) pertain to the states with a zero projection of the electron angular momentum on the dipole axis ($\Lambda = 0$). For $\Lambda \neq 0$, the g factor is well below the estimate (V.7) [279]. We draw the conclusion that the g factor is very small in the states (101), whence we arrive at the conclusion (102).

We now consider the laboratory frame of reference. It follows from expression (V.1) that the characteristic electron velocity equals

$$v_\mathrm{e} \sim \frac{\sqrt{R}}{r}\,,$$

and the frequency of its orbital motion is estimated as

$$\omega_\mathrm{e} \sim \frac{v_\mathrm{e}}{r} \sim \frac{\sqrt{R}}{r^2}\,.$$

For $r < r_1 = R^{1/4}\omega^{-1/2} \sim 3$ a.u., we have $\omega_e > \omega$, and therefore the electron is a fast subsystem and the atomcule is a slow one. For $r > r_1$, the situation reverses. Hence we conclude that the calculation of excited electronic states of an ioncule in the laboratory frame is more complicated than in the rotating frame of reference: if advantage is taken of the conventional Born–Oppenheimer (BO) approximation, the nonadiabatic terms cannot be neglected and should be rigorously taken into account. The advantages of the rotating coordinate system are compelling if our reasoning is within the framework of the approximation of classical nuclear trajectories. The limit of fast nuclei ($r > r_1$) corresponds to discarding the terms with $m \neq 0$ in the expansion (IV.11). This is analogous to the Kramers–Henneberger approximation [278, 279] known in the theory of atomic stabilization in a strong electromagnetic field.

The $V_0(\mathbf{r})$ potential corresponding to $m = 0$ is, for $r \to \infty$, the field of a quadrupole ($V_0 \sim 1/r^3$), which may contain only a finite number of weakly bound states. Going over to the rotating coordinate system makes it possible to take into account in an exact way all V_m for $m \neq 0$. As shown above, this leads to an infinite number of bound quasi-stationary states (for $R > R_c$). The theory [280] allows the terms with $m \neq 0$ to be approximately taken into account when performing the calculation in the laboratory frame. Based on Ref. [280] and Section 5, we conclude that the problem involves, in addition to r_1, one more characteristic distance

$$r_2 = (\Delta E)^{-1/2} \sim 10 \text{ a.u.}$$

For $r > r_2$, we have a polarization interaction between the electron and the atomcule:

$$U(r) = -\frac{\alpha_A}{2r^4}\,, \tag{V.8}$$

where $\alpha_A \sim R^2/(\Delta E)$ is the atomcule polarizability (we note that it is very high). Formula (V.8) describes the virtual atomcule transitions induced by the field of an immobile electron. For $r < r_2$, we have $\omega_e > \Delta E$, and the electron can no longer be treated as immobile. In the $R < r < r_2$ range, instead of formula (V.8) we therefore have [280]

$$U(r) \sim -\frac{R^2}{r^2}\,. \tag{V.9}$$

Estimates by the Levinson theorem [219] on the basis of the phase equation [281] allow the conclusion that there exist several weakly bound states in the potential (V.8), (V.9) (the relation between these and Efimov states [282] is traced in Ref. [280]). However, the conclusions of Ref. [280] apply to the ground state of the complex (in this instance, this is the ground $n = 1$ state of the atomcule). In the $n \gg 1$ states corresponding to the classical limit, the calculation should be performed in the rotating frame of reference, as discussed above. However, this statement is approximate, because the question of how to choose the optimal frequency Ω of rotation of the frame of reference arises. If the characteristic dimension r of the electron cloud is small enough, viz.

$$r < r_1\,, \tag{V.10}$$

then $\omega_e > \omega$. In this case, the BO approximation holds good, when the first stage involves consideration of the electron motion for immobile α and $\bar{p}$. It is evident that $\Omega = \omega$ should then be the choice. In combination with expression (V.1), the condition (V.10) is equivalent to $|\varepsilon| > \omega \approx 3$ eV. One can see that the choice $\Omega = \omega$ is correct for the ground electronic state of an ioncule (see Section 4).

For excited states, we have $|\varepsilon| \ll \omega$. In this case $\omega_e \ll \omega$ and the first stage should consider the motion of α and $\bar{p}$ in the field of an immobile electron. Since $R < r_1$, it may be assumed that $r \gg R$. The electron moves in the field of the dipole moment $\mathbf{d} = \langle \mathbf{R} \rangle$ of the Keplerian orbit described by the endpoint of the $\mathbf{R}(t)$ vector. What is more, this orbit precesses with a frequency ΔE owing to the screening by the strongly bound electron and the weak disturbance of the Coulomb degeneracy (see Section 2.6). Hence it follows that the correct choice is $\Omega = \Delta E$. For this K'-frame rotation frequency, the orbit precession in K' vanishes and the antiproton orbit becomes closed, i.e. the Coulomb symmetry is restored. There exists a quasi-continuum of electron bound states in the field of the $\mathbf{d}$ dipole. Since $\Delta E \ll \omega$, the true Auger-decay rate of excited electronic states will be many orders of magnitude lower than that estimated from expression (V.4).

The (n, l, m) states for fixed n and l are of equal parity $(-1)^l$, and therefore $\hat{d} = 0$ for an antiproton in the (n, l) state, because all matrix elements in this subspace of states vanish. In fact, for the orbits (99)–(101), the interaction with the weakly bound electron mixes the (n, l) states with close l, and therefore $\langle \mathbf{d} \rangle \neq 0$, as assumed above.

The above estimates for the characteristics of excited electronic states of an ioncule invite an additional, more rigorous substantiation. They should rather be considered as a supposition, though confirmed by experimental data (see Sections 5–7).

References

1. Wheeler J A *Phys. Rev.* **71** 143 (1947)
2. Fermi E, Teller E *Phys. Rev.* **72** 399 (1947)
3. Conversi M et al. *Phys. Rev.* **71** 209 (1947)
4. Zel'dovich Ya B, Gershteĭn S S *Usp. Fiz. Nauk* **71** 581 (1960) [*Sov. Phys. Usp.* **3** 593 (1961)]
5. Gershteĭn S S et al. *Usp. Fiz. Nauk* **97** 3 (1969) [*Sov. Phys. Usp.* **12** 1 (1969)]
6. Burhop E H S *Contemp. Phys.* **11** (4) 333 (1970) [*Usp. Fiz. Nauk* **106** 527 (1972)]
7. Kirillov-Ugryumov V G, Nikitin Yu P, Sergeev F M *Atomy i Mesony* (Atoms and Mesons) (Moscow: Atomizdat, 1980)
8. Balashov V V, Korenman G Ya, Eramzhyan R A *Pogloshchenie Mesonov Atomnymi Yadrami* (Absorption of Mesons by Atomic Nuclei) (Moscow: Atomizdat, 1978)
9. Hughes V W, Wu C S (Eds) *Muon Physics* Vols 1–3 (New York: Academic Press, 1975–1977)
10. Scheck F *Leptons, Hadrons and Nuclei* (Amsterdam: North-Holland, 1983)
11. Backenstoss G *Ann. Rev. Nucl. Sci.* **20** 467 (1970) [*Usp. Fiz. Nauk* **107** 405 (1972)]
12. Batty C J *Fiz. Elem. Chastits At. Yadra* **13** 164 (1982) [*Sov. J. Part. Nucl.* **13** 71 (1982)]
13. Batty C J *Rep. Prog. Phys.* **52** 1165 (1989)
14. Gershteĭn S S, Petrov Yu V, Ponomarev L I *Usp. Fiz. Nauk* **160** (8) 3 (1990) [*Sov. Phys. Usp.* **33** 591 (1990)]
15. Men'shikov L I, Somov L N *Usp. Fiz. Nauk* **160** (8) 47 (1990) [*Sov. Phys. Usp.* **33** 616 (1990)]
16. Petitjean C *Nucl. Phys. A* **543** 79c (1992)
17. Batty C J, Friedman E, Gal A *Phys. Rep.* **287** 385 (1997)
18. *Proc. Int. Symposium on Exotic Atoms, Molecules and Muon Catalyzed Fusion* (*EXAT'98*) (Ascona, Switzerland, July 1998); *Hyp. Int.* **118/119** (1999)
19. *Proc. Workshop 'Physics and Detectors for DAΦNE'* (Frascati, Italy, 1999); *Frascati Phys. Ser.* **XVI** (1999)

20. *Proc. Int. Symposium on Muon Catalyzed Fusion and the Physics of Exotic Atoms and Molecules (μCF-95)* (Dubna, 1995); *Hyp. Int.* **101/102** (1996)
21. Nagamine K et al. *Hyp. Int.* **101/102** 521 (1996)
22. Dzhelepov V P et al. *Zh. Eksp. Teor. Fiz.* **50** 1235 (1966) [*Sov. Phys. JETP* **23** 796 (1966)]
23. Bystritskiĭ V N et al., Preprint OIYaI No. D-12690 (Dubna: Joint Institute for Nuclear Research, 1979); *Pis'ma Zh. Eksp. Teor. Fiz.* **31** 249 (1980) [*JETP Lett.* **31** 227 (1980)]
24. Kammel P *Hyp. Int.* **119** 323 (1999)
25. Hayano R S et al. *Phys. Lett. B* **231** 355 (1989)
26. *Institut Yadernoĭ Fiziki im. G I Budkera SO RAN. Ezhegodnyĭ Otchet — 1999* (G I Budker Institute of Nuclear Physics, Siberian Branch of the Russian Academy of Sciences: Annual Report – 1999) (Novosibirsk: Izd. GNIs IYaF SO RAN, 2000)
27. Solodov E P *Frascati Phys. Ser.* **XV** (1999)
28. Aul'chenko V M et al. *Yad. Fiz.* **62** 2142 (1999) [*Phys. At. Nucl.* **62** 1976 (1999)]
29. Akai K et al. *Proc. 1999 Particle Accelerator Conf. (PAC-99)* (New York, 1999)
30. Guaraldo C et al. *Hyp. Int.* **119** 253 (1999)
31. Leon M, Bethe H A *Phys. Rev.* **127** 636 (1962)
32. Borie E, Leon M *Phys. Rev. A* **21** 1460 (1980)
33. Men'shikov L I, Ponomarev L I *Z. Phys. D: At., Mol. Clusters* **2** 1 (1986)
34. Koike T, Harada T, Akaishi Y *Phys. Rev. C* **53** 79 (1996)
35. Terada T P, Hayano R S *Phys. Rev. C* **55** 73 (1997)
36. Markushin V E *Phys. Rev. A* **50** 1137 (1994)
37. Reifenröther G, Klempt E *Nucl. Phys. A* **503** 885 (1989)
38. Reifenröther G, Klempt E *Phys. Lett. B* **245** 129 (1990)
39. Men'shikov L I *Yad. Fiz.* **63** 920 (2000) [*Phys. At. Nucl.* **63** 850 (2000)]
40. Faifman M P et al. *Frascati Phys. Ser.* **XVI** 637 (1999)
41. Day T B, Snow G A, Sucher J *Phys. Rev. Lett.* **3** 61 (1959); *Phys. Rev.* **118** 864 (1960)
42. Simons L M *Phys. Scripta T* **22** 90 (1988)
43. Vermeulen J L *Nucl. Phys. B* **12** 506 (1969)
44. Lisitsa V S, Sholin G V *Zh. Eksp. Teor. Fiz.* **61** 912 (1971) [*Sov. Phys. JETP* **34** 399 (1972)]
45. Demkov Yu N, Ostrovskiĭ V N, Solov'ev E A *Zh. Eksp. Teor. Fiz.* **66** 125 (1974) [*Sov. Phys. JETP* **39** 61 (1974)]
46. Men'shikov L I *Muon Catalyzed Fusion* **2** 173 (1988)
47. Bracci L, Fiorentini G *Nuovo Cimento A* **43** 9 (1978)
48. Ponomarev L I, Solov'ev E A *Pis'ma Zh. Eksp. Teor. Fiz.* **64** 129 (1996) [*JETP Lett.* **64** 135 (1996)]
49. Crowford J E et al. *Phys. Rev. Lett.* **56** 1043 (1986); *Phys. Rev. D* **43** 46 (1991)
50. Aschenauer E C et al. *Phys. Rev. A* **51** 1965 (1995)
51. Schottmuller J et al. *Hyp. Int.* **119** 95 (1999)
52. Ito T M et al. *Phys. Rev. C* **58** 2366 (1998)
53. Men'shikov L I, Ponomarev L I *Pis'ma Zh. Eksp. Teor. Fiz.* **39** 542 (1984) [*JETP Lett.* **39** 663 (1984)]; **42** 12 (1985) [*JETP Lett.* **42** 13 (1985)]
54. Breunlich W H et al., Preprint BNL BNL-21174 (Berkeley: BNL, 1986)
55. Jones S E et al. *Phys. Rev. Lett.* **56** 588 (1986)
56. Breunlich W H et al. *Annu. Rev. Nucl. Part. Sci.* **39** 311 (1989)
57. Ackerbauer P et al. *Hyp. Int.* **82** 243, 357 (1993)
58. Lauss B et al. *Hyp. Int.* **101/102** 285 (1996); **118** 79 (1999)
59. Sakamoto S, Nagamine K *Hyp. Int.* **101/102** 277 (1996)
60. Averin Yu P et al. *Hyp. Int.* **118** 111 (1999)
61. Kravtsov A V et al. *Muon Catalyzed Fusion* **2** 183 (1988)
62. Kravtsov A V et al. *Muon Catalyzed Fusion* **2** 199 (1988)
63. Chaplinski W et al. *Muon Catalyzed Fusion* **5/6** 59 (1990/91)
64. Gorelkin V N, Smilga V P *Zh. Eksp. Teor. Fiz.* **66** 1201 (1974) [*Sov. Phys. JETP* **39** 1586 (1974)]
65. Varlamov V G et al. *Nuovo Cimento B* **36** 131 (1976)
66. Bashkirov V A et al. *Pis'ma Zh. Eksp. Teor. Fiz.* **29** 302 (1979) [*JETP Lett.* **29** 271 (1979)]
67. Gurevich I I, Ponomarev A N "Myuonnoi spinovoi relaksatsii metod" ("Muon spin relaxation method"), in *Fizicheskaya Entsiklopediya* (Encyclopedia of Physics) Vol. 3 (Moscow: BSE, 1992) p. 226; Smilga V P, Belousov Yu M *Myuonnyĭ Metod Issledovaniya Veshchestva* (Substance Research with Muon Method) (Moscow: Nauka, 1991) [Translated into English: *The Muon Method in Science* (New York: Nova Science, 1994)]
68. Bin'ko V N et al. *Hyp. Int.* **87** 905 (1994)
69. Gorelkin V N, Soloviev V R, Dobretsov Yu P *Hyp. Int.* **101/102** 169 (1996)
70. Gorelkin V N, Konchakov A M, Kotova L P *Hyp. Int.* **87** 997 (1994)
71. Pikaev A K *Sovremennaya Radiatsionnaya Khimiya* (Modern Radiation Chemistry) Vols 1 – 3 (Moscow: Nauka, 1985, 1986, 1987)
72. Balin D V et al. *Pis'ma Zh. Eksp. Teor. Fiz.* **40** 318 (1984) [*JETP Lett.* **40** 1112 (1984)]
73. Men'shikov L I Preprint IAE-3810/12 (Moscow: Institute of Atomic Energy, 1983)
74. Faifman M P, Men'shikov L I *Hyp. Int.* **118** 187 (1999)
75. Kottmann F, in *Fundamental Interactions in Low-Energy Systems* (Ettore Majorana Int. Science Ser.: Physical Sciences, Vol. 23, Eds P Dalpiaz, G Fiorentini, G Torelli) (New York: Plenum Press, 1985) p. 481
76. Hauser P et al. *Phys. Rev. A* **46** 2363 (1992)
77. Zavattini E, in *Laser Spectroscopy: Proc. Second Int. Conf.* (Lecture Notes in Physics, Vol. 43, Eds S Haroche et al.) (Berlin: Springer-Verlag, 1975) p. 370
78. Udem T et al. *Phys. Rev. Lett.* **79** 2646 (1997)
79. Taqqu D et al. *Hyp. Int.* **119** 311 (1999)
80. Bernaben J, Ericson T E O, Jariskog C *Phys. Lett. B* **50** 467 (1974)
81. Feinberg G, Chen M Y *Phys. Rev. D* **10** 190 (1974)
82. Vorobyov G et al. *Hyp. Int.* **118** 13 (1999)
83. Carboni G et al. *Nuovo Cimento A* **34** 493 (1976)
84. Carboni G et al. *Nucl. Phys. A* **278** 381 (1977)
85. Carboni G et al. *Phys. Lett. B* **73** 229 (1978)
86. Borie E, Rinker G A *Phys. Rev. A* **18** 324 (1978); *Rev. Mod. Phys.* **54** 67 (1982)
87. Placci A et al. *Nuovo Cimento A* **1** 445 (1971)
88. Bertin A et al. *Nuovo Cimento B* **26** 433 (1975)
89. Carboni G, Pitzurra O *Nuovo Cimento B* **25** 367 (1975)
90. Mueller R O et al. *Phys. Rev. A* **11** 1175 (1975)
91. Cohen J S, Bardsley J N *Phys. Rev. A* **23** 46 (1981)
92. Cohen J S *Phys. Rev. A* **25** 1791 (1982)
93. Men'shikov L I, Ponomarev L I, Sukhanov L P *Z. Phys. D: At., Mol. Clusters* **7** 203 (1987)
94. Von Arb H P et al. *Phys. Lett. B* **136** 232 (1984)
95. Eckhause M et al. *Phys. Rev. A* **33** 1743 (1986)
96. De Vries C P, Oskam H J *Phys. Rev. A* **22** 1429 (1980)
97. Cohen J S, Martin R L, Wadt W R *Phys. Rev. A* **27** 1821 (1983)
98. Dolinov V K et al. *Muon Catalyzed Fusion* **4** 169 (1989)
99. Gol'danskiĭ V I, Firsov V G *Usp. Khim.* **40** 1353 (1971)
100. Bethe H A, Salpeter E E *Quantum Mechanics of One- and Two-Electron Atoms* (New York: Academic Press, 1957)
101. Landau L D, Lifshitz E M *Teoriya Polya* (The Classical Theory of Fields) (Moscow: Nauka, 1988) [Translated into English (Oxford: Pergamon Press, 1983)]
102. Landua R, Klempt E *Phys. Rev. Lett.* **48** 1722 (1982)
103. Dey W et al. *Nucl. Phys. A* **326** 418 (1979)
104. Leon M *Phys. Lett. B* **50** 425 (1974); *B* **53** 141 (1974); *Nucl. Phys. A* **260** 461 (1976)
105. Bradbury J N et al. *Phys. Rev. Lett.* **34** 303 (1975)
106. Wheeler J A *Rev. Mod. Phys.* **21** 133 (1949)
107. Diaz J A, Kaplan S N, Pule R V *Nucl. Phys.* **40** 54 (1963)
108. Cojocaru V et al. *Phys. Lett.* **20** 53 (1966)
109. Ganzorig Dz et al. *Nucl. Phys. A* **350** 278 (1980)
110. Frank F C *Nature* **160** 525 (1947)
111. Sakharov A D, Report of the P N Lebedev Physics Institute, USSR Academy of Sciences (Moscow: 1948)
112. Alvarez L W et al. *Phys. Rev.* **105** 1125 (1957)
113. Putvinskiĭ S V *Usp. Fiz. Nauk* **168** 1235 (1998) [*Phys. Usp.* **41** 1127 (1998)]
114. Golovin I N, Kadomtsev B B *At. Energ.* **81** 364 (1996) [*At. Energy* **81** 793 (1996)]
115. Alekseev P N et al. *Nucl. Eng. Design* **173** 151 (1997)
116. Alekseev P N et al. *At. Energ.* **79** 243, 327 (1995) [*At. Energy* **79** 651, 733 (1995)]
117. Karelin A I *Radiokhimiya* **38** 289 (1996)

118. Alekseev P N et al., Preprint IAE-6110/3 (Moscow: IAE, 1998)
119. Adamov E O et al. *At. Energ.* **82** 3 (1997) [*At. Energy* **82** 1 (1997)]
120. Okun L B *Leptony i Kvarki* (Leptons and Quarks) (Moscow: Nauka, 1981) [Translated into English (Amsterdam: North-Holland, 1982)]
121. Gorbunov D S et al., Preprint IYaI-0960/97 (Moscow: Institute for Nuclear Research, 1997)
122. http://www.jnf.kek.jp/
123. Dalitz R H, in *Proc. Conf. on Hypernuclear and Kaon Physics* (Ed. B Povh) (Heidelberg: MPI, 1982)
124. Dalitz R H *Strange Particles and Strong Interactions* (Oxford: Oxford University Press, 1962) [Translated into Russian (Moscow: IL, 1964)]
125. Kunselman R *Phys. Rev.* **134** B485 (1971); *Phys. Rev. C* **9** 2469 (1974)
126. Backenstoss G et al. *Phys. Rev. B* **43** 431 (1973)
127. Cheng S C et al. *Nucl. Phys. A* **254** 381 (1975)
128. Roberson P et al. *Phys. Rev. C* **16** 1945 (1977)
129. Roberts B L *Phys. Rev. D* **17** 358 (1978)
130. Negele J W *Phys. Rev. C* **1** 1260 (1970)
131. Bethe H A, Siemens P J *Nucl. Phys. B* **21** 589 (1970)
132. Schmidt R et al. *Hyp. Int.* **118** 67 (1999)
133. Deser S et al. *Phys. Rev.* **96** 774 (1954)
134. Trueman T L *Nucl. Phys.* **26** 57 (1961)
135. Beer G A *Hyp. Int.* **118** 3 (1999)
136. Toki H, Yamazaki T *Phys. Lett. B* **213** 129 (1988)
137. Toki H et al. *Nucl. Phys. A* **501** 653 (1989)
138. Sivukhin D V *Obshchiĭ Kurs Fiziki: Optika* (Textbook of General Physics: Optics) (Moscow: Nauka, 1980)
139. Toki H, Hirenzaki S, Yamazaki T *Nucl. Phys. A* **530** 679 (1991)
140. Hirenzaki S, Toki H, Yamazaki T *Phys. Rev. C* **44** 2472 (1991)
141. Iwasaki M, Trudel A, Celler A *Phys. Rev. C* **43** 2472 (1991)
142. Yamazaki T et al. *Z. Phys. A: Hadrons Nucl.* **355** 219 (1996)
143. Baird S et al. *Nucl. Phys. A* **392** 297 (1983)
144. Akaishi Y, Yamazaki T, in *Proc. Workshop 'Physics and Detectors for DAΦNE'* (Frascati, Italy, 1999)
145. Wiegand C E, Pehl R H *Phys. Rev. Lett.* **27** 1410 (1971)
146. Batty C J et al. *Nucl. Phys. A* **326** 455 (1979)
147. Caso C et al. *Eur. Phys. J. C* **3** 1 (1998); http://pdg.lbl.gov/
148. Fano U *Phys. Rev.* **124** 1866 (1961)
149. Bardsley J N *Phys. Rev. B* **1** 349 (1968)
150. *Nucl. Data Tables* **14** (1973)
151. Bour G et al. *Phys. Lett. B* **368** 251 (1996)
152. Meshkov I, Skrinsky A N *Nucl. Instrum. Meth. A* **379** 41 (1996)
153. Kartavtsev O I, Meshkov I N *JINR Rapid Communications* (Dubna, 1996)
154. Gabrielse G et al. *The Production and Study of Cold Antihydrogen* (CERN, 1997); http://hussle.harvard.edu/ atrap/
155. Halzscheiter M et al. *Nucl. Phys. B* **56** 336 (1997); http://athena.wednet.edu/project/document/proposal.html; http://varming.homecern.ch/varming/athena/publicathena.html
156. Budker G I, Skrinskiĭ A N *Usp. Fiz. Nauk* **124** 561 (1978) [*Sov. Phys. Usp.* **21** 277 (1978)]
157. Gabrielse G *Hyp. Int.* **44** 349 (1988)
158. Hughes R J *Hyp. Int.* **76** 3 (1993)
159. Pauli W, in *Niels Bohr and the Development of Physics* (Eds W Pauli, L Rosenfeld, V Weisskopf) (New York: McGraw-Hill, 1955); Lüders G *Det. Kon. Dan. Vid. Sel. Mat.-fys. Medd.* **28** 1 (1954)
160. Walraven J T M *Hyp. Int.* **76** 205 (1993)
161. Artsimovich L A *Upravlyaemye Termoyadernye Reaktsii* (Controlled Thermonuclear Reactions) 2nd ed. (Moscow: Fizmatgiz, 1963) [Translated into English (New York: Gordon and Breach, 1964)]
162. Dehmelt H G *Nature* **262** 777 (1976)
163. Hänsch T W, Schawlow A L *Opt. Commun.* **13** 68 (1975)
164. Minogin V G, Letokhov V S *Davlenie Lazernogo Izlucheniya na Atomy* (Laser Light Pressure on Atoms) (Moscow: Nauka, 1986) [Translated into English (New York: Gordon and Breach, 1987)]
165. Letokhov V S, Minogin V G, Pavlik B D *Zh. Eksp. Teor. Fiz.* **72** 1328 (1977) [*Sov. Phys. JETP* **45** 698 (1977)]
166. Andreev S V et al. *Pis'ma Zh. Eksp. Teor. Fiz.* **34** 463 (1981) [*JETP Lett.* **34** 442 (1981)]; *Zh. Eksp. Teor. Fiz.* **82** 1429 (1982) [*Sov. Phys. JETP* **55** 856 (1982)]
167. Kazantsev A P *Usp. Fiz. Nauk* **124** 113 (1978) [*Sov. Phys. Usp.* **21** 58 (1978)]
168. Doyle J M et al. *Phys. Rev. Lett.* **67** 603 (1991)
169. Luiten O J et al. *Phys. Rev. Lett.* **70** 544 (1993); Setija I D et al. *Phys. Rev. Lett.* **70** 2257 (1993)
170. Hänsch T W, Zimmermann C *Hyp. Int.* **76** 47 (1993)
171. Vasilenko L S, Chebotaev V P, Shishaev A V *Pis'ma Zh. Eksp. Teor. Fiz.* **12** 161 (1970) [*JETP Lett.* **12** 113 (1970)]
172. Letokhov V S, Chebotaev V P *Printsipy Nelineĭnoĭ Lasernoĭ Spectroskopii* (Nonlinear Laser Spectroscopy) (Moscow: Nauka, 1975) [Translated into English (Berlin: Springer-Verlag, 1977)]
173. Schmidt F et al. *Phys. Rev. A* **51** 2789 (1995)
174. Gabrielse G et al. *Phys. Lett. B* **455** 311 (1999)
175. *Proc. Int. Workshop on Antimatter Gravity and Antihydrogen Spectroscopy; Hyp. Int.* **109** (1–4) (1997)
176. Penning F M *Physica* **3** 873 (1936)
177. Paul W *Rev. Mod. Phys.* **62** 531 (1990) [*Usp. Fiz. Nauk* **160** (12) 109 (1990)]
178. Van Dyck R S, Schwinberg P B, Dehmelt H G *Phys. Lett.* **38** 310 (1977)
179. Brown L S, Gabrielse G *Rev. Mod. Phys.* **58** 233 (1986)
180. Gabrielse G et al. *Phys. Rev. Lett.* **57** 2504 (1986)
181. Gabrielse G et al. *Phys. Rev. Lett.* **63** 1360 (1989); **65** 1317 (1990)
182. Walls F L, Dehmelt H G *Phys. Rev. Lett.* **21** 127 (1968)
183. Rolston S L, Gabrielse G *Hyp. Int.* **44** 233 (1988)
184. Men'shikov L I *Usp. Fiz. Nauk* **169** 113 (1999) [*Phys. Usp.* **42** 107 (1999)]
185. Gabrielse G et al. *Phys. Lett. A* **129** 38 (1988)
186. Glinsky M E, O'Neil T M *Phys. Fluids B* **3** 1279 (1991)
187. Men'shikov L I, Fedichev P O *Zh. Eksp. Teor. Fiz.* **108** 144 (1995) [*JETP* **81** 78 (1995)]
188. Fedichev P O *Phys. Lett. A* **226** 289 (1997)
189. Wolf A *Hyp. Int.* **76** 189 (1993)
190. Delone N B, Kraĭnov V P, Shepelyanskiĭ D L *Usp. Fiz. Nauk* **140** 355 (1983) [*Sov. Phys. Usp.* **26** 551 (1983)]
191. Mansbach P, Keck J *Phys. Rev.* **181** 275 (1969)
192. Schramm U et al. *Phys. Rev. Lett.* **67** 22 (1991)
193. Neumann R *Hyp. Int.* **44** 305 (1988)
194. Kolybasov V M "Adronnye atomy" ("Hadronic atoms"), in *Fizicheskaya Entsiklopediya* (Encyclopedia of Physics) Vol. 1 (Moscow: BSE, 1988) p. 28
195. Fetkovich J G, Pewitt E G *Phys. Rev. Lett.* **11** 290 (1963)
196. Block M M et al. *Phys. Rev. Lett.* **11** 301 (1963)
197. Block M M, Kopelman J B, Sun C R *Phys. Rev.* **140** 143 (1965)
198. Fetkovich J G et al. *Phys. Rev. D* **2** 1803 (1970)
199. Fetkovich J G, Riley B R, Wang I-T *Phys. Lett. B* **35** 178 (1971)
200. Comber C et al. *Nuovo Cimento A* **24** 294 (1974)
201. Fetkovich J G et al. *Nucl. Phys. A* **240** 485 (1975)
202. Iwasaki M et al. *Phys. Rev. Lett.* **67** 1246 (1991)
203. Condo G T *Phys. Rev. Lett.* **9** 65 (1964)
204. Russel J E *Phys. Rev. Lett.* **23** 63 (1969); *Phys. Rev.* **188** 187 (1969); *Phys. Rev. A* **1** 721, 735, 742 (1970); *A* **6** 2488 (1976); *J. Math. Phys.* **12** 1906 (1971)
205. Men'shikov L I, Preprint IAE-6036/1 (Moscow: Institute of Atomic Energy, 1997)
206. Men'shikov L I *Hyp. Int.* **119** 245 (1999)
207. Azuma T et al. CERN/SPSC 97-19; CERN/SPSC P-307; http://tkynx0.phys.s.u.-tokyo.ac.jp/asacusa/
208. Horvath D *Hyp. Int.* **119** 263 (1999)
209. Knudsen H, Reading J F *Phys. Rep.* **212** 107 (1992)
210. Galitskiĭ V M, Nikitin E E, Smirnov B M *Teoriya Stolknoveniĭ Atomnykh Chastits* (Theory of Atomic Particle Collisions) (Moscow: Nauka, 1981)
211. Nikitin E E, Umanskiĭ S Ya *Neadiabaticheskie Perekhody pri Medlennykh Atomnykh Stolknoveniyakh* (Theory of Slow Atomic Collisions) (Moscow: Atomizdat, 1979) [Translated into English (Berlin: Springer-Verlag, 1984)]
212. Briggs J S, Greenland P T, Solov'ev E A *Hyp. Int.* **119** 235 (1999)
213. Ahlrichs R et al. *Z. Phys. A: Hadrons Nucl.* **306** 297 (1982)
214. Beck W A, Wilets L, Alberg M A *Phys. Rev. A* **48** 2779 (1993)
215. Belyaev S T, Budker G I, in *Fizika Plazmy i Problema Upravlyaemykh Termoyadernykh Reaktsiĭ* (Plasma Physics and Thermonuc-

lear Research) (Ed. M A Leontovich) Vol. 3 (Moscow: Izd. AN SSSR, 1958) p. 41
216. Lifshitz E M, Pitaevskiĭ L P *Fizicheskaya Kinetika* (Physical Kinetics) (Moscow: Nauka, 1979) [Translated into English (Oxford: Pergamon Press, 1981)]
217. Baz' A I, Zel'dovich Ya B, Perelomov A M *Rasseyanie, Reaktsii i Raspady v Nerelyativistskoĭ Kvantovoĭ Mekhanike* (Scattering, Reactions and Decays in Nonrelativistic Quantum Mechanics) 2nd ed. (Moscow: Nauka, 1977) [Translation of the 1st Russian ed. (Jerusalem: Israel Program for Scientific Translations, 1966)]
218. Heitler W *The Quantum Theory of Radiation* (Oxford: Oxford University Press, 1970)
219. Landau L D, Lifshitz E M *Kvantovaya Mekhanika. Nerelyativistskaya Teoriya* (Quantum Mechanics: Non-Relativistic Theory) (Moscow: Nauka, 1974) [Translated into English (Oxford: Pergamon Press, 1977)]
220. Yamazaki T et al. *Phys. Rev. A* **55** R3295 (1997)
221. Korobov V I *Phys. Rev. A* **54** R1749 (1996)
222. Korobov V I, Bakalov D D *Phys. Rev. Lett.* **79** 3379 (1997)
223. Bakalov D D et al. *Hyp. Int.* **101/102** 487, 493 (1996)
224. Elander N, Yarevsky E *Phys. Rev. A* **56** 1855 (1997)
225. Kino Y, Kamimura M, Kudo H *Proc. XV Int. Conf. 'Few-Body Problems in Physics'* (Gröningen, 1997)
226. Demkov Yu N, Ostrovskiĭ V N *Metod Potentsialov Nulevogo Radiusa v Atomnoĭ Fizike* (Zero Radius Potentials and Their Applications in Atomic Physics) (Leningrad: Izd. LGU, 1975) [Translated into English (New York: Plenum Press, 1988)]
227. Delone N B, Kraĭnov V P *Atom v Sil'nom Svetovom Pole* (Atom in a Strong Light Field) (Moscow: Energoatomizdat, 1984) [Translated into English (Berlin: Springer-Verlag, 1985)]; *Multiphoton Processes in Atoms* (Heidelberg: Springer-Verlag, 1994)
228. Smirnov B M *Vysokovozbuzhdennye Atomy* (Highly Excited Atoms) (Moscow: Energoatomizdat, 1982)
229. Delone N B, Kraĭnov V P *Usp. Fiz. Nauk* **165** 1295 (1995) [*Phys. Usp.* **38** 1247 (1995)]
230. Bureeva L A, Lisitsa V S *Vozmushchennyĭ Atom* (Perturbed Atom) (Moscow: IzdAT, 1997)
231. Davydkin V A, Zon B A *Opt. Spektrosk.* **51** 25 (1981) [*Opt. Spectrosc.* **51** 13 (1981)]
232. Kim L, Pratt R H *Phys. Rev. A* **36** 45 (1987)
233. Yamazaki T et al. *Nature* **361** 238 (1993)
234. Yamazaki T *Hyp. Int.* **101/102** 451 (1996)
235. Smirnov B M *Fizika Slaboionizovannogo Gaza v Zadachakh s Resheniyami* (Physics of Weakly Ionized Gases: Problems and Solutions) (Moscow: Nauka, 1972) [Translated into English (Moscow: Mir Publ., 1981)]
236. Radzig A A, Smirnov B M *Parametry Atomov i Atomnykh Ionov: Spravochnik* (Parameters of Atoms and Atomic Ions) 2nd ed. (Moscow: Energoatomizdat, 1986)
237. Radzig A A, Smirnov B M *Spravochnik po Atomnoĭ i Molekulyarnoĭ Fizike* (Reference Data on Atoms, Molecules, and Ions) [Translated into English (Berlin: Springer-Verlag, 1985)]
238. Morita T, Ohtsuki K, Yamazaki T *Nucl. Instrum. Meth. A* **33** 439 (1993)
239. Morita N et al. *Phys. Rev. Lett.* **72** 159 (1994)
240. Yamazaki T et al. *Chem. Phys. Lett.* **265** 137 (1997)
241. Widmann E et al. *Phys. Rev. A* **53** 3129 (1996)
242. Widmann E et al. *Phys. Rev. A* **51** 2870 (1995)
243. Hellmann H *Kvantovaya Khimiya* (Quantum Chemistry) (Moscow-Leningrad: GTTL, 1937); *Einführung in die Quantumchemie* (Leipzig: Deuticke, 1937)
244. Feynman R P *Phys. Rev.* **56** 340 (1939)
245. Smirnov B M *Atomnye Stolknoveniya i Élementarnye Protsessy v Plazme* (Atomic Collisions and Elementary Processes in Plasmas) (Moscow: Atomizdat, 1968)
246. Berestetskiĭ V B, Lifshitz E M, Pitaevskiĭ L P *Relyativistskaya Kvantovaya Teoriya* (Relativistic Quantum Theory) (Moscow: Nauka, 1968 – 1971) [Translated into English (Oxford: Pergamon Press, 1971 – 1974)]
247. Korobov V I, Shimamura I *Phys. Rev. A* **56** 4587 (1997)
248. Kartavtsev O I, Fedotov S I, Monakhov D E *Hyp. Int.* **109** 125 (1997); **119** 207 (1999)
249. Hori M et al. *Phys. Rev. A* **57** 1698 (1998)
250. Korenman G Ya, Preprint NIIYaF MGU No. 97-1/452 (Moscow: D V Skobeltsyn Scientific Research Institute of Nuclear Physics at the M V Lomonosov Moscow State University, 1997)
251. Kondrat'ev V N *Konstanty Skorosti Gazofaznykh Reaktsiĭ* (Gas-Phase Reaction Rates) (Moscow: Nauka, 1971) [Translated into English as *Rate Constants of Gas Phase Reactions* (Washington: Office of Standard Reference Data, 1972)]
252. Kondrat'ev V N, Nikitin E E *Kinetika i Mekhanizmy Gazofaznykh Reaktsiĭ* (Kinetics and Mechanisms of Gas Phase Reactions) (Moscow: Nauka, 1974); see also *Gas-Phase Reactions: Kinetics and Mechanisms* (Berlin: Springer-Verlag, 1981)
253. Conroy H, Bruner B *J. Chem. Phys.* **47** 921 (1967)
254. Nikitin E E *Teoriya Elementarnykh Atomno-Molekulyarnykh Protsessov v Gasakh* (Theory of Elementary Atomic and Molecular Processes in Gases) (Moscow: Khimiya, 1970) [Translated into English (Oxford: Clarendon Press, 1974)]
255. Levin J L, Sanders T M *Phys. Rev.* **154** 138 (1967)
256. Kukushkin L S, Shikin V B *Zh. Eksp. Teor. Fiz.* **63** 1830 (1972) [*Sov. Phys. JETP* **36** 969 (1973)]
257. Shikin V B *Usp. Fiz. Nauk* **121** 457 (1977) [*Sov. Phys. Usp.* **20** 226 (1977)]
258. Harrisson H R, Springett B E *Phys. Lett. A* **35** 73 (1971)
259. Halperin B, Gomer R *J. Chem. Phys.* **43** 1069 (1965)
260. Gachechiladze I A, Keshishev K O, Shal'nikov A I *Pis'ma Zh. Eksp. Teor. Fiz.* **12** 231 (1970) [*JETP Lett.* **12** 159 (1970)]
261. Lebedenko V N, Rodionov B U *Pis'ma Zh. Eksp. Teor. Fiz.* **16** 583 (1972) [*JETP Lett.* **16** 411 (1972)]
262. Brushi L, Mazzi G, Sautini M *Phys. Rev. Lett.* **28** 1504 (1972)
263. Laveland R J, Lecomber P G, Spear W E *Phys. Lett. A* **39** 225 (1972)
264. Sommer W T *Phys. Rev. Lett. A* **12** 271 (1964)
265. Woolf M A, Rayfield G W *Phys. Rev. Lett.* **15** 235 (1965)
266. Budrick B *Phys. Rev. Lett.* **14** 11 (1965)
267. Grimes C C, Adams G *Phys. Rev. B* **41** 6366 (1990)
268. Yamazaki T, Ohtsuki K *Phys. Rev. A* **45** 7782 (1992)
269. Widmann E *Hyp. Int.* **119** 195 (1999)
270. Ketzer B et al. *J. Chem. Phys.* **109** 424 (1998)
271. Perelomov V M, Popov V S, Terent'ev M V *Zh. Eksp. Teor. Fiz.* **50** 1393 (1966) [*Sov. Phys. JETP* **23** 924 (1966)]
272. Men'shikov L I *Yad. Fiz.* **42** 1449 (1985) [*Sov. J. Nucl. Phys.* **42** 918 (1985)]
273. Men'shikov L I, Faĭfman M P *Yad. Fiz.* **43** 650 (1986) [*Sov. J. Nucl. Phys.* **43** 414 (1986)]
274. Men'shikov L I et al. *Zh. Eksp. Teor. Fiz.* **92** 1173 (1987) [*Sov. Phys. JETP* **65** 656 (1987)]
275. Scrinzi A et al. *Phys. Rev. A* **47** 4691 (1993)
276. Petitjean C et al. *Hyp. Int.* **118** 127 (1999)
277. Dzhelepov V P et al. *Pis'ma Zh. Eksp. Teor. Fiz.* **53** 581 (1991) [*JETP Lett.* **53** 604 (1991)]
278. Henneberger W C *Phys. Rev. Lett.* **21** 838 (1968)
279. Komarov I V, Ponomarev L I, Slavyanov S Yu *Sferoidal'nye i Kulonovskie Sferoidal'nye Funktsii* (Spheroidal and Coulomb Spheroidal Functions) (Moscow: Nauka, 1976)
280. Kirzhnits D A, Pen'kov F M *Zh. Eksp. Teor. Fiz.* **85** 80 (1983) [*Sov. Phys. JETP* **58** 46 (1983)]
281. Babikov V V *Metod Fazovykh Funktsiĭ v Kvantovoĭ Mekhanike* (Phase Function Method in Quantum Mechanics) (Moscow: Nauka, 1968)
282. Efimov V N *Yad. Fiz.* **12** 1080 (1970)
283. Demkov Yu N *Zh. Eksp. Teor. Fiz.* **45** 195 (1963) [*Sov. Phys. JETP* **18** 128 (1964)]
284. Demkov Yu N, Kunike M *Vestn. Leningrad. Univ.* **16** 39 (1969)
285. Men'shikov L I *Zh. Eksp. Teor. Fiz.* **85** 1159 (1983) [*Sov. Phys. JETP* **58** 675 (1983)]
286. Nelipa N F *Fizika Élementarnykh Chastits* (Elementary Particle Physics) (Moscow: Vysshaya Shkola, 1977)
287. Lee T D *Particle Physics and Introduction to Field Theory* (Chur: Harwood Academic Publ., 1981)
288. Feynman R P *Usp. Fiz. Nauk* **157** 163 (1989); Feynman R P, in *Elementary Particles and the Laws of Physics: the 1986 Dirac Memorial Lectures* (Cambridge: Cambridge University Press, 1987)
289. Gershteĭn S S, in *Fizicheskaya Entsiklopediya* (Encyclopedia of Physics) Vol. 4 (Moscow: BRE, 1994)

290. Gol'danskiĭ V I, Kuz'min V A *Usp. Fiz. Nauk* **157** (1) 3 (1989) [*Sov. Phys. Usp.* **32** 1 (1989)]
291. Landau L D *Zh. Eksp. Teor. Fiz.* **32** 407 (1957) [*Sov. Phys. JETP* **5** 337 (1957)]
292. Lee T D, Yang C N *Phys. Rev.* **105** 1671 (1957)
293. Salam A *Nuovo Cimento* **5** 299 (1957)
294. Christenson J H et al. *Phys. Rev. Lett.* **13** 138 (1964)
295. Danilov M V *Usp. Fiz. Nauk* **168** 631 (1998) [*Phys. Usp.* **41** 559 (1998)]
296. Sakharov A D *Pis'ma Zh. Eksp. Teor. Fiz.* **5** 32 (1967) [*JETP Lett.* **5** 24 (1967)]
297. Kuz'min V A *Pis'ma Zh. Eksp. Teor. Fiz.* **12** 335 (1970) [*JETP Lett.* **12** 228 (1970)]
298. Ignat'ev A Yu, Kuz'min V A, Shaposhnikov M E *Pis'ma Zh. Eksp. Teor. Fiz.* **30** 726 (1979) [*JETP Lett.* **30** 689 (1979)]
299. Rubakov V A, Shaposhnikov M E *Usp. Fiz. Nauk* **166** 493 (1996) [*Phys. Usp.* **39** 461 (1996)]
300. Grib A A, Mamaev S G, Mostepanenko V M *Kvantovye Éffekty v Intensivnykh Vneshnikh Polyakh* (Quantum Effects in Intense External Fields) (Moscow: Atomizdat, 1980)
301. Birrell N D, Davies P C W *Quantum Fields in Curved Space* (Cambridge: Cambridge University Press, 1982) [Translated into Russian (Moscow: Mir, 1984)]
302. Kadomtsev B B *Dinamika i Informatsiya* (Dynamics and Information) (Moscow: Red. Zh. "Usp. Fiz. Nauk", 1997)
303. Bogolyubov N N, Shirkov D V *Vvedenie v Teoriyu Kvantovannykh Poleĭ* (Introduction to the Theory of Quantized Fields) (Moscow: Nauka, 1976) [Translated into English (New York: John Wiley, 1980)]
304. Itzykson C, Zuber J-B *Quantum Field Theory* (Cambridge: Cambridge University Press, 1978) [Translated into Russian (Moscow: Mir, 1984)]
305. Ryder L H *Quantum Field Theory* (Cambridge: Cambridge University Press, 1984) [Translated into Russian (Moscow: Mir, 1987)]